The influence of solid surfaces on the structure and dynamics of polymer melts

TECHNISCHE UNIVERSITÄT DARMSTADT

Vom Fachbereich Chemie
der Technischen Universität Darmstadt

zur Erlangung des akademischen Grades eines
Doktor rerum naturalium (Dr. rer. nat.)

genehmigte
Dissertation

vorgelegt von

Sulivan Dias Borges Vianna, (Eng.) Engenheiro de Materiais

aus São Paulo (Brasilien)

Referent: Prof. Dr. Florian Müller-Plathe
Korreferent: Prof. Dr. Hans-Jürgen Butt
Tag der Einreichung: 1. März 2012
Tag der mündlichen Prüfung: 16 April 2012

Darmstadt 2013
D17

Die vorliegende Arbeit wurde im Zeitraum von Februar 2009 bis Januar 2012 am Max-Planck-Institut für Polymerforschung in Mainz unter der Anleitung von Herrn Prof. Dr. H.-J. Butt, Herrn Prof. Dr. W. Steffen und Frau Prof. Dr. Hatice Duran angefertigt.

As we enjoy great advantages from the inventions of others,
we should be glad of an opportunity to serve others
by any invention of ours,
and this we should do freely and generously.

Benjamin Franklin

Summary

The structure and dynamics of polymer melts in the proximity of a solid substrate was investigated. This issue is relevant due to its basic scientific aspects as well as for technological applications in the field of interfaces and composite materials. For this, polystyrene of various molecular weights (in the entangled and non-entangled regime) were spin coated on gold surfaces which were created by thermal evaporation. Polystyrene was chosen due to its vast technological application range and for being a well characterized material. The polymer films were characterized using resonance enhanced dynamic light scattering (REDLS) and kinetic surface plasmon resonance spectroscopy (SPR). For this an appropriate REDLS setup adapted for the problem was built. The film thickness ranged from about 4 nm to 440 nm. For different molecular weights, the glass transition temperatures (T_g) were measured by kinetic SPR and compared to the value of T_g of bulk polymer measured by DSC at corresponding heating or cooling rates. Within the experimental errors, no differences in T_g were observed for the entangled and non-entangled polystyrenes samples (350 000 g/mol and 1821 g/mol respectively) measured down to 4 nm for the entangled polymer and 8 nm for the non-entangled molecular weight.

The behavior of the dynamics investigated by REDLS revealed two main processes, a slow- and a fast-mode. The slow-mode was shown to be attributed to the free-surface dynamics, specifically the dynamics of thermally activated capillary waves. The signal of the fast-mode originated throughout the entire film thickness and was correlated to the presence of solvent (toluene) residues. Thoroughly annealed films did not show a fast-mode.

From the theory of thermally activated capillary waves it is possible to infer physical properties of these supported polymer films, such as *e.g.* viscosity (η) and shear modulus (G). The results obtained by REDLS of thin films at a given temperature and capillary wave frequency were compared with rheological measurements of bulk polystyrene at the same temperature and

frequency. No differences of η and G were observed between thin films and the bulk polymer. It was also possible to state that the dynamics of the free-surface is described by a Vogel-Fulcher-Tamman like behavior (VFT) instead of fitting to the Arrhenius equation as proposed by some authors. However, the solid surface with a no-slip boundary condition at the polymer-solid contact leads to the dynamics of the free-surface to slow down while decreasing the film thickness. This should not be confused with a chain confinement effect, but it is simply a hydrodynamic effect governed by the film thickness h and the no-slip boundary condition. Even though the film thickness has an impact on the measured capillary wave frequency, it was possible to show that the temperature and frequency dependence of η and G remain unaltered with film thickness. The relevant factor changing the dynamics is in fact the film thickness itself.

Zusammenfassung

Der Einfluss von festen Substraten auf Struktur und Dynamik von Polymerschmelzen wurde untersucht. Diese Fragestellung ist, sowohl für das grundlegende wissenschaftliche Verständnis, als auch für technologische Anwendungen wie z.B. im Bereich der Grenzflächen und Verbundwerkstoffen wichtig. Zur Untersuchung wurden ultradünne Filme von Polystyrol mit verschiedenen Molekulargewichten (im verknäulten und unverknäulten Bereich) durch Aufschleudern (spin coating) auf thermisch aufgedampfte Goldoberflächen hergestellt. Polystyrol wurde wegen seines großen technologischen Anwendungsbereiches und der guten Charakterisierung ausgewählt. Die Polymerfilme wurden mittels resonanzverstärkter dynamischer Lichtstreuung (REDLS) und kinetischer Oberflächenplasmonen Resonanz Spektroskopie (SPR) untersucht. Für diesen Zweck wurde eine geeignete und an das Problem angepasste REDLS Apparatur aufgebaut. Es wurden Filmdicken im Bereich von etwa 4 nm bis 440 nm verwendet. Die Glasübergangstemperaturen (T_g) der Filme für unterschiedliche Molekulargewichte (350 000 g/mol und 1821 g/mol) mit Dicken von bis zu 4 bzw. 8 nm herab wurden durch kinetische SPR Messungen bestimmt und mit T_g von Bulk Polystyrol verglichen (differential scanning calorimetry–DSC–bei entsprechenden Heiz- oder Kühlraten). Dabei wurden innerhalb des Messfehlers keine Unterschiede in T_g beobachtet.

Das mittels REDLS untersuchte dynamische Verhalten von dünnen Schichten zeigte zwei dynamische Prozesse, einen sogenannten langsamen (slow-mode) und einen schnellen (fast-mode). Die langsame Relaxation zeigt die Dynamik der freien Oberfläche, insbesondere die der thermisch aktivierten Kapillarwellen. Die schnelle Relaxation, deren Signal aus dem gesamten Film stammt, resultiert aus der Diffusion von verbliebenem Lösungsmittel (Toluol). Gründlich getemperte Filme haben keinen schnellen Prozess gezeigt.

Aus der Theorie der thermisch aktivierten Kapillarwellen kann auf physikalische Eigenschaften der Polymerfilme, wie z.B. Viskosität (η) und Scher-

modul (G) geschlossen werden. Durch den Vergleich der Ergebnisse von REDLS von dünnen Schichten bei einer gegebenen Temperatur und Wellenfrequenz der Kapillarwelle mit rheologischen Messungen bei der gleichen Temperatur und Frequenz wurden keine Unterschiede von η und G zwischen dünnen Filmen und Bulk Polymer beobachtet. Desweiteren war es möglich, die Dynamik der freien Oberfläche mit der Vogel-Fulcher-Tamman (VFT) Gleichung zu beschreiben, anstelle der von viele Autoren vorgeschlagenen Arrhenius Gleichung. Unter Annahme einer "no-slip" Randbedingung an der Polymer-Feststoff Grenzfläche beim Verringern der Filmdicke verlangsamt sich die Dynamik der freien Oberfläche. Das sollte nicht mit einem Confinement Effekt der Kette verwechselt werden, es handelt sich lediglich um eine hydrodynamische Wechselwirkung bedingt durch die Schichtdicke h und die "no-slip" Randbedingungen. Auch wenn die Schichtdicke Auswirkungen auf die gemessene Wellenfrequenz der Kapillarwelle hat, war es möglich zu zeigen, dass die Viskosität η und der Schermodul G unverändert mit der Schichtdicke bleiben und der relevante Faktor für die Veränderung der Dynamik die Schichtdicke selbst ist.

Erklärung zur Dissertation

Hiermit versichere ich, die vorliegende Dissertation ohne Hilfe Dritter nur mit den angegebenen Quellen und Hilfsmitteln angefertigt zu haben. Alle Stellen, die aus Quellen entgenommen wurden, sind als solche kenntlich gemacht. Diese Arbeit hat in gleicher oder ähnlicher Form noch keiner Prüfungsbehörde vorgelegen.

Darmstadt, den Februar 23, 2012

Sulivan Dias Borges Vianna

Contents

Introduction

Motivation

The properties of polymeric materials confined to nanoscopic dimensions have been extensively studied throughout the last 20 years due to their great technological importance and in order to improve basic scientific understanding [1, 2]. Materials like small molecular glass formers and polymers are thought of to display deviations from bulk properties when submitted to confinement [3, 4], *i.e.*, under geometries of dimensions similar to the molecular length scale. Although enormous theoretical and experimental efforts have been spent to reach a precise view of the dynamical behavior of ultrathin polymer films, both supported and free-standing, many controversial and disagreeing results have been reported [4–14]. One of the most contemplated properties studied in these systems is the glass transition related to the primary or α-relaxation, which is attributed to the reorientational motion of chain segments and therefore to the main chain backbone [15]. There is a vivid ongoing discussion whether or not the glass transition temperature, T_g, of ultrathin films suffers influence of the confinement imposed by the nanoscopic dimensions of the films, by the polymer-solid contact (*e.g.* van der Waals forces), or simply by the presence of a solid support with no-slip boundary conditions on it (hydrodynamic effects). The polymer-gas or polymer-vacuum interface, the so-called free-surface is also believed to play a role on the dynamics of ultrathin polymer films (the schematics showing the relevant parts of a polymer thin film is shown in Figure 1.1).

Furthermore, some groups reported an enhanced mobility of the free-surface dynamics [16, 17]. Such experiments were primarily designed to be sensitive solely to the topmost molecular layers. They concluded that the observed increased mobility of the free-surface of polymer ultrathin films was the reason behind the commonly detected T_g deviations in comparison to the bulk material. The idea supported by those authors is that a highly

mobile free-surface would expand its mobility to the central region of the films, thus, decreasing T_g. It was also pointed out that the dynamics of the free-surface is Arrhenius-like.

However, in a recent set of publications [18–22] it was shown by broadband dielectric spectroscopy (BDS), ellipsometry, and AC-calorimetry that a careful sample preparation is a crucial aspect in these studies, otherwise undesired side effects could mimic disagreements of the T_g between bulk and ultrathin films. It was reported that down to a film thickness of ≈ 4.5 nm no deviations in T_g were observed in entangled polystyrene (PS) films if their sample preparation and handling procedures were followed. Actually, much earlier in a pioneer work, Efremov [23] showed by ultra sensitive DSC that down to 3 nm no T_g deviations were observed in entangled PS in comparison to bulk. He performed careful sample preparation, but did not mention that this procedure was the reason for a non-deviating T_g.

Another open question regards the interphase region between the solid-surface and the polymer. What happens to the chain mobility at the vicinity of an interface? How thick is this interphase region? What is the role of the chemical composition of both, the solid surface and the polymer? To which extend these effects can change the intrinsic properties of a material (as T_g, density, viscosity, surface tension, refractive index, etc) throughout the film thickness?

Although all these questions have been addressed from the experimental, theoretical and from the simulation point of view, no clear phenomenological picture is widely accepted in the scientific community. The answer to these important basic questions could lead to the improvement and complete development of technological fields where the dynamics of thin films and interfaces play a significant role. Some examples are: data storage; abrasion and friction; static & dynamic wetting; organic and inorganic solar cells; physical and chemical properties of nanocomposites; materials for drug delivery; biomembranes and bio-systems in general; coatings and paintings; rheological properties while processing composite materials; catalysts; electrochemistry; medical applications where surface properties are of vital importance; growing of cells and tissues, and innumerous others.

For a company producing nano-devices based on polymeric ultrathin films, it is fundamental to know if the softening temperature or the T_g of a polymer is going to happen at 100 °C or 30 °C. This knowledge is important for both, the product performance and its final price. If a certain application requires working temperatures of 30 °C and the polymer suggested is polystyrene, it would be crucial to know whether or not it will

fulfill the product requirements. Another example would be the case where a lower softening temperature is desired, as *e.g.* while processing materials or even in the case of data storage in thin films, where high softening temperatures mean the necessity of more heating while processing or in applications, therefore increasing costs. This is an example of tuning properties in these fields. Surface dynamics is a relatively new field in physical-chemistry and surely, a topic of general and major interest for basic research and technology nowadays.

Organization of this thesis

Chapter 1 introduces the main concepts about polymer physics and dynamics necessary for the comprehension of the experimental results obtained by REDLS (resonance enhanced dynamic light scattering) and kinetic SPR (surface plasmon resonance) in polymer ultrathin films. Here, both bulk and ultrathin films are revisited, the state-of-the-art research and remaining open scientific questions are introduced, including the discussion about the anomalies found in the glass transition of ultrathin films and the developed theories trying to explain them. A second part of this chapter introduces the theories about capillary waves in viscoelastic media of arbitrary thickness. The here so-called "slow-mode" behaves as capillary waves and, therefore, can be regarded as the manifestation of capillary wave dynamics on polymer ultrathin films. From this dynamical behavior one can infer about physical properties of the films, enabling a direct comparison to the bulk properties. Mathematical corrections of the existing capillary wave theories, will be presented at this point.

Chapters 2 refers to the experimental part, *i.e.*, the methods used to prepare the samples and characterize them. Every key aspect of each procedure is explained in detail. Introductions to SPR and DLS as well as REDLS and WEDLS are also given.

Chapter 3 includes the main results obtained by REDLS and kinetic SPR in polymeric and oligomeric ultrathin films (from 4 nm up to about 440 nm), covering a broad behavioral range where a sort of transition from confinement effects to bulk features can be observed. Here, the main relaxation modes detected by REDLS and kinetic SPR are introduced: the "slow-mode", the "fast-mode", and indirectly, the α-relaxation. All these dynamical processes are treated on the theoretical basis provided in the initial chapters. A discussion is carried out in each section together with the results.

Chapter 4 relates all the most important features observed by REDLS in those polymeric systems with the known world of polymer physics and polymer dynamics, and brings a new point of view to this field. Many of the long standing and still currently open questions, including those that inspired this research project were regarded and ultimately resolved. Some new scientific questions generated by this research work are mentioned with suggestions about how to possibly clarify them. An outlook on the future of both REDLS and WEDLS techniques is also given. Accounting for their major importance as these powerful techniques revealed to be capable of resolving dynamics at interfaces for a great variety of relevant systems.

Chapter 1

Theory

The main concepts of polymer chain dynamics were long ago developed by scientists as Rouse (1953), who launched one of the first successful models intending to describe the single chain movements and relaxations, culminating with the work of Pierre Gilles de Gennes (1971) about chain reptation and the molecular theory ("tube model") of Doi and Edwards. After a certain period, the scaling concepts in polymer physics were established and even the deviations of the scaling laws from the reptation theory observed in experiments could be accurately explained. In this way, the rheology of polymers, their flow, and the main ideas about this topic were developed. In the meanwhile, an old problem in condensed-matter physics, the glass transition, was being treated by many researchers as Adam, Gibbs, DiMarzzio, later on C.A. Angell, H. Sillescu, E.W. Fischer, W. Götze, F. Kremer, W. Spiess and others, without ultimately conclusive results. The glass transition is still one of the most challenging and important open questions in physics. This chapter treats the main relaxation processes in bulk polymeric materials and on their surfaces, in order to give a broad view about the here relevant polymer dynamics and finally to be the basis of comparison with the results obtained by kinetic SPR (Surface Plasmon Resonance), and by the recently developed technique, REDLS (Resonance Enhanced Dynamic Light Scattering) in ultrathin polymeric and oligomeric films. A discussion about the glass transition in ultrathin films, a controversial question raised about 20 years ago in polymer physics, is carried out, and the state-of-the-art research in this field is presented in detail.

1.1 Polymer Dynamics

Polymers became widely used products in industry at the end of 1940's and early 1950's, and economically extremely important for many countries, being frequently a sort of sensor for development of a nation. For these reasons, to understand the behavior of polymeric materials while processing, their final performance, how to produce them in the least expensive ways possible, etc, became of primordial importance.

Dynamical-mechanical and rheological tests were crucially important to determine final mechanical properties of polymeric pieces as well as the flow of these materials when injected into molds, while blowing them or stamping polymeric sheets. Dielectric properties of polymeric materials became of fundamental interest when the use of polymers as insulators in electric cables and capacitors for example, spread in an incredibly fast way.

1.1.1 Dynamics of bulk polymers

In the following, the main concepts describing polymer relaxation behavior in the bulk material will be introduced.

1.1.1.1 Molecular theories of relaxation

Before starting to describe the known relaxations in polymers let us introduce the common system of nomenclature for labeling some of the different loss regions found in these materials.

Deutsch, Hoff and Reddish proposed in 1954 to use the Greek letters α, β, γ, etc, for the relaxation peaks following the order that they appear [24]. The α-relaxation corresponds to the dynamical process observed at the highest temperature (at a constant probing frequency), or the lowest frequency at a given constant probing temperature. The β, γ, δ-relaxations are the ones with higher frequency, *i.e.*, they are faster than the α-relaxation; in the case of a constant frequency, they are the ones that appear in lower temperatures [24, 25]. At that time not all relaxations we nowadays know were identified and understood. Therefore, although their definitions fail in being rigorously precise, they are still widely used. The physical meaning of many of these relaxations and to what they are attributed is still a matter of discussion (as the precise interpretation of the α-relaxation), but the most accepted views will be treated herein.

Amorphous and semi-crystalline polymers undergo a "glass transition" at the temperature defined as T_g also called – glass-rubber transition – that takes place at temperatures below the melting point T_m in the case of semi-crystalline polymers (T_m is the melting point of the crystalline regions). The glass transition temperature is characterized, *e.g.*, by an abrupt change in the slope of the specific volume as a function of temperature. This abrupt change of expansion coefficient in the transition from the glassy state to the rubbery state (or to the liquid state in materials where the rubber plateau does not exist), as well as the heat capacity and other properties are normally used to determine the transition region [25]. The T_g is not an unique temperature, *i.e.*, a sharp first-order transition like, *e.g.*, the melting of ice, but occurs over a certain range of temperatures. It is important to notice that this transition is related to the amorphous state, being present in all glass forming materials. The amorphous state is not at thermodynamic equilibrium. Another feature of the glass transition temperature (also due to the non-equilibrium of the amorphous glass state) is that it is dependent on the rate of cooling or heating being applied while the material is tested, also suffering hysteresis. Higher rates deliver higher T_g values [25]. Therefore, this temperature is called "the dynamic or kinetic glass transition" [25]. The reason for the cooling or heating rate dependence of the T_g may be explained by the inefficiency of the polymer chains to relax to the new equilibrium states and therefore to the equilibrium volumes at a specific temperature if its cooling or heating rate is greater than the relaxation rate at the corresponding temperatures. An explanation in terms of density of free-volume in the glassy and in the liquid state that results to be analogous to this latter explanation, is given in ref. [25]. Some other aspects of this topic will be further discussed in section 1.1.1.3.

The α-relaxation, also called α-process, segmental-relaxation or primary-relaxation, is experimentally related to the glass transition. The cooperativity size of this relaxation (or of the glass transition) is shown to be in the range $\approx$ 1-4 nm [26, 27]. It was estimated that a kinetic segment of three repeat units (monomers) relaxing in the presence of free volume fluctuations participate in this relaxation for the specific case of cis-polyisoprene [28]. Other polymers will show a segment probably different from this specific number, but in general this is the characteristic length scale of this relaxation. Normally, by comparing the glass transition temperature T_g obtained by DSC (Differential Scanning Calorimetry) with rheological experiments, T_g is said to be the temperature at which the α-relaxation (or the enthalpy relaxation time in this case) exhibits relaxation time $\tau_\alpha \approx 100$ s determined at the "standard" scan rate 20° C/min [29] (some authors consider 10 s or even

1 s when other rates are used). In the past, T_g was determined in terms of viscosity, *i.e.* T_g is defined as the temperature at which $\eta \approx 10^{12}$ Pa s and for laboratory time-scales, the material behaves as an extremely viscous liquid or in other words, as a solid. If the T_g is determined by the first approach, then the viscosity will not be $\eta \approx 10^{12}$ Pa s [29]. It is important to keep in mind that these latter definitions are not *a priori* meaningful, but somewhat arbitrary. These definitions are simply based on the empirical comparison between the calorimetric glass transition temperatures obtained by DSC with the rheological data.

The β, γ, etc, relaxations, also called "localized processes", are Arrhenius-like and for many years thought to be related to quite small portions of the polymeric chain, such as side groups (*e.g.*, rotations or bouncing of side groups). For the case of methacrylate polymer series, the β-relaxation is thought to be related to –COOR side-group [25]. These relaxations are also sometimes attributed to the glass transition itself [30]. These ideas seem to be contradictory since some polymers as polyvinyl chloride and polyvinyl acetals also show β-peaks which cannot be attributed to side group rotations [25]. It is important to note that even though no voluminous side groups are present in some of the polymers having those localized relaxations, these polymers also show a glass transition, and therefore it seems intuitive that some theories relate local relaxations to the amorphous state itself. Small portions of the main chain backbone may be able to show some degree of mobility, even under T_g in the "frozen" glassy state, as experimentally revealed for these local processes.

In the past, attention was driven towards these local processes, even though, a fully comprehensive understanding was never achieved. The glass transition problem and the α-relaxation are still a strong matter of discussion.

The latter definitions given for the α, β, γ, δ peaks did not take into account that modes slower than the α peak exist at a given temperature. In fact, there are well known modes related to longer pieces of chain that relax with times longer than τ_α [28, 31].

The so-called normal mode or terminal-relaxation or end-to-end-vector relaxation are names given to the relaxation of the complete chain. Considering a polymer chain, the complete relaxation of all chain segments will lead to the relaxation of the end-to-end vector, a fact that can be observed, *e.g.*, by BDS (Broadband Dielectric Spectroscopy) for polymers showing strong dipole moments along the chain contour. An example of those measurements and their characteristics can be found in [28], where cis-polyisoprene

was studied.

This terminal relaxation is related to the whole chain flow and, for a given probing temperature it relaxes on time-scales much longer than those of the α-relaxation. In a master curve obtained by rheology, the terminal region can be observed in frequencies much slower than the α-relaxation, so that the α-relaxation does not play a strong role in this terminal range anymore. τ_α at the reference temperature T_r is given by the cross-over point between G' and G'' (the storage and loss shear moduli, respectively) and can be obtained at other temperatures by multiplying this value by the shift factor a_T^i corresponding to the temperature T^i at which one wants to calculate τ_α^i, *i.e.*, $\tau_\alpha^i = \tau_\alpha^r \cdot a_T^i$, as shown in appendix D.

The first theory that described this terminal region successfully (or the normal mode) was the Rouse model [32], in which it was established that the relaxation time of the terminal relaxation of low molecular weight polymers was proportional to the square of the molecular weight [25, 33]:

$$\tau_R = \frac{n^2 l^2 \zeta_0}{6\pi^2 p^2 k_B T} \propto M^2 \tag{1.1}$$

where, n is the number of segments with length l in which the chain was arbitrarily divided, p is the order of the mode (as the harmonic modes in a string), ζ_0 is the friction coefficient of a single link, k_B is the Boltzmann constant and T the temperature.

The Rouse viscosity is given by:

$$\eta_R = \frac{\pi^2}{12}\left(\frac{\rho N_A k_B T}{M}\right)\tau_R \propto \rho M^1 \tag{1.2}$$

η_R is the Rouse viscosity for low molecular weights (M) polymers, N_A is the Avogadro's number, k_B is the Boltzmann constant, and ρ is the density [34].

It was experimentally shown that low molecular weight polymers (non-entangled) follow these scaling laws but higher molecular weight polymers showed another scaling dependence:

$$\tau_{max} \propto M^{3.4} \tag{1.3}$$

and

$$\eta_0 \propto M^{3.4} \tag{1.4}$$

The scaling power of the long relaxation time, τ_{max} (the normal mode relaxation time), with molecular weight was experimentally found to vary

from 3.4 to 3.7, just as the viscosity (η_0) [35, 36]. It was observed that this deviation from the Rouse theory was happening in molecular weights where chain entanglements take place, *i.e.*, for molecular weights higher than the entanglement molecular weight, M_e, the model fails.

As a conclusion, the Rouse theory is applicable to low molecular weight polymers (oligomers), where the rubber plateau region essentially disappears due to the absence of entanglements in these materials, and the glass-rubber and the terminal regions merge [25]. This leads to the conclusion that the rubber-plateau found in rheology master curves of high molecular weight polymers is originated due to chain entanglements. The higher the molecular weight, the more pronounced is the rubber-plateau [35].

De Gennes suggested in 1971 [37] that the presence of entanglements would lead the polymer chains to move through these obstacles by doing a kind of movement that he named "reptation", *i.e.*, the polymer chains "crawl" within the polymeric mass formed by other chains. Out of this idea, a relaxation time proportional to M^3 comes out:

$$\tau_{rep} = \frac{(Na)^3}{\pi^2 \rho b^2 \Delta} \propto M^3 \tag{1.5}$$

where a is the length of a chain monomer, N is the number of monomers of the whole freely jointed chain, b is the stored length of a "chain defect", Δ is the diffusion coefficient of the defects along the chain, and ρ is the equilibrium density of defects per unit length of the extended chain. Actually, de Gennes developed this model by considering a gel network and extracting the diffusion of a single polymer molecule through it. The disagreement between theory and experiments was still remaining though, as the experimental scaling exponent observed was 3.4 and therefore higher than the expected value 3.

Many years later, this long standing problem was resolved. Modifications of the original reptation theory incorporating additional relaxation mechanisms, such as contour length fluctuations and constraint release seemed to describe the experimental results quite well [38, 39].

Another successful theoretical approach that delivered explicitly the power law $\tau_{max} \propto M^{3.4}$ was the "double reptation model" derived by des Cloizeaux [40–43]. He also showed that other parallel relaxations were leading to the factor varying from 3.4 to 3.7 instead of the pure reptation of de Gennes. The double reptation model considers a pair of entangled polymer chains with the reptation modeled with a time dependent diffusion coefficient [44].

Nowadays it is fully accepted that linear polymers of low molecular weight will flow following the Rouse relaxation time τ_R scaling with M^2 and that due to the presence of entanglements, high molecular weight polymers ($M >> M_e$) show a rubber plateau and deviate from the Rouse model, scaling with $M^{3.4}$ to $M^{3.7}$, instead.

Apart from the normal mode, it was experimentally observed by the group of E. W. Fischer that a much slower hydrodynamic mode of diffusive nature was present in a series of glass formers [31]. This mode was attributed to long range density fluctuations originated from non-homogeneous distribution of free-volume in the amorphous state. In other words, this ultra-slow mode was attributed to an intrinsic presence of "quasi-crystals", similar to the polyamorphic regions cited in ref. [29] or even agglomerates of fractals diffusing in a correlated way inside the amorphous liquid material. Finally, it is referred to as the diffusion of one kind of amorphous liquid within another type of amorphous matrix. These agglomerates were named "Fischer Clusters", after E. W. Fischer who developed a thermodynamic theory intending to explain their origin [45].

In the context of the present work it is relevant to take into account that this hydrodynamic mode relaxes at rates following a square-law of the modulus of scattering vector q :

$$\frac{1}{\tau_{F.C.}} = D_{\phi\phi} \cdot q^2 \tag{1.6}$$

where $\tau_{F.C.}$ is the relaxation time of the Fischer cluster, $D_{\phi\phi}$ is a sort of apparent diffusion coefficient and $q = |\mathbf{q}| = (4\pi n_i/\lambda_0) \cdot sin(\theta_s/2)$. The autocorrelation function obtained in DLS (Dynamic Light Scattering) is a single exponential.

Some groups attribute this mode to the presence of defects in the amorphous liquid state originated from the topological insufficiency of tetrahedra to fulfill the real space [46]. These calculations found clusters with size in the order of 100 - 200 nm, which is in full agreement with the experimental values found [46].

Apart from these modes related to the intrinsic nature of glasses and high molecular weight materials, polymers naturally show modes related to the solid state as sound waves of different wave lengths as phonons, shear waves, compression waves, longitudinal and transverse waves etc. The bulk melt (in the liquid or rubbery state) displays a variety of hydrodynamic modes of different nature and physical behavior (dispersion relations). Some are propagating modes and some others are overdamped due to the high viscosities

of these systems. Examples of these modes can be found in [47, 48]. An example of dispersion relation for such a mode is:

$$\omega = -i\frac{\eta}{\rho}k^2 \tag{1.7}$$

where ω is the relaxation frequency, η the viscosity, ρ density and k the wave-vector of the mode. This is an example of a bulk overdamped mode. More about these issues and definitions relevant to surface dynamics will be introduced in section 1.2.

1.1.1.2 Empirical models

Molecular theories were not successful in fully describing and predicting the existence and the features of the glass transition in glass formers and polymeric materials and their main relaxation (the α-relaxation), fit equations and empirical models were proposed in order to describe this process in a systematic way.

Photon correlation techniques observe the relatively slow relaxational components of a system in the spectrum of scattered light [49]. Extremely fast processes including thermal diffusion of polymer chains and Brillouin modes cannot be detected [49]. By collecting the whole scattered light from polystyrene in the range of DLS, a third of the radiation is due to isotropic scattering and two thirds are related to anisotropic scattering [49, 50]. The isotropic scattering has been linked to a longitudinal stress relaxational experiment at constant longitudinal strain [49, 51–53], and the dynamic properties of this mode are determined by the relaxational components of the compressional or bulk modulus (K) and by the shear modulus (G) [49].

A main feature of the relaxation behavior of the α-relaxation is that a stretched exponential (also called KWW after Kohlrausch-Williams-Watts– similar to equation 1.19) with $0 < \beta_{KWW} < 1$ is needed to describe the autocorrelation function C obtained in DLS [54]:

$$C(t) = a \cdot e^{(-t/\tau)^{\beta_{KWW}}} \tag{1.8}$$

where $C(t)$ is the autocorrelation function, a is the contrast, t is the real time, τ is the relaxation time and β_{KWW} is the stretching parameter (also called Kohlrausch parameter). β_{KWW} describes a distribution of relaxation times. For polymers as polystyrene and cis-polyisoprene, $\beta_{KWW} \approx 0.4$ [28, 49, 54] and it is always independent of temperature [28].

The α-relaxation was long ago measured in bulk polystyrene by Depolarized Dynamic Light Scattering (DDLS) by Patterson [54] (what corresponds to the above mentioned two thirds of the overall scattered light, *i.e.*, the anisotropic scattering). The autocorrelation functions obtained were not single exponentials, *i.e.*, they did not show a single decay time of a single exponential function, but the α-relaxation appeared to have a distribution of relaxation times. A stretched exponential having stretching parameter $\beta_{KWW} \approx 0.4$ was needed to fit the experimental autocorrelation functions. This distribution of relaxation times delivering $\beta_{KWW} \approx 0.4$ is experimentally observed for a variety of systems and can be measured by different experimental techniques as DLS, BDS, etc. Other values for the stretching parameter are possible tough.

Another feature of the α-relaxation is that its relaxation times are, in the range accessible to DLS, always q-independent at a given temperature, *i.e.*, it is not related to diffusional or translational processes within that range of **q**-vectors observed in those DLS experiments (a more detailed view of q-dependence is given in section 1.2 and Chapter 2.1). This relaxation was then related to the orientation fluctuations of chain units.

Finally, a plot of the relaxation times, τ_α, as a function of temperature, displayed as -log(τ_α) *vs.* 1000/T (normally called Arrhenius plot or activation plot) delivers a curve that can be conveniently fitted by the so-called Vogel-Fulcher-Tamman-Hesse equation (VFTH or just VFT) instead of the linear[1] Arrhenius type. The Arrhenius equation is given by:

$$\tau(T) = \tau_0 \cdot exp\left(\frac{-E_a}{RT}\right) \tag{1.9}$$

or alternatively the equation may be expressed as:

$$\tau(T) = \tau_0 \cdot exp\left(\frac{-E_a}{k_B T}\right) \tag{1.10}$$

where E_a is the activation energy, R is the universal gas constant and k_B is the Boltzmann constant.

The VFT has several equivalent expressions [29]:

$$\tau(T) = \tau_0 \cdot exp\left(\frac{B}{T - T_0}\right) \tag{1.11}$$

[1]The Arrhenius curve is just linear in an activation plot. Otherwise it is an exponential function of temperature.

$$\tau(T) = \tau_0 \cdot exp\left(\frac{DT_0}{T - T_0}\right) \tag{1.12}$$

$$\tau(T) = \tau_0 \cdot exp\left(\frac{f}{T - T_0}\right) \tag{1.13}$$

where, τ_0, B, D, f and T_0 are constants; f is called the "fragility" of the liquid, and it is a measure for the deviation from the Arrhenius law, *i.e.*, the bending of the observed experimental curves.

This kind of behavior of the relaxation times from the α-relaxation with temperature is also found for the viscosity as a function of temperature in rheology experiments, where the shift factors, a_T, also follow the same type of curve, but there the fit equation is normally called Williams-Landel-Ferry (WLF):

$$log(a_T) = \frac{-C_1 \cdot (T - T_r)}{C_2 + (T - T_r)} \tag{1.14}$$

where T_r is the reference temperature at which the master curve is taken and C_1 and C_2 are universal constants if $T_r = T_g$. Their values are $C_1^g = 17.44$ and $C_2^g = 51.6$ [25]. Such equations were found to apply in the temperature range $T_g < T < T_g$+100 °C [25].

In 1965 Adam and Gibbs developed a theory that relates the relaxation times with the configurational entropy (S_c) and the temperature of viscous liquids [55]. They suggested that for densely packed liquids the conventional transition state theory for liquids, which is based on the notion of single molecules passing over energy barriers established by their neighbors, was not adequate to describe these materials. They proposed that, viscous flow occurs by increasingly cooperative rearrangements of groups of particles called CRRs (cooperative rearrangement regions). It was supposed that each CRR was acting independently of other such groups, but the minimum size of such a group was temperature dependent. The relationship between the minimum sized group and the total configurational entropy of the liquid delivers the Adam-Gibbs equation (AG):

$$\tau(T) = \tau_0 \cdot exp\left(\frac{C}{TS_c}\right) \tag{1.15}$$

It has been shown that the VFT equation is mathematically equivalent to the WLF equation [56] and to the Adam-Gibbs model (AG) [57] if the

temperature dependence of the configurational entropy ($S_c(T)$) is taken into account. Other equations are also equivalent to those ones as the equation proposed by Cohen and Turnbull [58] that is equivalent to the empirical formula based on free volume proposed by Doolittle in 1951 [59]. This means all these equations are mathematically equivalent and are a trial to describe the features of viscous liquids in the same way, *i.e.*, they can all be derived based on the empirical free volume equation [25] primary proposed by Doolittle:

$$\eta(T) = a \cdot exp\left(\frac{b}{f_v}\right) \tag{1.16}$$

where a and b are constants and $f_v = V_f/V$, the fractional free volume.

The real behavior of viscous and viscoelastic liquids deviates from the VFT/WLF universal formulas in the range of extremely high or extremely low temperatures as summarized by McKenna [60]. Actually, the widespread belief that glasses cease to flow under T_g seems to be equivocal. In this work McKenna collected data for polystyrene in a broad range of temperatures from several groups and, it turned out that the actual behavior of viscous materials diverges from the VFT for extremely high and extremely low temperatures (in other words, the VFT cannot "bend" enough to fit the α-relaxation times or the viscosity on the long range temperature scale). This means that the nature of the glass transition is not that predicted by the VFT, *i.e.*, there is no T_0 temperature, or "Vogel temperature" at which the material freezes completely. Consequently, as the VFT, WLF, Adam Gibbs and some other less used fit equations are all equivalent to each other, all these models fail to fully explain the nature of glasses in a broad range of temperatures. Hence, these equations are just convenient fit functions that approximately describe the behavior of the α-relaxation or the viscosity in glasses within a certain range of temperatures.

As pointed out before, the α-relaxation shows a distribution of relaxation times characterized by $0 < \beta_{KWW} \leq 1$ (being $\beta_{KWW} \approx 0.4$ for a variety of polymers). A reasonable explanation for this characteristic of the glass transition is given by the main idea behind what exactly happens at the glass transition, and the nature of the α-relaxation. It has been thought for many years that the α-relaxation is a large scale conformational rearrangement of the main chain backbone [15, 25] involving long range cooperative thermal motions of individual chain segments [25]. The hindrance of these "micro-Brownian" motions can be described in terms of frictional or viscous forces, resulting from the interactions of the moving chain segments with their neighboring molecules and between segments of the same molecule [25].

These molecules have an intrinsic relaxation, *i.e.*, the chains change their conformations in given rates that are temperature and probing rate dependent. It is important to note here that external forces applied to probe the system should be small enough in order to rely on being within the linear response regime.

Theories describing the α-relaxation as being the relaxation of segmental conformations involve the solution of diffusion equations in multidimensional chain space (fractal dimensions) and yield results involving distributions of relaxation times instead of a single relaxation time. For the same reason the stretching exponential parameter is expected to be in the range $0 < \beta_{KWW} \leq 1$, more precisely $\beta_{KWW} \approx 0.399$ as normally found in accurate experiments [28, 54] ($\beta_{KWW} = 1$ indicates a unique relaxation time, while $0 < \beta_{KWW} < 1$ stands for a distribution of relaxation times). The nature and physical meaning of the stretching parameter, β_{KWW}, also called Kohlrausch parameter is a 165 year old problem, considered by some scientists as one of the most intriguing and important problems in contemporaneous physics [61, 62]. Before introducing this problem, it is of valuable interest to show the simple derivation of the KWW equation, and the nature of the phenomena behind it. While treating the problem of decay of residual charge in Leyden jars, Kohlrausch found that this decay was not single exponential, and that the relaxation rate decreases with time, following a power law function:

$$\frac{dQ(t)}{dt} = -\gamma(t) \cdot Q(t) \tag{1.17}$$

where $\gamma(t)$ is the relaxation rate and decreases with time following a power law:

$$\gamma(t) \propto t^{-(1-\beta)} = \frac{1}{t^{1-\beta}} \tag{1.18}$$

by integrating equation 1.17 one finds:

$$Q(t) = Q(0) \cdot e^{(-t/\tau)^{\beta}} \tag{1.19}$$

that is exactly the form of the well known stretched exponential or KWW, equation 1.8. Kohlrausch found the value $\beta = 0.43$ for this specific problem.

Phillips [61, 62] found that the physical meaning of the stretching parameter is related to the fractal dimension at which the relaxation process is taking place and, is simply given by:

$$\beta = \frac{d}{d+2} \tag{1.20}$$

where d is the dimensionality of the configuration space at which the micro-Brownian motion occurs [61, 62].

The following question arises: Why does the α-relaxation of the glass transition show relaxation decays with a stretching parameter $\beta_{KWW} = 0.399$ for a variety of polymers? What is the dimensionality, or in other words, the fractal dimension of the glass transition? Why do different kinds of polymers, show the same stretching parameter, *i.e.*, the same segmental relaxation behavior? What do these materials have in common? Why polymers such as polystyrene or cis-polyisoprene have the same α-relaxation characteristics, even though their chemical structure is completely different?

A non-understood characteristic of the α-relaxation in glass formers: when studying the α-relaxation in different glass forming systems, where distributions of relaxation times are obtained, experimental relaxation data can be well described by a correlation function with the form of equation 1.19:

$$C(t) = a \cdot e^{(-t/\tau)^{\beta_{KWW}}} \tag{1.21}$$

Some specific values of stretching parameter, β_{KWW}, repeat for materials of completely different chemical nature. One of these values, that is the same for polystyrene, cis-polyisoprene and others, is $\beta_{KWW} = 0.4$, and is independent of temperature [28]. Why this happens? These questions remained unsolved so far, and their answer would bring a deeper understanding about the α-relaxation and, therefore, the glass transition itself.

The nature of the phenomena described by stretched exponential functions was introduced while deriving the stretched exponential function. The stretching parameter β_{KWW} is related to d, where d is the dimensionality of the configuration space in which the micro-Brownian motion occurs [61, 62]. Considering that one of the common features of glasses of completely different chemical nature is that they are formed by random walks, let us take this as a starting point. The mathematician Benoit Mandelbrot showed that in average a 2-dimensional random walk has the fractal dimension $d \approx 1.33$ [2]. By substituting this value in equation 1.20, one finds:

[2]Note that $R \approx N^{1/2}b$, where $D = 1/2$ is the one-dimensional fractal dimension of random walks [33], while $D = 1.33$ is the two-dimensional fractal dimension of a random

$$\beta = \frac{1.33}{1.33 + 2} \approx 0.399 \tag{1.22}$$

that is exactly the searched stretching parameter for the α-relaxation.

Could it be the reason for the well known value found for the stretching parameter in several glass former materials? Is the tetrahedral symmetry of these systems the reason for these relaxation characteristics? If so, then more attention should be brought to this issue since the glass transition in itself is a topic of major importance in our times.

Systems where other stretching parameters are involved should show different types of dimensionality for the micro-Brownian motions, likely because different numbers of chain segments are involved in the relaxation process. The normal mode however, shows stretching parameter larger than 0.5 and increases with temperature [36]. Does it mean that the chain conformation, or more precisely the number of segments participating in this relaxation is dependent on temperature? If so, this changes our classical view of the reptation motion itself and brings another view to the chain self-diffusion within the polymeric mass.

1.1.1.3 Open questions concerning the glass transition in bulk

The glass transition is one of the most intriguing open questions in the field of condensed-matter physics. It is characterized by a strong slowing down of the dynamic relaxations (except for the localized modes) in glass-former materials. Here, it is important to notice that the term "glass-formers" involves a broad range of materials such as ceramics, metals, polymers, molecular glasses, ionic glasses, etc. These materials can be classified in terms of their ability to form stable glasses, the so-called "glass forming ability"(GFA). At this point several open questions are still remaining unsolved [29].

All these open questions, make the glass transition a "hard-to-solve" problem. Therefore, a full picture of the microscopic behavior of bulk glasses requires a deeper understanding of their dynamics in both, the liquid and the glassy state. It is important to point out that these general questions are related to the glass transition in bulk glass former materials in general, making it an even harder topic when confinements are involved.

The glass transition is the transition from a liquid or rubbery state at high temperatures to a super viscous, solid-like state, achieved by cooling them

walk, the same as the dimensionality of a cloud [63, 64].

under a certain temperature, T_g. Naturally, it can also be observed during heating from the glassy towards the liquid or rubbery state. This enables to introduce the scope of this work, that is to understand the broad dynamical behavior of polymers at interfaces. In this dissertation, polymer ultrathin films at interfaces were studied. In this geometry, polymer molecules are confined to distances similar to their own size. However, this is not a real confinement geometry as the molecules have degrees of freedom in the direction perpendicular to the solid surface, and also due to the dimensions related to the glass transition (about 1–4 nm) being much smaller than the films normally studied. A point that is worth to clarify is that this work does not treat the glass transition in thin films as a priority, but regards it as one part of the spectrum of relaxation found in supported polymer ultrathin films. The following sections focus on these issues and serve as background for the conclusions driven by the present work.

1.1.2 Dynamics of ultrathin polymer films

In the following, the main concepts describing polymer relaxation behavior in ultrathin films will be introduced.

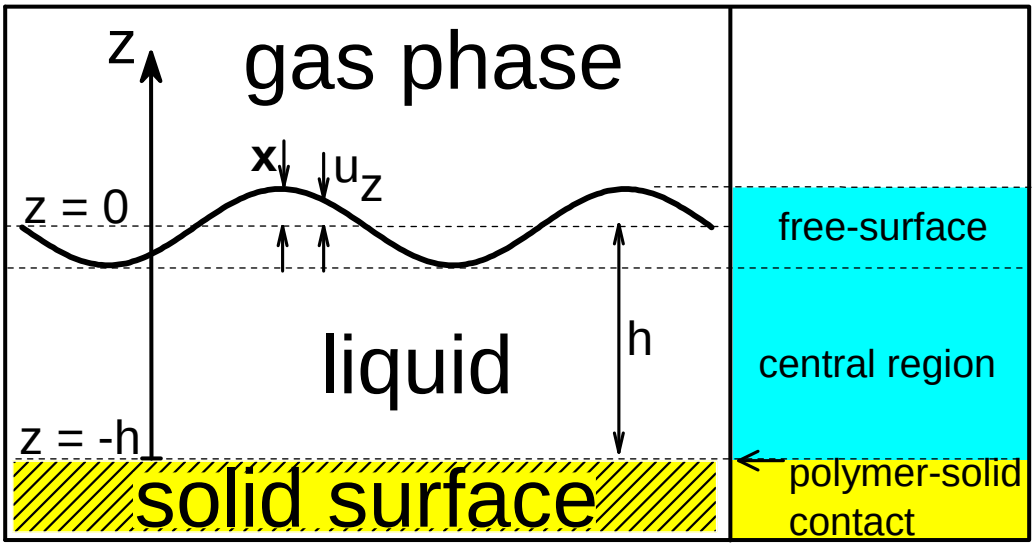

Figure 1.1: Schematics of a supported polymer film of thickness h. The three regions of importance in films are defined: free-surface, central region and the polymer-solid contact. This nomenclature is used throughout this work. The undulation of the free-surface shown, is due to thermally activated capillary waves.

The properties of polymeric materials confined to nanoscopic dimensions, *i.e.*, to the order of their radius of gyration (R_g), have been extensively studied throughout the last 20 years [4–14, 16–21, 65]. There are many ways to submit a system to confinements: to force the polymer into a given geometry as a nano-pore (as alumina nano-pore), porous silica, or other porous materials; Into layered materials as mica or layered clays (in principle the layers can be swollen and the polymers submitted into the gap region between layers); or simply to prepare an ultrathin film by methods as spin coating in which the film thickness can be well controlled and determined. The great majority of the studies related to polymers under confinements applied the thin film geometry, where spin coating was by far the most frequently used technique to produce the films.

The reason for such a big interest in polymeric films is justified by the great technological importance of thin layer systems and by the basic scientific understanding that can be obtained from such systems [1, 2]. Materials such as low molecular weight glass formers and polymers were for several years thought to display deviations from bulk properties when they are under confinements, starting with the work of Jackson and McKenna [3] culminating with the hundreds of works related to the topic. The massive number of publications on this area surely reflects its importance within the scientific community (cf. table 1.1).

One of the most contemplated properties studied in these systems is the glass transition related to the α-relaxation or primary relaxation. Although enormous theoretical and experimental efforts have been made to reach a precise view of the dynamical behavior of ultrathin polymeric films, both supported and free-standing, controversial and disagreeing results have been reported [4–14, 18–21, 65]. There is an ongoing discussion regarding to whether or not the T_g of ultrathin films suffers the influence of the confinement imposed by the nanoscopic dimensions of the films, by the presence of a solid support (due to hydrodynamics or due to van der Waals forces), or by the free-surface, *i.e.*, the interface between polymer-gas or polymer-vacuum.

In a recent set of research studies, it was shown by dielectric spectroscopy, ellipsometry, and AC-calorimetry that careful sample preparation is a crucial aspect in these studies, otherwise undesired side effects will mimic disagreements of the T_g between bulk and ultrathin films. It was reported that down to a film thickness of $h \approx 5$ nm no deviations in T_g were observed in entangled polystyrene films if a careful sample preparation and handling procedures were followed [18–22]. In fact, earlier in 2003, Efremov [23] has shown by means of ultra sensitive DSC that down to 3 nm thickness no deviations from

bulk properties could be observed in ultrathin polystyrene films.

An enhanced mobility of the dynamics of the free-surface has been reported as well [16, 17]. Here it was concluded that an increased mobility of the free-surface of polymer ultrathin films is the reason for the observed deviations of T_g in comparison to bulk. It was also pointed out that the dynamics of the free surface is Arrhenius-like. These latter authors (and others) defend the idea that the top free-surface is a liquid like layer that has a propagating effect towards the central region of the films, expanding its high mobility towards the whole film, leading the thin films to deviate their properties from the bulk material. Further, a detailed review on these ideas and some quantitative results will be presented. The theoretical approaches used to sustain all those views are introduced and finally this section will be part of the basis for the argumentation at the conclusions chapter placing the found results within this context.

1.1.2.1 A 20 year old problem: what happens to the T_g of glasses under confinements ?

As mentioned before, the glass transition temperature, T_g, in ultrathin polymer films became a matter of extreme importance and triggered a large amount of studies performed by many groups. Actually, before T_g deviations under confinements were found for polymer thin films, Jackson and McKenna [3] found T_g reduction of 8.8 °C in o-terphenyl confined into porous glasses treated with hexamethyldisilazane, with an average pore diameter of 8.5 nm. Later, Reiter found that polystyrene films with thickness $h < 8$ nm supported by a glass substrate could dewet at temperatures below the bulk T_g, concluding that the T_g of these films could be reduced in comparison to the bulk value [66].

Many groups reported declined T_g values ranging from deviations of some few degrees Celsius up to $\Delta T_g \approx 50$ °C [14] in supported films and $\Delta\, T_g \approx 70$ °C in free-standing films [6] in comparison to the T_g in bulk materials. These supported films were normally entangled polystyrene or poly(methyl methacrylate) on glass or on fused silicon, but also alternative substrates such as gold, aluminum, platinum and others were used. On the contrary, some few groups reported increased T_g values, normally for poly(methyl methacrylate) on glass or silicon. These groups concluded that the α-relaxation is influenced by the attractive forces present between this polymer and the substrate [67]. For polystyrene, most of the reports point towards a T_g reduction due to "confinements", while some few groups found an increase in T_g [68,69]. Only

a handful of groups however, found no deviations of T_g in ultrathin films, apparently under the same conditions [19–21, 23, 70, 71]. These contradictory reports brought even more attention towards this issue, reinforcing the possibility that those observed deviations of T_g could be related to artifacts and not a confinement effect on the glass transition.

An intricate aspect of this topic is the common disagreements found while comparing results obtained for films having exactly the same properties (M_w, polydispersity, thickness, substrate and so on) between different groups and even by comparing the results of the same authors throughout the years. A small collection of results about T_g fluctuations was published in [19]. Table 1.1 (based on a table from ref. [19]) shows a comparison of T_g deviations found in polystyrene. An extra column named "annealing" was added, where it is pointed out whether or not the sample was annealed. The reason for the addition of this extra column will be clarified. The irreproducibility of results became a tremendous problem, and naturally brings mistrust towards the deviations reported.

The remaining question is: why are these results in complete disagreement even within the same branch of research groups defending a diminishing glass transition temperature and sometimes an increased one? Naturally the only quite reproducible results are from groups that found no T_g shifts at all, a fact that drives a primary credibility towards these "zero-shift" results.

A. Serghei et al. [18, 65] proposed that sample preparation and handling procedures are crucial factors related to T_g disagreements. Samples not submitted to annealing before testing might have remaining solvent, that can work as a plasticizer, leading to a T_g decrease. Furthermore, they showed that if the annealing procedure is ignored, metastable states would result in a decreased T_g value. Their group also showed that annealing under air environment could lead to chain scission or cross-linking in some polymers, changing the T_g values to lower or to higher temperatures respectively.

In fact, even though these preparative effects were meticulously studied by the group of Friedrich Kremer, unfortunately many researchers ignore completely those facts and keep producing ultrathin films without caring about simple procedures as annealing. Examples of recently published works performed without taking the necessary care of sample preparation (as it was explicitly pointed out in those papers) can be found in [17, 72]. A question that can hardly be answered is: what other crucial sample preparation details are being ignored by those groups finding T_g deviations in ultrathin films?

On the other hand, some groups have performed annealing respecting

the acceptable limits of minimum annealing time, temperature, pressure, and handling during measurement time, and even though they found T_g deviations [73]. A detailed description of the annealing procedure and sample handling of the works summarized in Table 1.1 is given in Table 1.2. These tables show the irreproducibility of results of similar experiments and puts forward the idea that annealing and sample handling are important factors as pointed out by A. Serghei, but unfortunately are not the final answer for all T_g deviations observed. Some other ignored factors must be influencing the dynamics of polymer ultrathin films in the results obtained by some research groups. It seems that these factors must have a sort of random character, as sometimes their influence on dynamics are much more pronounced than others. Therefore, the source of error is not systematic when comparing different groups. This would mean that most likely random parameters commonly ignored are playing a role in this type of experiments. A possibility is an unintentional introduction of contaminants that work as plasticizers leading to diminishing T_g. Here, one should look carefully to each step of the sample preparation itself, and focus on eliminating any source of undesired contamination. A quite critical effect would be originated by using dirty containers and filters while handling polymer solutions. A hidden source of contamination is the broadly used accessory to prepare solutions: needles and syringes destined for medical applications. They are believed to be extremely clean due to their final destination, but in fact they are solely sterile (free of alive organisms), being commonly covered internally and externally with anticoagulant substances as heparin and sometimes even lubricants in order to decrease friction. Some types of syringes and needles even contain PDMS (polydimethylsiloxane) oil for this purpose.

The non-systematic addition of such molecules would surely lead to the conventionally random T_g deviations reported in thin films in comparison to bulk material, as well as to thin film dewetting, as phase separation would likely to be favorable. In thin films these effects are of great magnitude because the ratio between volume per area is quite small, therefore tiny amounts of contaminants would play a significant role. On the other hand, increased T_g values in thin films are probably originated due to cross-linking that might have taken place in some cases, where the samples were handled under oxygen rich atmospheres, or extremely high temperatures.

Table 1.1: Comparison of systems studied by several groups. The T_g deviations of PS found by different authors show the non-systematic behavior normally reported. Even direct comparisons give irreproducible behavior as G2 and G11. Few groups found zero T_g deviations, despite the fact that all films were annealed.

	author (year)	method	M_w (kg/mol)	h (nm)	ΔT_g (°C)	substrate	annealing
G1	Keddie [4] (1994)	ellipsometry	501	12	−25	H-passivated Si	annealed
			2900	12	−25	H-passivated Si	annealed
G2	Forrest [7] (1997)	ellipsometry	767	29	−12	SiO_x	annealed
G3	Ge [68] (2000)	AFM	65	20	+5	SiO_x	annealed
			6500	20	+5	SiO_x	annealed
G4	Tsui [74] (2001)	X-ray reflectometry	96	11	−15	SiO_x	annealed
G5	Fukao [75] (2001)	thermal expansion/BDS	280	11	−20	Al (cap)	annealed
			6670	12	−8	Al (cap)	annealed
G6	Efremov [70] (2004)	DSC	120	3	0	Pt	annealed
			10200	3	0	Pt	annealed
G7	Fakhraai [11] (2005)	ellipsometry	641	6	−32	Pt	annealed
G8	Ellison [76] (2005)	fluorescence	440	13	−35	glass	annealed
			3000	13	−35	glass	annealed
G9	Lupascu [69] (2005)	BDS	160	5	+10	Al (cap)	annealed
G10	Huth [71] (2006)	AC calorimetry	160	8	0 (± 3)	SiO_x	annealed
G11	Raegen [14] (2008)	ellipsometry	734	25	0	SiO_x	annealed
				6	−50	SiO_x	annealed
G12	Serghei [21] (2008)	BDS	700	12	0	Al (cap)	annealed
G13	Mapesa [20] (2010)	BDS	319	5	+1 (± 1)	SiO_x	annealed
		BDS	319	6	−1 (± 1)	Al (cap)	annealed
		ellipsometry	319	17	0 (± 2)	SiO_x	annealed
G14	Tress [19] (2010)	BDS	1103	11	−2 (± 1)	SiO_x	annealed
		BDS	749	17	+1 (± 1)	Al (cap)	annealed
		ellipsometry	1103	10	−2 (± 2)	SiO_x	annealed
		ellipsometry	749	12	−2.5 (± 2)	SiO_x	annealed
		X-ray reflectometry	319	19	−1 (± 3)	SiO_x	annealed
G15	This work (2009-2011)	kinetic SPR	1.8	8	0 (± 2)	Au	annealed
		kinetic SPR	189	20	0 (± 2)	Au	annealed
		kinetic SPR	350	4	0 (± 2)	Au	annealed

Table 1.2: sample handling procedures.

author (year)	annealing procedure	annealing temperature	annealing time	measured in
Keddie [4] (1994)	vacuum	160 °C	48h	air
Forrest [7] (1997)	atmosphere not mentioned	100–130 °C	12–20h	air
Ge [68] (2000)	vacuum (10^{-4} Torr)	170 °C	4 h	dry N_2
Tsui [74] (2001)	vacuum	150 °C–180 °C	2–5 h	vacuum (10^{-2} Torr)
Fukao [75] (2001)	vacuum	70 °C	several days	air
Efremov [70] (2004)	vacuum	140 °C	1000 s	vacuum (1–4 × 10^{-8} Torr)
Fakhraai [11] (2005)	dry N_2	120 °C	15 h	air (Linkam stage)
Ellison [76] (2005)	atmosphere not mentioned	T_g+40 °C	15min	air
Lupascu [69] (2005)	atmosphere not mentioned	120 °C	12h	N_2
Huth [71] (2006)	in situ annealed?	150 °C	before the 2^{nd} cycle	N_2
Raegen [14] (2008)	air or N_2 or vacuum	150 °C	1 hour	N_2 or vacuum
Serghei [21] (2008)	N_2	"well above the T_g"	"several hours"	N_2
Mapesa [20] (2010)	high oil-free vacuum (10^{-6} mbar)	152 °C	> 24 h	dry Ar
Tress [19] (2010)	Ar	T_g+30 °C	at least 12 h	Ar
This work (2009-2011)	dry & filtered N_2, p <1 mbar	T_g+30 °C	>24 h	dry and filtred N_2

1.1.2.2 Theories for the T_g anomalies

Throughout the years, many ideas were developed in order to explain qualitatively and quantitatively the experimental results found about the T_g of ultrathin films. One of the most spread and accepted concepts among those groups defending T_g variations in thin films is surely the so-called **"layered model"** as described in [77]. This model assumes that the chain segments close to the polymer free-surface show higher mobility (relax with faster relaxation times) than the bulk segments, "spreading" mobility to the inner part of the film, decreasing its overall T_g. Some groups defend the idea that chain ends segregate near the polymer free-surface [73,78]. Others claim that at the polymer free-surface a reduction of chain entanglement occurs [73,79]. This model also proposes that the polymer chains close to the solid surface can move faster or slower than in bulk due to different kind of interactions between polymers and solid substrates, as cited in ref. [77]. As a result, this model postulates that the overall T_g is an interplay between all those relaxations, leading the film T_g to values higher or lower than the bulk value.

Even those authors supporting this theory, agree on the lack of predictive capacity of this model regarding both qualitative and quantitative results. In fact, it is a convenient model for those groups finding T_g deviations in thin films due to its flexibility, *i.e.*, no matter what comes out of a given experiment (increase, decrease or no change at all in T_g) can be taken into account by this model.

These ideas can be easily dropped using the simple argument that air, gas as N_2 or vacuum are not good solvents for polymer chains, which will tend to be more with the other polymer chains instead of being more mobile as if they were "dissolved in air". There are no strong explanations based on serious arguments showing that the free-surface should be more mobile than those chains in the central region of the film, and that these mobility would be expanded towards the whole film thickness.

A model trying to take into account the effect of the "highly mobile" free-surface, expanding its effects towards the whole films thickness is the **"capillary wave model"**, proposed by Herminghaus *et al.* [80, 81]. This model supposes that capillary waves present on the free-surface having wavelength similar or greater than the film thickness h, could penetrate across the film thickness and affect T_g. The capillary wave relaxation predicted by Herminghaus is of the form:

$$\omega(\mathbf{q}) = \frac{E}{\eta} + \frac{F(1)\gamma|\mathbf{q}|}{\eta} + \frac{1}{\tau_R} \approx \frac{E}{\eta} + \frac{F(1)\gamma|\mathbf{q}|}{\eta} \tag{1.23}$$

where, $\omega(\mathbf{q})$ is the relaxation frequency (or relaxation rate) of the capillary wave with modulus of wave vector, $q = |\mathbf{q}|$, elastic modulus E of the polymer film, $F(1)$ is a constant depending on the thickness h and on the wave vector of the capillary wave $\mathbf{q}$, η is the viscosity of the polymer thin film, γ is the surface tension of the polymer film, and τ_R is the Rouse relaxation time for the slowest harmonic mode (p = 1) expressed in equation 1.1. Since τ_R is much higher (slower) than the capillary wave dynamics, the third term in the equation 1.23 can be neglected.

In fact, a similar mathematical form was proposed in ref. [82]:

$$\tau(q_{\|}) \approx \frac{\tau_0(q_{\|})}{1 + \tau_0(q_{\|})(\mu/\eta)} \tag{1.24}$$

that can be rewriten as:

$$\frac{1}{\tau(q_{\|})} \approx \frac{1}{\tau_0(q_{\|})} + \frac{\mu}{\eta} \tag{1.25}$$

here μ, the frequency independent shear modulus is used instead of the elastic modulus E, while both η and γ are included in $\tau_0(q_{\|})$. In fact, the constant $F(1)$ in eq.1.23 is included in $\tau_0(q_{\|})$. This equation was shown to describe well the dynamical behavior of capillary waves on viscoelastic media of arbitrary depth [82], however a coupling between capillary waves dynamics and the α-relaxation was never experimentally explicitly shown. The influence of the film thickness is taken into account in $\tau_0(q_{\|})$ and is related to hydrodynamics (no slip boundary condition) and nothing else. This topic will be discussed in detail in section 1.2.

The **"sliding chain model"** was proposed by De Gennes [79] to explain the experimental T_g reductions normally found in free-standing films. His arguments were based on the assumption that loops having two end points close to the free-surfaces could slide along their own chain contour as they do not have a huge energy barrier to overcome and therefore this barrier could be ignored. Those long loops having two ends on the free-surface, could reach the central region of the film and influence the overall T_g. For this, the film thickness should be thinner than a threshold of the order of its end-to-end vector, R_{EE}. This model predicts a linear decrease of the bulk T_g for films thinner than $h \approx R_{EE}$, so that $T_g(slide) < T_g(\infty)$ in this thickness range. The

model fails though in predicting the experimental results [77]. Another example of model trying to describe T_g anomalies is the **"percolation model"**, which considers that different domains with slow dynamics exist, and when they percolate the sample the glass transition occurs. It predicts a decrease of T_g by decreasing the film thickness to values lower than a 3D threshold, *i.e.*, the percolation length [83].

All these models intending to describe T_g anomalies found by different groups, arrive at different functional forms for $T_g(h)$ (if they are able to predict a functional form at all). Some broadly spread equations that take into account the T_g shifts have so many free parameters with no clear physical meaning, that they could basically fit anything that is possible to come out of an experiment, and therefore these equations are well appreciated by those groups finding T_g deviations. Therefore, although these equations are widely used to interpret experimental results, their outcome must be regarded as essentially arbitrary if not unphysical. In fact, I will show further evidences that the vast majority of T_g anomalies found experimentally result from insufficient sample preparation procedures. No agreements are found between these models, even though they aim to describe the very same system: a polymer film.

1.2 Surface Dynamics

Surface waves are those that exist at the interface between different media. There are many types of surface waves, being of mechanical or electromagnetic nature. Some electromagnetic surface waves used in this work, such as surface plasmons and waveguided modes will be described in Chapter 2. Examples of mechanical surface waves are Love waves (L waves) [84, 85], Rayleigh waves, which are called Lamb waves or Rayleigh-lamb waves when they are waveguided in layers [86]. These type of waves are of relevance in *e.g.*, seismology. Thermally activated capillary waves are one part of the broad spectrum of surface waves that can be found at the free-surface of a liquid or soft material [87] (as simple liquids, viscoelastic materials and so forth). In the REDLS spectrum, capillary waves are related to the major fraction of the scattered light when polymer ultrathin films are studied (thickness–h < 200 nm). The dynamic characteristics of these type of waves are driven by the experimental conditions (as **q**-vector, temperature, pressure, etc), and by the intrinsic properties of the material as *e.g.*, viscosity (η), elastic or shear modulus (E or G, respectively), density (ρ) and sur-

face tension (γ). Film thickness (h) also plays a relevant role on surface dynamics: thinner films show slower relaxations. The surface tension itself combined with thermal fluctuations is both, the cause and the responsible for the restoring force of capillary waves [88,89]. Therefore to understand the behavior of capillary waves in ultrathin films and measure them is of great interest because rich information about the material as η, G', etc, can be directly extracted from these studies. This is of importance considering that to perform rheological or any mechanical measurements in such small volumes is unlikely to be feasible. Apart from that, fundamental knowledge about liquid and soft interfaces can be obtained in relevance to adhesion, interfacial mass transport phenomena, friction and lubrication, etc. This section treats the basic theory of these surface waves and finally these predictions will be explicitly compared with the results obtained by REDLS that are presented in Chapter 3.

1.2.1 Length scales of surface waves

A liquid surface is characterized by a spectrum of height fluctuations *e.g.*, thermally activated capillary waves [87,88]. The origin of these displacements as well as the restoring force that keeps it constantly moving is related to the existence of surface tension [87] and thermal fluctuations in the material [89]. Density fluctuations occur inevitably in all materials even if they remain at rest for an infinitely long time, and being so the same happens to the surface tension. Under these conditions the surface of liquids and soft materials (under constant local stress due to these fluctuations) tries to reestablish the local equilibrium by minimizing the surface area and, as a result, thermally activated capillary waves are formed.

There are many kinds of surface waves other than capillary waves. A surface wave will be denoted capillary wave if it satisfies the inequality $\lambda << (\gamma/\rho g)^{1/2}$ [88] where g is the acceleration of gravity. If the waves are originated solely due to gravitational forces, the inequality $\lambda >> (\gamma/\rho g)^{1/2}$ is satisfied and therefore these waves are called "gravity-waves" [88]. As the nature of the wave motion depends upon the relation between the thickness of the liquid layer and the wavelength of the capillary wave, two regimes can be distinguished, namely surface waves ($\lambda << h$) and tides ($\lambda >> h$) [88].

1.2.2 Capillary waves in simple liquids

Surface roughness, defined as amplitude ξ of the surface waves of a simple liquid, is given by [90]:

$$\xi = \sqrt{\frac{k_B T}{\gamma}} \tag{1.26}$$

where $k_B T$ is the thermal energy, γ is the surface tension. The lateral correlation length (ζ) is given by:

$$\zeta = \sqrt{\frac{\gamma}{g\Delta\rho}} \tag{1.27}$$

where $\Delta\rho$ is the mass density differences between the liquid phase and the phase on top of it (a gas for example). For a liquid as water at room temperature, the surface roughness is about 2 Å, and the correlation length about 3 mm.

Smoluchowski (1908) was the first to predict the existence of such waves on liquid surfaces [91]. The first theoretical hydrodynamic descriptions of surface waves as capillary waves on simple liquids are almost a century old and were further developed by many others including Levich [87,88], where among other results the lubrication approximation to the Navier-Stokes is applied for the case of shallow liquids where the thickness h is much smaller when compared to both the lateral wave length $2\pi/|\mathbf{q}|$ and the viscous penetration depth $(2\nu/\omega)^{1/2}$, where $\nu = \eta/\rho$ is the kinematic viscosity [47]. The lubrication approximation however, lacks the contribution of elastic high-frequency waves in vicoelastic thin films [47].

It was experimentally shown by means of X-Ray Photon Correlation Spectroscopy (X-PCS) that, the latter well accepted theoretical description for simple liquids fails completely in describing the surface dynamics of the mixture water and glycerol [92]. Glycerol is a glass forming material and its viscosity can be tuned by varying the temperature. Instead, the description of thermal surface height fluctuations given in ref. [93] based on the linear response theory [94] gives a satisfactory description for viscous liquids of infinite thickness.

Due to the inefficiency of the theories for capillary waves in simple liquids in describing the actual observed phenomena in viscoelastic media as polymer thin films, the more complete description based on the theory of Jäckle [47], with the necessary corrections, is used in this work. An analogous derivation

of the capillary wave dynamics in viscoelastic media of arbitrary thickness was later derived by Stephan Herminghaus [81]. As both theories deliver analogous results, due to its relative simplicity the derivation given by Herminghaus will be shown.

1.2.3 Capillary waves in viscoelastic liquids of arbitrary thickness

The derivation of dispersion relations [3] for the case of surface waves in viscoelastic media of arbitrary thickness is useful because these relations can be directly compared to the results obtained by a DLS experiment as RELDS or by X-PCS. A useful theoretical model to describe the REDLS experiment should predict the relaxation time τ as a function of the wave-vector $\mathbf{q}$ of the capillary waves and the physical properties of the material as the viscosity η, surface tension γ, elastic modulus E or shear modulus[4] μ, the density ρ, the temperature T and film thickness h. Therefore a description of the following form is desired:

$$\tau = \tau(\mathbf{q}, T, \eta, \gamma, G^{'}, \rho, h) \tag{1.28}$$

For capillary waves, the derivation of dispersion relations is naturally more sophisticated than the classical Brownian diffusion case (this derivation is shown in the Appendix), but can be rather well predicted in an analogous way as the case of Brownian motion is derived (the principle for acquiring $\omega(k)$ is similar, their physics are not the same though). Next, the derivation of capillary wave dynamics in viscoelastic media of arbitrary depth as given by Herminghaus in [81] is described.

This derivation considers the viscoelastic material as a continuous medium and makes as few references as possible to the molecular structure of the film. However, implicitly, the material is considered as being formed by "parts" much smaller than the dimensions of the film, as the thickness h.

The internal strain of the film may be described by a tensor field, $\mathbf{S(r)}$, which tends to relax (if the temperature conditions are high enough), without

[3] Dispersion relations show the functional form of the function $\omega(q)$ and are of relevance in this work. A more detailed explanation about this topic can be found in the appendix.

[4] All these moduli are related to each other through the Poisson's ratio ν, which is labeled ψ by Herminghaus.

the presence of an external field. This relaxation takes place due to the self-diffusion of the molecules as:

$$\partial_t \mathbf{S} = -\omega_0 \mathbf{S} \tag{1.29}$$

where ∂_t is the time derivative [5] and ω_0 is the inverse of the slowest Rouse relaxation time τ_R (for $p = 1$, cf. equation 1.1), which is much slower than the α-relaxation at that temperature. Even for a non-entangled polymer melt (much above T_g) this frequency is much smaller than one per minute.

In this model, a single relaxation rate is considered, *i.e.*, its decay time function can be expressed by a single exponential (instead of a stretched exponential). Deviations from this simple model are included. Alternatively, $\mathbf{S}$ may decay by center-of-mass rearrangements of the molecules, in other words: flow in the polymer melt.

The spectrum of the interfacial eigenmodes for a viscoelastic polymer melt was derived earlier by Herminghaus et al in ref. [80]. This spectrum can take into account all possible boundary conditions, as slip, no-slip, for a polymer melt, or even to take into account the bulk free-surface dynamics and a free-standing film. For the present purpose just the direction parallel to the solid surface (x) and the normal direction (z) will be considered. It is convenient to define a vector potential, $\phi = (\phi_x, \phi_z)$, for the strain tensor which relates to the potential as follows:

$$\mathbf{S} =: \begin{pmatrix} \partial_x \phi_x & \frac{1}{2}(\partial_x \phi_z + \partial_z \phi_x) \\ \frac{1}{2}(\partial_x \phi_z + \partial_z \phi_x) & \partial_z \phi_z \end{pmatrix} \tag{1.30}$$

where ∂_x and ∂_z are the partial derivative with respect to x and to z, respectively. The flow field j (in units of flow), relates to the vector potential ϕ as

$$\partial_t \phi = -\omega_0 \phi + j - j\nabla\phi \tag{1.31}$$

As the aim of the present derivation is to describe thermally activated capillary waves, the amplitudes of these fluctuations are small, and therefore the non-linear term $-j\nabla\phi$ on the right side can be disregarded. Just linear terms will be kept.

[5] Herminghaus uses in his derivation $\partial_t f(t)$ instead of the common notation $\frac{\partial f(t)}{\partial t}$. Here, for this derivation, his notation is used.

By combining standard linear theory of elasticity [95] and hydrodynamics [96], in the limit of small Reynolds number, the force balance becomes

$$\eta \Delta j = \nabla p - \frac{E}{2(1-\psi)} \Delta \phi \tag{1.32}$$

where E is the Young's modulus, ψ the Poisson's ratio, p is the pressure field, and η is the viscosity. Herminghaus here assumes the liquid to be incompressible, therefore $\psi = 0.5$. This assumption neglects density fluctuations, considering that the only relevant fluctuations are that of strain. The equation of motion is obtained by combining equations 1.29 and 1.31:

$$\left\{ \partial_t + \omega_0 + \frac{E}{\eta} \right\} \Delta \phi = \frac{\nabla p}{\eta} \tag{1.33}$$

here, for supported films, the free-surface is considered to be at $z = 0$ and the polymer-solid contact at $z = -h$, where h is the film thickness. For such a system, equation 1.33 has harmonic solutions of the form

$$\phi = \begin{pmatrix} f(z) \\ g(z) \end{pmatrix} \cdot \exp(iqx - \omega t) \tag{1.34}$$

Considering the boundary condition in which the tangential stress at the free-surface is zero ($f'(0) = 0$), one gets

$$g(z) = (1 - \alpha q z) e^{qz} + (2\alpha - 2\beta - 1 - \beta q z) e^{-qz} \tag{1.35}$$

where α and β are functions of wavenumber q and film thickness h. As mass conservation is considered, $f(z) = ig'(z)/q$.

From the balance of forces at the substrate one obtains:

$$[(\omega_0 - \omega)\eta + E] f'(-h) = (\omega_0 - \omega)\kappa f(-h) \tag{1.36}$$

where κ is the coefficient of sliding friction. By considering a generalized form for the extrapolation length given in ref. [97],

$$L = \frac{2\eta}{\kappa} - \frac{2E}{(\omega - \omega_0)\kappa} \tag{1.37}$$

and as the solid-substrate is impenetrable ($g(-h) = 0$), follows that

$$2\alpha = \frac{e^{2qh} - 2qh + 3 + Lqh(e^{2qh} - 1)}{e^{2qh} + (qh-1)^2 + Lqh(e^{2qh} + qh - 1)} \tag{1.38}$$

and

$$\beta = \left(\frac{\alpha[qh(L+2) - 1] + 2}{Lqh + 1}\right) e^{-2qh} \tag{1.39}$$

If there is no friction at the surface, *i.e.*, if complete slip boundary conditions are applied ($\kappa = 0$), then $\beta = \alpha \cdot exp(-2qh)$ and

$$\alpha(q) = \left(\frac{1}{2}\right) \frac{e^{2qh} - 1}{e^{2qh} + qh - 1} \tag{1.40}$$

These modes are exactly the same as the symmetric modes for the case of a free standing film of thickness $H = 2h$. However, if the film sticks to the substrate, *i.e.*, considering no-slip boundary condition, $f(-h) = 0$, then $\beta = [\alpha(2qh - 1) + 2]exp(-2qh)$, and

$$\alpha(q) = \left(\frac{1}{2}\right) \frac{e^{2qh} - 2qh + 3}{e^{2qh} + (qh-1)^2} \tag{1.41}$$

In order to get the capillary wave mode spectrum, the additional boundary condition $p = -\gamma \partial_{xx} \zeta(x,t)$ is taken at the free-surface, where $\zeta(x,t)$ is the excursion of the latter, and γ is the surface tension. It turns out that

$$2\omega(q) = \omega_0 + \frac{E}{\eta} + \frac{\gamma q F(qh)}{\eta} \pm \sqrt{\left(\omega_0 + \frac{E}{\eta} + \frac{\gamma q F(qh)}{\eta}\right)^2 - 4\omega_0 \frac{\gamma q F(qh)}{\eta}} \tag{1.42}$$

where $F(qh) = \frac{\alpha - \beta}{\alpha + \beta}$. As the Rouse relaxation rate is much smaller than the capillary wave dynamics ($\omega_0 << \omega(q)$), one arrives at the simplified form

$$\omega(q) = \omega_0 + \frac{E}{\eta} + \frac{\gamma q F(qh)}{\eta} \tag{1.43}$$

as a good approximation for describing capillary wave dynamics on systems that can be compared to the here made assumptions. For the part inside the square root in equation 1.42, the frequency of the capillary waves for all q values are much smaller than the Rouse relaxation and therefore will be not taken into account.

Equation 1.43 is similar to equation 1.44 neglecting ω_0:

$$\frac{1}{\tau(q_{\|})} \approx \frac{1}{\tau_0(q_{\|})} + \frac{\mu}{\eta} \tag{1.44}$$

where

$$\tau_0(q_{\|}) \approx \frac{2\eta[cosh^2(q_{\|}h) + q_{\|}^2h^2]}{\gamma q_{\|}[sinh(q_{\|}h)cosh(q_{\|}h) - q_{\|}h]} \tag{1.45}$$

here $q_{\|}$ is the component of the wavevector $\mathbf{q}$ parallel to the free-surface. In equation 1.44, the Rouse frequency ω_0 is ignored for being much smaller than the other terms.

Equation 1.44 was derived in ref. [82] from the theory delivered by Jäckle in ref. [47], in spite of the fact that Herminghaus considers the Young modulus E in the second term of equation 1.43, while in equation 1.44 the frequency independent, real part of the shear modulus, μ is taken.

This confusion might be originated at the step where the Poisson's ratio appears in equation 1.32. If the minus sign in the denominator is taken as a plus signal, then:

$$\frac{E}{2(1+\psi)} = G \tag{1.46}$$

It is important to notice that μ is the storage modulus G' at infinite (or very high) frequencies. G' is the real part of the shear modulus G. At very high probing frequencies, polymer liquids exhibit a solid response, with storage modulus G' independent of frequency and equal to the glassy modulus G_g [33]. Common values of the glassy modulus of polymers are of the order 10^9 Pa [33]. The glassy modulus describes the linear elastic response of polymers at temperatures below their T_g [33]. The physical reason that the liquid's response in high frequencies is similar to that of the glass is that the monomers and even smaller parts of monomers, when the polymer is in the liquid state, do not have time to relax stress under high frequencies [33].

Since for an incompressible melt $\phi = 0.5$, it is possible to visualize from equation 1.46 that

$$E = 3G \tag{1.47}$$

therefore a factor of 3 is expected between the corresponding terms in both equations. Another error that the derivation from Herminghaus leads to is the frequency independence of the elastic contribution on the dynamics of capillary waves.

Finally, some corrections have to be made to both derivations. Herminghaus equivocally used the Young modulus E in equation 1.43 instead of the shear modulus G. Jiang *et al.* [82], arrived at the correct dispersion relation (equation 1.44) using the shear modulus instead of the Young modulus, but they equivocally assumed that the frequency of capillary waves in polymeric films is always very high, leading to the use of the frequency independent shear modulus μ instead of $G'(\omega, T)$. Therefore the correct dispersion relation for capillary waves in viscoelastic media of arbitrary depth should have the form:

$$\frac{1}{\tau(q_{||})} \approx \frac{1}{\tau_0(q_{||})} + \frac{G'(\omega, T)}{\eta} \tag{1.48}$$

From equation 1.48 one finds the following asymptotic behaviors:

- if $\tau_0(q_{||}) << \eta/G'$, $\tau(q_{||})$ is reduced to $\tau_0(q_{||})$, the purely viscous model used in ref. [98] to describe a free-surface without elastic effects [82].

- In the limit when $\tau_0(q_{||}) >> \eta/G'$, $\tau \approx \eta/G'$, which is the manifestation of viscoelasticity [82]. In this case the relaxation times are $q_{||}$ independent! This happens, *e.g.*, at low q values.

Note that the α-relaxation in the bulk is also $q_{||}$ independent and is visible in the depolarized DLS spectra. Therefore, one has to be careful when judging to have measured the α-relaxation simply because the dynamics observed reveals to be q-independent.

1.2.3.1 Scattering from surface waves

The theoretical description of scattering from capillary waves needed for these studies are introduced next.

The measured time-correlation function from thermally activated capillary waves measured by REDLS in any system can be compared to the correlation function delivered by X-PCS, which is described as a combination of heterodyne and homodyne terms [92]:

$$G(q,t) = \alpha Re\{G_1(q,t)\} + \beta G_2(q,t) + \gamma \tag{1.49}$$

where α, β and γ are q-dependent but time-independent functions [6]. In the case of REDLS the reference signal is much greater than the diffuse scattered signal, so the equation 1.49 is dominated by the heterodyne term G_1.

The heterodyne time-correlation function (G_1) obtained from thermally activated capillary waves can be described by [82, 92]:

$$G_1 = a \cdot e^{(-t/\tau)} \cdot \cos(\omega_p t) \tag{1.50}$$

The effect of gravity has to be negligible [92], which is the case for thermally activated capillary waves. Indeed, a function of this type can picture all the features of the experimental correlation functions obtained by REDLS. This form of G_1 (Figure 1.2 A1) is derived from the fact that its Fourier transform, the power spectrum $S(\omega)$ [99], is composed by two Lorentzians, cf. Figure 1.2 A2. When the propagation frequency of the wave (ω_p) goes to zero, G_1 becomes a single exponential and the power spectrum becomes the overlapping of both Lorentzians centered in $\omega_p = 0$, which in general is considered as a single Lorentzian [82]. Surface dynamics depends on the film thickness and since polymer thin films have some degree of roughness and imperfections considerably higher than that of simple liquids, an effective height h is taken leading to a distribution of relaxation times (corresponding to different localized thicknesses). In order to take this into account, a stretching parameter β_{KWW} is added to the single exponential above:

$$G_1 = a \cdot e^{(-t/\tau)^{\beta_{KWW}}} \cdot \cos(\omega_p t) \tag{1.51}$$

Equation 1.51 shows that if the propagation frequency $\omega_p = 0$, *i.e.*, if the wave is overdamped (non-propagating), the obtained time-correlation function will be reduced to a stretched exponential with relaxation time τ and contrast a (cf. simulation in Figure 1.2 C1). Experimentally, it is normally observed that for smooth surfaces the stretching parameter $\beta_{KWW} \approx 1$ (single-exponential). For propagating capillary waves ($\omega_p > 0$) the heterodyne time-correlation function is expressed by the stretched exponential modulating the cosine term, which fluctuates between $-1a$ and $+1a$ (if the baseline is taken as being zero, Figure 1.2 A1 and B1).

Entangled polymers at moderate temperatures (few degrees Celsius above their T_g) show higher viscosity than low molecular weight materials in the

[6] G_1 and G_2 are the heterodyne and the homodyne autocorrelation functions defined in the Chapter 2.

liquid state, and therefore, the nature of the capillary waves in polymeric systems is normally overdamped. This can be seen from measured correlation functions in ref. [98] and [82] (the same is valid for the oligomers of Styrene here studied as *e.g.*, PS 1821 g/mol). The transition from propagating to overdamped behavior in low molecular weight liquids has been studied in ref. [92], showing that by decreasing the viscosity of the mixture water-glycerol, propagating capillary waves exist (thus, $|\omega_p| > 0$ and the effect of the cosine term in the time-correlation function can be observed).

For the overdamped case, $\omega_p = 0$, is actually centered at the laser frequency, ω_{laser}, and was arbitrarily centered at zero. $\Gamma = 1/\tau$ is the relaxation rate, or more precisely, the inverse of the relaxation time τ obtained in REDLS [7].

Fourier transforms: as for the derivation of the theory of capillary waves from Jäckle [47], the power spectrum, $S(\omega)$ is needed, Figure 1.2 shows both, autocorrelation functions and their corresponding power spectra. The power spectrum is measured by spectroscopy techniques, such as interferometry, therefore to know what to expect from these spectra is of relevance. The power spectrum is mathematically described as [99, 100]:

$$S(\omega) = \frac{a}{\Gamma}\left[\frac{\Gamma^2}{\Gamma^2 + (\omega - \omega_p)^2} + \frac{\Gamma^2}{\Gamma^2 + (\omega + \omega_p)^2}\right] = \frac{a}{\Gamma}\left[\frac{2\Gamma^2(\Gamma^2 + \omega_p^2 + \omega^2)}{(\Gamma^2 + \omega_p^2 - \omega)^2 + 4\Gamma^2\omega^2}\right] \tag{1.52}$$

[7] Some spectroscopic methods as Fabry-Perot interferometry deliver $S(\omega)$ instead of G_1 [99].

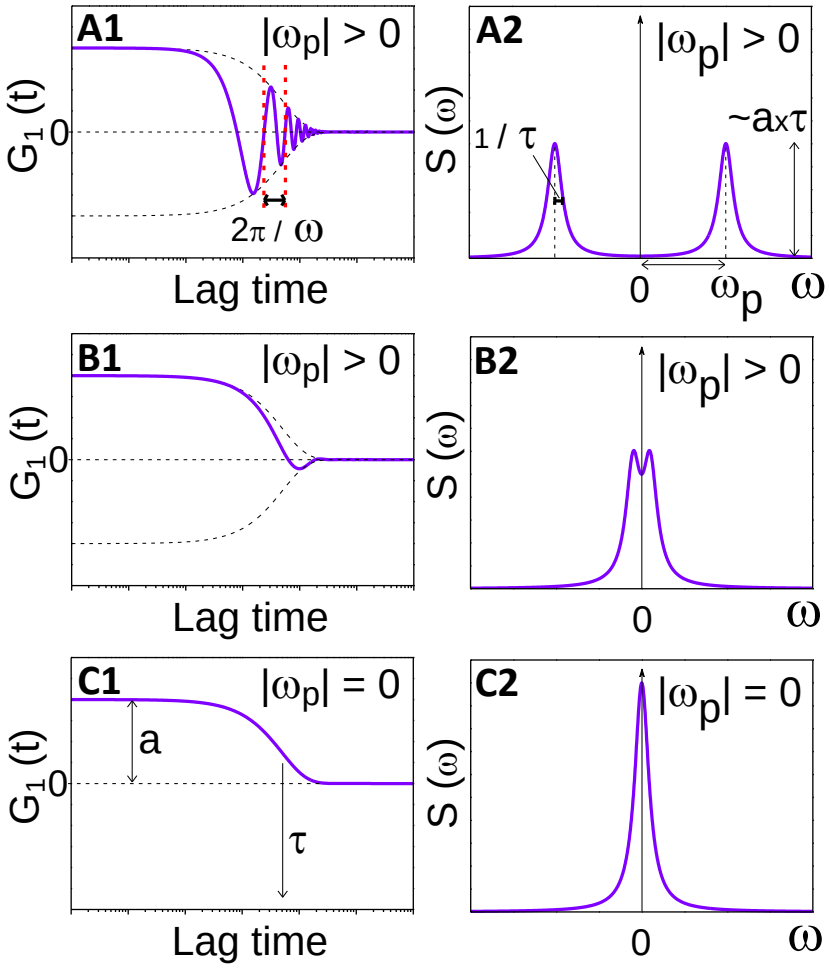

Figure 1.2: **A1**, **B1**, **C1**: Field autocorrelation function, G_1, expected from REDLS for propagating and non-propagating capillary waves. The propagating modes ($|\omega_p| > 0$) show the effect of the cosine term in the correlation function (**A1** and **B1**). The overdamped capillary waves ($|\omega_p| = 0$) show single exponential decay (**C1**). The higher the propagation frequency, $|\omega_p|$, the higher the "waviness" in such curves, deviating from the exponential decay (**C1**). **A2**, **B2**, **C2**: The power spectrum is a sum of two Cauchy–Lorentz distributions (Lorentzians). Propagating capillary waves ($|\omega_p| > 0$), exhibit two Lorentzians, shifted from the origin by a factor $\pm\omega_p$ (**A2**, **B2**). The half-width at half-maximum (HWHM) is the inverse of the relaxation time, $1/\tau$ (sometimes called relaxation rate Γ). For overdamped capillary waves ($|\omega_p| = 0$), it is centered at the original laser frequency plus a broadening due to relaxation (in the example it is centered in zero by subtracting the laser frequency), cf. **C2**.

1.2.3.2 Propagating and overdamped capillary waves

Capillary waves can be propagating or overdamped [92]. The propagation frequency in simple liquids, of low damping (low viscosity) is here called ω_0, and is given by [87, 92]:

$$\omega_0 = q^{3/2}\sqrt{\frac{\gamma}{\rho}} \tag{1.53}$$

where q is the modulus of the scattering vector, γ the surface tension and ρ the material density. In Figure 1.3, ω_0 is represented by the dashed red line. In this example the q-dependence of the propagation frequency of a material with surface tension $\gamma = 0.033$ N/m, viscosity $\eta = 1000$ Pa s and density, $\rho = 1000$ kg/m^3, is simulated. Experiments performed in ref. [92] have shown that ω_0, which is the propagating frequency derived by Levich [87] does not represent the real behavior of capillary waves in a mixture of water and glycerol. For this, they used the theory of Jäckle and Kawasaki [93] and obtained:

$$\omega_p \approx \frac{2}{3} Re\left\{\sqrt{\omega_0^2 - \frac{5\eta^2 q^4}{4\rho^2}}\right\} \tag{1.54}$$

This form of the propagation frequency described quite well the experimental results in ref. [92]. Figure 1.3 shows the behavior of capillary waves at the transition from propagating to overdamped. For q-vectors higher than a specific critical scattering vector, q_c, $\omega_p = 0$, and the capillary waves become overdamped. q_c is given by:

$$q_c = \frac{4\gamma\rho}{5\eta^2} \tag{1.55}$$

Equation 1.55 shows that if the viscosity is high, the critical scattering vector, q_c, becomes extremely small. This leads to overdamped capillary waves in the experimental achievable q-range.

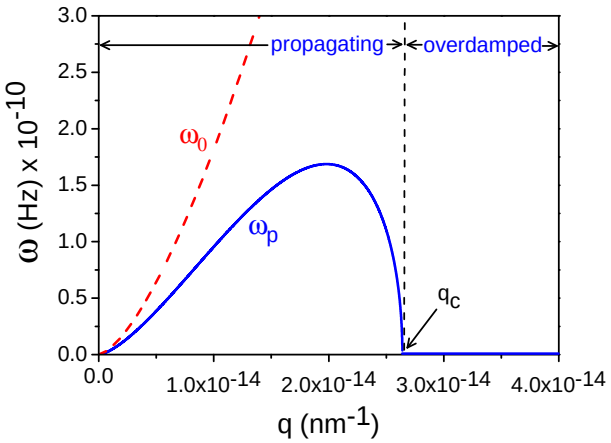

Figure 1.3: The blue curve shows the transition from propagating to overdamped capillary waves. The transition point is the critical angle q_c. The red dashed curve is the propagation frequency derived by Levich [87]. The condition simulated is similar to that of PS 1821 g/mol at T $\approx$ 93 °C: γ = 0.033 N/m, $\eta \approx$ 1000 Pa s and $\rho \approx$ 1000 kg/m^3. To study the propagating range experimentally is not possible due to the low critical angle, q_c. Therefore, this situation will deliver overdamped capillary waves in such a material.

1.2.4 Factors impacting on the dynamics of capillary waves

In order to compare directly the experimental results obtained from REDLS with the theoretical predictions for thermally activated capillary waves, it is important to know the effect of experimental conditions and material properties on the dynamics of capillary waves. Next, these concepts are developed on the basis of the capillary wave dynamics theory described previously.

1.2.4.1 q-dependence

A broad spectrum of wavelengths $\lambda_{C.W.}$ of capillary waves exists on a liquid or soft surface. From the **q**-dependence of $\tau(q_{\|})$ obtained in equation 1.48, one can simulate the relaxational behavior $\tau(q_{\|})$ of waves of different $\lambda_{C.W.}$, cf. Figure 1.4.

As an example, the prediction in Figure 1.4 is taken considering a viscous material with viscosity η = 1500 Pa s, surface tension γ = 33 mN/m and no elastic behavior ($G^{'}$ = 0 Pa), varying the thicknesses from 1 nm to 100 μm.

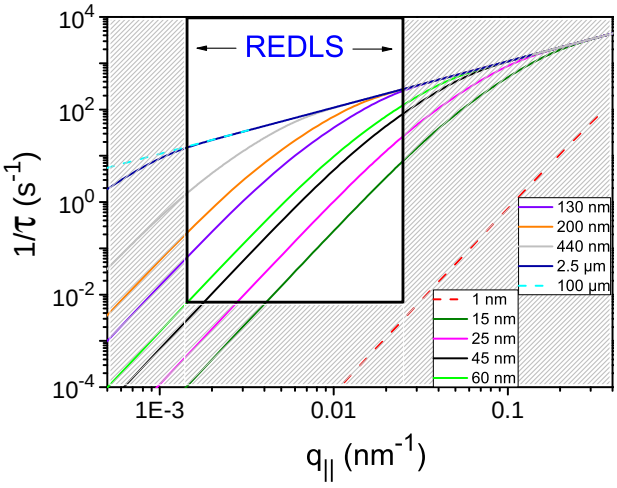

Figure 1.4: Prediction for the q-dependence of capillary waves on viscous liquids of arbitrary thickness. Here films having 1 nm < h < 100 μm are shown. Note that at very high $q_{||}$ values, no differences can be observed for the relaxation behavior of different film thicknesses. Within the REDLS window, films thicker than 2.5 μm behave equally. In this example the effect of elasticity was not taken into account ($G' = 0$). The viscosity for all thicknesses was η = 1500 Pa s. The maximum frequencies REDLS is able to resolve are not shown (in relaxation times it is $\approx$ 0.1 μs).

The REDLS experiment is able to resolve dynamic processes in the q range $1.4{\times}10^{-3}$ nm^{-1} < $q_{||}$ < $2.5{\times}10^{-2}$ nm^{-1} and relaxation times in the range 0.1 μs < τ < 1000 s. This experimental wavevector limitation comes from the wavelength available to excite surface plasmons in the here used configuration (λ = 632.8 nm was used) and the experimental geometry (very low or high angles are not achieved). The time constraint comes from the fact that for relaxation times higher than 1000 s the measurement times required are practically unachievable for acceptable statistical levels. To measure relaxation times faster than 0.1 μs would require faster correlators and better detectors. The REDLS window is indicated in Figure 1.4.

The simulation of the **q**-dependence from capillary waves shows that the thinner films relax slower than thick ones. This is a result from the no-slip boundary condition used to derive equations 1.43 and 1.44, *i.e.*, the flow profile goes to zero at the solid surface. Therefore, thinner films are expected to show capillary wave dynamics slower than thick ones due to hydrodynamics. It is crucial to note that no electrostatic potentials were assumed between the solid and the free-surface dynamics in this derivation.

Another important feature of capillary waves is that, for high $q_{||}$ values (small wave lengths $\lambda_{C.W.}$), no differences in dynamics are expected even if the thickness increases infinitely starting from films having h≈ 130 nm in this example. For lower **q** values no differences are observed in the REDLS time frame for films thicker than 2.5 μm. For films thicker than about $h = 5$ μm, no differences at all can be detected for the broad spectrum of wavelengths and amplitudes of capillary waves in a film under analogous conditions to the here simulated one.

The main idea behind these results is that capillary waves with small wavelengths do not differ in behavior in thick films $h > 130$ nm, while bigger wavelengths and amplitudes still feel the effect of the solid surface until about 1 μm. The film with thickness $h = 1$ nm shows extremely slow surface dynamics at any $q_{||}$ value, so that it cannot be seen in the REDLS time frame.

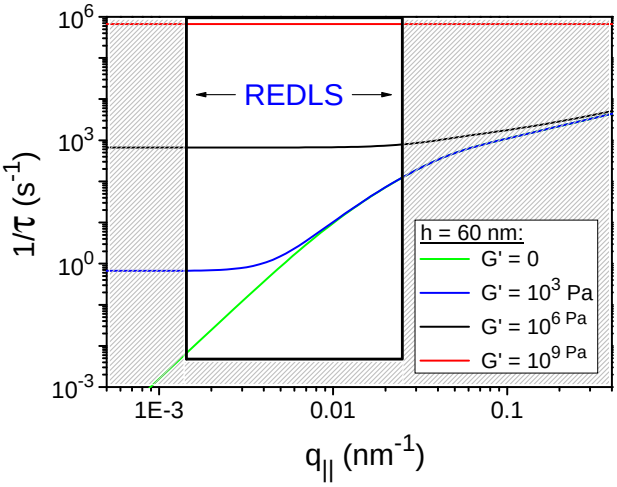

Figure 1.5: This example shows the effect of elasticity on the dynamics of capillary waves on a h = 60 nm film. Higher values of G' shift the curves towards higher frequencies, *i.e.*, the relaxation becomes faster.

If the elastic contribution is considered ($G' > 0$), then the relaxation frequency of capillary waves for this viscoelastic material will be higher than for the simple case of a Newtonian viscous liquid ($G' = 0$ Pa), as predicted by equation 1.48, cf. Figure 1.5. Therefore, if one compares two materials in a gedankenexperiment with exactly the same viscosity but one of them is viscoelastic and the other is a Newtonian viscous liquid, then the curves of the viscoelastic ones will appear shifted towards smaller times (faster dynamics), *i.e.*, the curves will shift to higher values of frequency.

1.2.4.2 Temperature dependence

One can ask what to expect from capillary wave dynamics while varying temperature. This is well predicted by the theory of capillary waves here described. As temperature increases, the viscosity $\eta(T)$ goes down following a VFT curve (section 1.1.1.2). Therefore, by considering the temperature dependence of the viscosity ($\eta(T)$) and plugging this term into equation 1.48, a first approximation to the temperature dependence of capillary wave dynamics can be obtained.

Next, one has to consider the temperature dependence of the surface tension $\gamma(T)$. For a material as PS for example, this dependence is linear in a broad range of temperatures for any molecular weight [101]. The variation of $\gamma(T)$ in a broad range of temperatures is negligible in comparison to the variation of the viscosity $\eta(T)$, in the same temperature range, due to the VFT temperature dependence of $\eta(T)$. Further, the thickness dependence of the relaxation times is considered in $\tau_0(q_{\|})$. The temperature dependence of the thickness, $h(T)$, can be neglected and h can be assumed as a constant considering the very small expansion coefficients of the polymers here studied ($\approx 10^{-3}$/K to 10^{-4}/K).

Finally, the storage shear modulus $G^{'}(\omega, T)$ for a constant thickness h has to be analyzed. Its temperature dependence at constant thickness, h, is quite unusual in thin films. While in bulk it decreases by increasing temperature, at the free-surface of thin films it decreases by increasing temperature, but at the same time, with increasing temperature, higher frequencies of capillary waves are generated, increasing the storage shear modulus, $G^{'}(\omega, T)$, at the free-surface. The final result is a competition between two opposite effects of temperature and frequency. Experimentally, it is verified that the net effect is a decrease of $G^{'}(\omega, T)$ by increasing temperature for a given film thickness. (cf. Chapter 3). This behavior is different from that reported in ref. [82], in which it is claimed that the storage shear modulus is weakly dependent on temperature.

A simulation is given in Figure 1.6, where it becomes clear that a VFT behavior should be expected for this mode. Just for comparison, the α-relaxation from bulk rheology of the oligomer PS 1821 g/mol is plotted together. The viscosity $\eta(T)$ of this oligomer PS 1821 g/mol was also considered in the calculations.

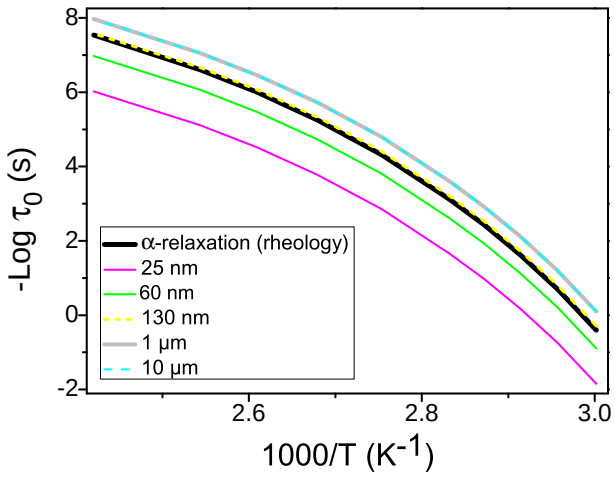

Figure 1.6: Activation-plot of capillary wave dynamics for a material with the viscosity dependence on temperature similar to PS 1821 g/mol. For this, the α-relaxation determined by rheology from this polymer was used. Thicker films relax faster than thinner ones. Films thicker than about 1 μm behave similarly. The effect of elasticity was neglected ($G' = 0$). The curves are approximately parallel shifts of the α-relaxation (or of the viscosity) in bulk material. Note that the α-relaxation is not an upper theoretical limit determining the fastest relaxation possible. For this example, a scattering angle $\theta_s = 60°$, was considered. At different scattering angles, different activation plots would be delivered.

1.2.4.3 Molecular weight dependence

By changing the molecular weight considerably, a strong impact on dynamics is expected. This is due to the molecular weight dependence of viscosity and shear modulus. The scaling laws that predict these dependences are given in section 1.1.1.1. For low molecular weight polymers (non-entangled) η scales with the first power of the molecular weight:

$$\eta_0 = \frac{\pi^2}{12}\left(\frac{\rho N_A k_B T}{M}\right)\tau_R \propto \rho M^1 \tag{1.56}$$

While for high molecular weight polymers (entangled) it scales with the power 3.4:

$$\eta_0 \propto M^{3.4} \tag{1.57}$$

At high frequencies, polymer liquids exhibit a solid response, with storage modulus $G' = \mu$ independent of frequency and equal to the glassy modulus G_g [33]. This value can be obtained for different molecular weights from rheological experiments at high frequencies (or low temperatures). This shear independent storage modulus μ was used in ref. [82]. Therefore, high molecular weight polymers show capillary wave dynamics slower than ones with small molecular weight.

1.2.4.4 Surface tension dependence

In liquid materials in general the surface tension does not vary considerably as the viscosity does. As an example, the surface tension in room temperature of a polymer as PS has values about $\gamma \approx 33$ mN/m [101] while water has $\gamma = 71.99$ mN/m [102], a factor of about two in difference. Therefore, the effect of the absolute values of surface tension on different materials does not vary much. In the outlook of Chapter 4.1 new ideas about tuning surface tension properties are given.

1.2.4.5 Thickness dependence

The thickness dependence of the dynamics of capillary waves is contained in the term τ_0 of equation 1.48. As explained before, in thinner films, capillary waves will relax slower than in thicker films, simply due to hydrodynamic effects. It no longer differs for films thicker than about 1 μm in the example of Figure 1.4.

A question that follows is: what is the effect of roughness on the dynamics of capillary waves of thin polymer melts? This problem can be seen as a polymer film with a varying thickness across the film plane-xy ($h = h(x, y)$). Here, each spot on the plane x-y of thickness h_i will show a correspondent relaxation time, τ_i. In this case, a distribution of relaxation times is expected, and the autocorrelation functions obtained by REDLS should be fit by stretched exponentials with β_{KWW} slightly smaller than one (the stretching parameter, β_{KWW}, gives the distribution of relaxation times). Smooth films are therefore expected to show $\beta_{KWW} = 1$.

1.2.4.6 Surface dependence

What is the effect of interactions between the solid substrate and the free-surface for very thin films? This problem requires to calculate the van der Waals forces between the solid surface and the very last layer of molecules at the free-surface. This is estimated as [102]:

$$f = -\frac{A_H}{6\pi D^3} \tag{1.58}$$

where f is the force per unit area, A_H is the Hamaker constant and $D = h$ in this case is the film thickness.

By considering the order of magnitude for the Hamaker constant for the supported polymer films studied here ($A_H \sim 10^{-20} J$) and the decay of the van der Waals forces with the inverse of the cubic thickness, it is simple to estimate that these forces can be neglected for the thickness range possible to be analyzed within the REDLS window shown in Figure 1.4. Thus, the only relevant impact of the solid surface on dynamics of capillary waves expected is the imposition of the no-slip boundary condition at the solid-polymer contact, therefore simply a hydrodynamic effect.

Chapter 2

Experiment

Despite the large amount of research during the last 20 years on the understanding of polymer ultrathin films dynamics, a lot of fundamental mistakes concerning the sample preparation are still remaining even in recently published works. The preparation of polymer ultrathin films seems *a priori* to be an easy task. Experiments show however that to achieve high quality supported and free standing polymer thin films requires extreme care and cleanness. This chapter will treat the basic concepts about obtaining supported thin films and how to prepare properly clean and smooth metallic surfaces for REDLS studies. This chapter will also deal with the basic concepts about the combination of SPR (surface plasmon resonance spectroscopy) and DLS (dynamic light scattering), leading to the technique named REDLS (resonance enhanced dynamic light scattering), which was the core method used in this work to study the dynamics of polymer ultrathin films at the vicinity of solid surfaces. An additionally developed technique called WEDLS (waveguide enhanced dynamic light scattering), based on leaky modes of wave guides, will be introduced and its possible future usage is put forward.

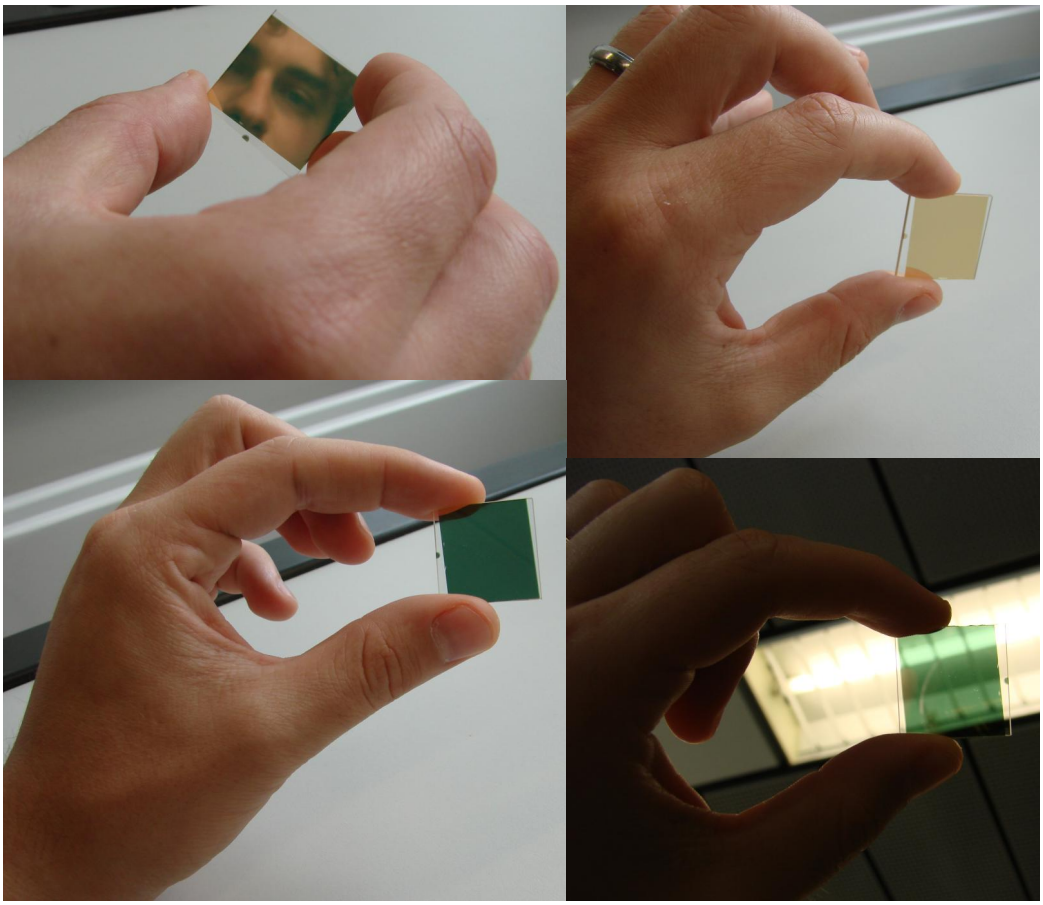

Figure 2.1: Sample on glass substrates: high refractive index glasses as LaSFN9 (n = 1.81) are covered with a 47 nm thick layer of gold, which is deposited by thermal evaporation on top of a pre-layer of chromium (1 nm thick) in order to promote a good adhesion between gold and glass. The freshly evaporated gold layers are then covered with polymer ultrathin films by means of spin-coating, and subsequently annealed. The final result is a homogeneous layered system of high surface quality.

2.1 Materials and Methods

2.1.1 Sample preparation

2.1.1.1 Metal evaporation

Smooth gold surfaces are required for a fairly good surface plasmon coupling. Apart from that, the characteristics of the polymer-solid contact should be well known to achieve an understanding of the impact of structure and roughness on the dynamics of polymer ultrathin films. In this work all glass substrates (LaSFN9 or NLAK8) were first coated with about 1 nm of chromium to achieve a good adhesion of the gold layer on the glass surface. Gold was thermally evaporated at the constant rate of 1 Å/s during the whole procedure, what delivers a final roughness (rms) of approximatelly 5 Å over an area of 2.5 μm per 2.5 μm. This value is considered to correspond to a smooth surface. Higher evaporation rates should not be used, otherwise rougher interfaces will be formed. After metal evaporation, the substrates should be kept under clean and inert atmosphere, preferably nitrogen or argon. The best choice is to proceed with the spin coating right after the metal thermo-evaporation took place.

2.1.1.2 Polymer ultrathin films by spin-coating

Some general rules have to be followed for obtaining fairly good quality (smooth and free of impurities) polymer thin films. The most important are:

- **Molecular weight:** the molecular weight should be preferentially higher than the entanglement molecular weight M_e, otherwise the necessary mechanical stability to keep the film wetting the surface in high temperatures can be hardly reached, *i.e.*, the higher the M_w, the higher the film quality in high temperatures compared to T_g. The production of stable oligomeric ultrathin films is possible though. In this case an extreme care over the cleanness should be taken since even tiny amounts of contaminants work as plasticizers decreasing strongly the film stability and its T_g. Contaminants have the same effect on the T_g of high molecular weight polymer films, but in these systems it is not always the case that small amounts of plasticizers will lead to a sample damage due to dewetting as in oligomeric ones.

- **Solvent:** for spin coating, a good solvent for the specific polymer has to be used, otherwise the polymer will not be completely dissolved producing a turbid solution, which normally can be observed by the naked eye. These concentration fluctuations normally have dimensions in the meso-scale range, deposited on the solid surface leading to extremely rough surfaces. This can be observed on PMMA thin films spin coated from a PMMA-toluene solutions. It is also evident that ultra high purity solvents have to be used for the solution preparation. The solvent chosen has to show a considerably high boiling point (normally higher than 100 °C). If this is not the case, a skin will form on the surface during the application of the solution on the solid substrate, not allowing a homogeneous drying during spinning. This leads to extremely rough films. An example is when films are produced by spin-coating PMMA dissolved in acetone. Acetone has a low boiling point (≈ 57 °C), whereas MEK (methyl ethyl ketone) another good solvent for PMMA, has a higher but still low boiling point of 79.64 °C. A good solvent for PMMA having a quite high boiling point (155.65 °C) is cyclohexanone, which is recommended for spin coating of PMMA. However, this solvent can suffer oxidation, what brings a yellow color to the solutions, if kept in ambient air atmosphere and exposure to light. For polystyrene a good choice is toluene, which has a boiling point of 110.6 °C. All PS films in this work were prepared by spin coating using a PS-toluene solution.

- **Spinning time:** as good solvents are necessary for a high film quality, it also means that the interactions between polymer and solvent are strong. Consequently, the solvent will hardly leave the polymer film completely (even under high temperature and ultra high vacuum). If the spinning time is short (less than 2 minutes), a considerable amount of solvent will remain on the film. Handling the coated surface makes this remaining solvent to flow across the film, leading to waviness in the film. This phenomenon can be observed by the naked eye if one watches thicker films under white light right after a short spinning time: Newton rings are formed and different colors appear, creating a very inhomogeneous coloration. In fact, when observed by the naked eye, a high quality film should appear to have a homogeneous color over the whole surface. Drying during spinning happens mostly due to diffusion of the solvent to the adjacent air layers and this slows down the drying process in ultrathin films. For these reasons all polymer films prepared in the present work were spun for 10 minutes at constant speed.

- **Spinning speed:** moderate spinning rates should be used in order not to have chain scission and further increase the polydispersity (speeds higher than 6000 rpm should be avoided). A general accepted number is around 3000 rpm [65]. If thinner films are needed, one should play with the concentration of polymer in the solution, rather than increasing the spinning rate.

- **Application of the solution:** the surface to be coated should be completely covered with the solution before spinning, otherwise the lateral inhomogeneity caused in the borders of the solution droplet can affect the smoothness several millimeters into the central part of the film. Therefore, applying a single droplet to the center of the substrate expecting to achieve a complete surface coverage by spinning is a common mistake.

- **Deposition time:** the solution should be carefully applied on the complete area of the solid surface (this procedure should not take more than 5 seconds), and afterwards one should wait around 5 seconds before start spinning. If a longer interval is taken between the deposition of the solution and spinning, a skin can be formed, resulting in a rough film. This systematic procedure also helps to achieve a reproducible way of preparing thin films.

- **Filtration of the solution:** dust is normally present in the polymer, solvent and in the laboratory environment. For these reasons, filtration is a necessary procedure. Some polymers form globules hard to be dissolved even under mixing for several minutes in a good solvent (as very high molecular weight polymers). Therefore, the filtration of the solution also helps to remove these clusters. In case the solutions are not dust free or contain undissolved polymer, these inhomogeneities will cause roughness and will work as centers of concentrated tension finally nucleating dewetting.

- **Filter cleaning:** another important procedure to be observed is the cleaning of the filters before filtering the solution. Filters are normally not dust free and can contaminate the solution with particles (as PTFE particles from the filter itself). For this reason the filters should be rinsed with about 10 ml of solvent and dried under clean atmosphere in an ideal case (to protect from new contamination by dust particles). In this work 0.2 μm pore size PTFE filters from Millipore were used.

- **Syringe cleanness:** plastic syringes must not be used. These syringes are normally made of semi-crystalline polymers as polypropylene, which will not easily dissolve and contaminate the solution in a considerably way, but they may contain plasticizers that can be released to the solution. Polymeric syringes may contain lubricants as PDMS oil or analogous in order to facilitate the sliding of the piston. These substances will lead to catastrophic results as phase separation and consequently to film dewetting. Of course, T_g reductions will also take place, just as it happens in bulk materials by the addition of plasticizers. In many cases the common needles for medical applications are believed to be ideal for this use due to their cleanness. In fact, those needles are sterile but often externally and internally coated with anti-coagulant materials as Heparin, which again will work as a plasticizer. Ideally, for this purpose special metallic needles and glass syringes selected for DLS should be used. The cleaning procedure of these needles and syringes is the same as the one for DLS cuvettes in hot acetone fountains.

- **Solution concentration:** high polymer concentrations (> 5 % w./w.) can make the filtering procedure impossible due to the high solution viscosity and, the formation of a skin on the film surface, leading to rough films. In general dilute solutions are used (1-2 % w./w.), with low enough intrinsic viscosity [103].

- **Surface cleanness:** impurities on the glass or metal surface (as dust or even imperfections) will lead to the formation of the so-called island effect, *i.e.*, the local induced inhomogeneity will extend its effect from the vicinities of the impurity to the range of millimeters, what can be easily observed by the naked eye. Therefore, it is clear that clean and smooth metal surfaces are crucial for obtaining high quality polymer thin films. Before depositing the metal film by thermal evaporation, the glass surface also has to be extremely smooth and clean.

- **Affinity between surface and polymer solution:** it is necessary that the polymer solution wets the surface to be coated. Otherwise a high quality polymer film will never be achieved.

- **Size of the substrate:** very small substrates are not recommended for spin coating when the here described spin coated method is applied. If the surface to be coated has lateral dimensions $<<$ 20 mm, border effects will be expanded towards the central part of the substrate so that a homogeneous film across the whole substrate will hardly be obtained.

2.1.1.3 Annealing of polymer films

A careful annealing procedure is essential in order to achieve thin films of high quality, which are as free of solvent as possible. As some polymers (as PS and PMMA [18,65]) can suffer degradation by oxidation under ambient air in high temperatures, the films should not be heated in air atmosphere, but under vacuum or some inert atmosphere as dry nitrogen or argon. After submitted to a non-aggressive atmosphere, the films can be heated to temperatures higher than T_g. The temperature should not be higher than T_g + 60 K in order not to stimulate dewetting. At high temperatures, chain scissions due to thermal degradation may take place [104–108]. UV light should always be avoided due to cross-linking and chain degradation. High vacuum should be slowly applied to prevent foaming of the film, what will be irreversible. Annealing should be performed for at least 24 hours in order to achieve a well dried film, and to reach (or to be as close as possible to) dynamical equilibrium [65].

2.1.1.4 Preparation of waveguides

As it will be further shown in section 2.1.2.3 and 4.1, thick polymer films [1] under the here used configuration, lead to the formation of waveguide systems. Waveguides have a broad application in several fields of optics. Their quality and smoothness are often critical and essential for some applications. A successful waveguide based technique named WEDLS (waveguide enhanced dynamic light scattering) [109] was developed within the framework of this project and for this specific application, polymeric waveguide films extremely stable under water were required [109], cf. section 4.1.

In general when a supported polymer film is submersed in water, it detaches from the surface, *i.e.*, it becomes free standing and, therefore, can no longer be used as a supported film. For these applications, water proof and stable waveguide films were produced. As WEDLS can also be used to study dynamics of larger polymeric systems, the WEDLS device, *i.e.*, the waveguide itself is of relevance for future studies on this issue. Hereafter the production of thick polymeric films are described.

The waveguides were prepared by spin coating a solution of PMMA (polymethylmetacrylate) M_w = 200 kg/mol, PDI≈ 1.05, with the concentration

[1] Depending on the material the minimum thickness to obtain waveguides can change, but the thicknesses are normally in the range of hundreds of nanometers or more.

of 11 % w./w., dissolved in high purity cyclohexanone. The solutions were filtered through a PTFE millipore filter (0.25 μm pore size).

Since the WEDLS measurements took place having water as add-layer, one had to care about the physical and chemical stabilities of the waveguide films. In order to achieve stable and high quality waveguide systems under these conditions, PMMA films were spin coated on gold surfaces, which were previously functionalized with 3-(4-benzoylphenoxy)-propanethiol (BPSH), annealed at 130 °C for about 24 h and finally cross-linked by applying UV radiation (λ = 254 nm) for 5 h.

These gold layers were produced by thermal evaporation on NLaK8 glass substrates at the controlled rate of 1 Å/s. The final gold film thickness was determined to be ≈ 47 nm, which was theoretically calculated to be ideal for having high coupling efficiencies in the case of p-polarized light (calculations show that using s-polarized light requires gold layers ≈ 30 nm thick). This type of calculations are explained throughout the next sections.

Right after being produced, gold covered substrates were coated with BPSH by submersion in solution for several hours (overnight) as described in ref. [110]. Applying UV-radiation (λ = 256 nm) during 5 h ensured to reach cross-linked PMMA films, which were covalently bonded to the BPSH layer [110] and thus to the gold surface. This gives the films the necessary physical and chemical stability required for this application. The PMMA films were optically isotropic as confirmed by the perfect coincident fit of the curves for s- and p-polarized light [109]. These waveguides layers were stable under water over weeks, a fact that is proven by the non-existing shift of the eigenmodes of the waveguide.

2.1.1.5 Characterization of thin films

- **Gold layer:** The roughness of the gold layer (rms) measured by AFM was smaller than 0.75 nm measured in an area of 2.5 μm × 2.5 μm. The thickness of the gold films was measured by a profilometer (Tencor P-10) and confirmed by SPR to be 47 nm ± 1 nm in all cases. This is the ideal thickness for the coupling efficiency of the surface plasmon at its resonance for λ = 632.8 nm, with polystyrene as an add-layer.

- **Polymer layer:** The films are characterized by profilometer, SPR, REDLS and in a few cases with AFM. The quality of the ultrathin polymer films can be optically determined by SPR, as well as its thickness. The thickness determined by SPR (assuming the refractive index

of bulk PS, n ≈ 1.59) agreed within the error of ± 0.5 nm with the profilometer results (Tencor P-10). The primary characterization of the thickness was done on test samples by means of a profilometer with resolution of approximately 1 nm. These films were not used in our measurements though (to be sure that no dewetting induced by the scratches will take place). Instead, films prepared with exactly the same parameters were used for our experiments with REDLS (SPR results confirmed the previously measured thicknesses from the profilometer on the primary test sample).

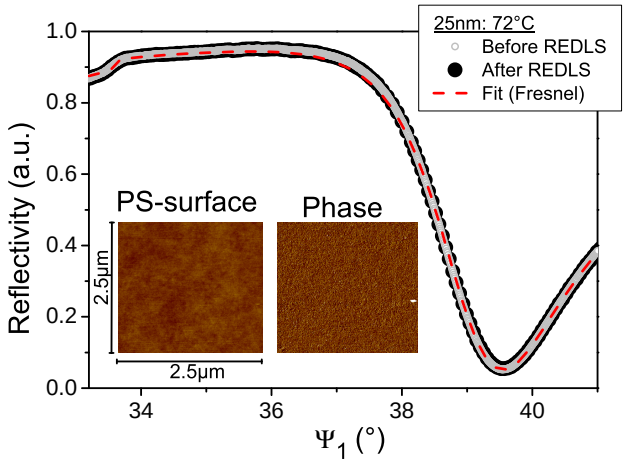

Figure 2.2: SPR was performed for all PS films before and after REDLS. The resonance curves show no shifts or change in shape after being measured at 72 °C (more than 20 °C above T_g). AFM measurements determined rms = 0.37 nm over a range of 2.5 μm × 2.5 μm for this example. The pictures above are the surface topography (left) and the phase contrast (right) for PS 1821 g/mol. This was taken after annealing under the conditions mentioned in the text. Thus, the initial roughness, rms = 0.53 nm, decreased with annealing. No dewetting was observed on the films, even in oligomeric ones (PS 1821 g/mol), in agreement with the zero-shift of the SPR resonance position and curve shape, before and after being submitted to high temperatures for considerably long times (several days in the case of the sample shown above).

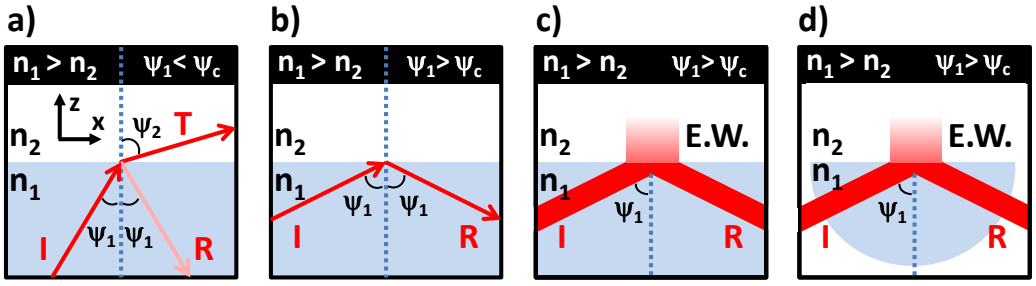

Figure 2.3: When light passes from a medium 1 (lower part (here glass), with refractive index n_1) to a medium 2 (with refractive index n_2), two situations are possible: if the incidence angle $\psi_1 < \psi_c$ part of the beam is transmitted and part reflected (a); if $\psi_1 > \psi_c$ no beam is transmitted and total internal reflection takes place (b, c and d). When light is totally reflected, an evanescent wave (E.W.) appears at the lower refractive index medium 2, at the boundary to medium 1. In both cases c) and d) the same phenomenon happens, the difference here is that in d) a half cylinder lens is the medium 1.

2.1.2 Surface Plasmon Resonance–SPR

2.1.2.1 Total Internal Reflection–TIR

To understand the characteristics of evanescent waves, first the case for evanescent waves at total internal reflection will be shown. Here, the main features can be explained and are more intuitively understood. When light passes from a medium having refractive index n_1 to another medium with refractive index n_2 (where $n_1 > n_2$), under an incidence angle ψ_1, two situations can happen:

- if $\psi_1 < \psi_c$, where ψ_c is the critical angle relative to medium 1 with respect to medium 2, then part of the incident beam (I) is transmited (T) and part is reflected (R). The transmitted beam forms an angle ψ_2 with the normal (Figure 2.3 a)). This phenomenon is called refraction and can be determined by the "Snell-Descartes law":

$$n_1 \cdot sin(\psi_1) = n_2 \cdot sin(\psi_2) \tag{2.1}$$

- if $\psi_1 \geq \psi_c$, no light is transmitted ($T = 0$), and the phenomenon of total internal reflection happens (Figure 2.3 b), c) and d)). This means

beam I is reflected, *i.e.*, I is completely converted into R. At angles higher than ψ_c however, an evanescent wave (E.W.) is formed at the medium 2, on the spot where reflection takes place, Figure 2.3 c) and d). This wave is called evanescent wave (from latin "*evanescere* = disappear") due to its evanescent character, *i.e.*, its optical field decays exponentially as far as one gets distant from the interface between both media, and vanishes at great distances.

The existence of the evanescent wave of the total internal reflection is an exigence from the Maxwell-equations, which states that an electromagnetic wave at the interface cannot change its direction of propagation abruptly, and therefore an evanescent wave has to be formed.

The wavevector of an electromagnetic wave with wavelength in vacuum λ_0 propagating in a medium with refractive index n_i is given by:

$$\vec{k} = \frac{2\pi n_i}{\lambda_0}\hat{k} \tag{2.2}$$

where $\hat{k}$ is the unity vector in the direction of $\vec{k}$. From now on, the wavevector of electromagnetic waves, $\vec{k}$, will be simplified to k. For the case of an evanescent wave of the total internal reflection, the wavevectors in both directions (x and z, cf. Figure 2.3) are given by:

$$k_x^{TIR} = \frac{\omega}{c} \cdot n_1 \cdot sin(\psi_1) \tag{2.3}$$

and

$$k_z^{TIR} = \frac{1}{i\xi} \cdot \frac{e_z}{|e_z|} \tag{2.4}$$

where ξ is the "penetration depth" or the decay length of the amplitude of the electric field, $(1/e \cdot \vec{E}_0(x,z) \approx 0.37 \cdot \vec{E}_0(x,z))$, for the evanescent wave into medium 2 and, $e_z/|e_z|$ is the canonic unity vector in the direction of z. The wavevector in z direction is complex due to its evanescent decay in this direction. The penetration depth of the field of such an evanescent wave in medium 2 is given by:

$$\xi^{TIR} = \frac{c}{\omega}\left[n_2\sqrt{\left(\frac{n_1}{n_2}\right)^2 \cdot sin(\psi) - 1}\right]^{-1} \tag{2.5}$$

The electric fields of evanescent waves of the total internal reflection (for both p and s-polarized light) can be found in ref. [111].

Depending on the direction of the electric field vector ($\vec{E}$) of the incident beam in respect to the plane of incidence, x, two relevant situations can occur: if $\vec{E}$ is contained in the x-z plane, and has a parallel component to the normal vector ($\hat{z}$) of the plane of incidence x (Figure 2.4–case a)), the polarization of light is named p-polarized (from German "parallel"), also called "TM" (transverse magnetic). If the incident beam has electric field $\vec{E}$ contained in the x-plane, *i.e.*, perpendicular to the normal vector $\hat{z}$ of the incidence plane-x, then the polarization of light is called "s-polarized" (from German "senkrecht" = perpendicular), also called "TE" (transverse electric)[2].

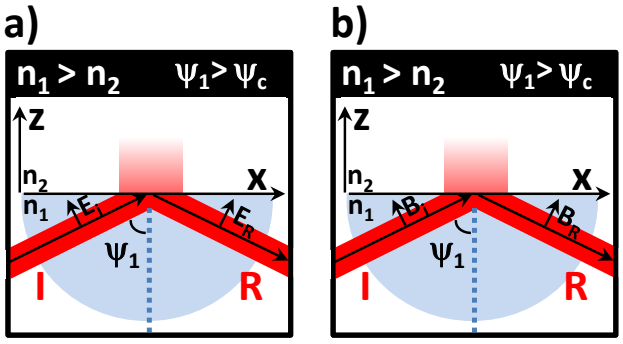

Figure 2.4: Case a): reflection of p wave (TM). Case b): reflection of s wave (TE). E_i and E_R are the incident and reflected electric field, respectively. B_i and B_R correspond to the magnetic field.

If one monitors the intensity of the reflected beam (with a photo-diode for example) as a function of incident angle ψ_1 for p-polarized light (R_p), the result is a curve as shown in Figure 2.5. Here the total internal reflection angle ψ_c can be observed. The black curve shows the case in which the beam totally reflected reaches the same intensity of the initial beam, and therefore goes to 100 % of its value (100 % ≡ 1). If one considers the reflections at the walls of the half cylinder lens, as the one in Figure 2.3 d), then part of the incident beam is lost and, therefore, the reflected beam does not reach the value 1 at total internal reflection (red curve). Here, the maximum value reached by the intensity of the beam will be named I_{max}, which is about 83 % for a half cylinder lens made out of LaSFN9 (as medium 1) and air (as medium 2).

[2]Some authors define in terms of the magnetic field, **B**. Then p-polarized light has the magnetic field parallel to the plane. Both definitions are analogous.

As both, prisms and half cylindrical lenses were used in this work (half cylindrical lenses in most of the cases), one should keep in mind that this phenomenon happened in all experiments and, therefore, at ψ_c, $R_p < 1$.

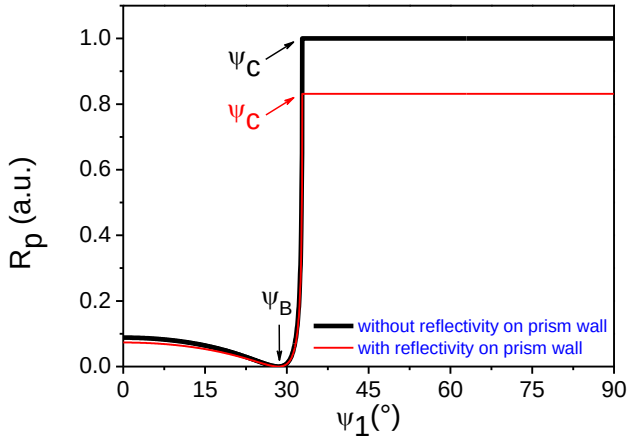

Figure 2.5: Reflectivity of a p-polarized beam as a function of incidence angle. Both curves show the phenomenon of total internal reflection (ψ_c), but the red curve considers the losses at the walls of the half cylinder lens. Therefore, $R_p(\psi_c) < 1$ when a cylinder lens (or prism) is used. ψ_B is the Brewster angle.

.

These reflectivity curves are simulated in a software called WinSpall, which can be freely downloaded from the internet[3]. This software is able to calculate reflectivity in multi-layer optical media. It is based on Fresnell equations [112, 113] and transfer-matrix formalism [114].

Figure 2.6 shows the behavior of the reflected beam and the transmitted beam (both p-polarized) with incidence angle ψ_1. Note that $I_{max} = \mathrm{T} + \mathrm{R}$, *i.e.*, when the transmission T reaches its maximum, the reflectivity R reaches its minimum. For angles higher than ψ_c, $R_p = I_{max}$ and $\mathrm{T} = 0$. There is a special angle called "Brewster angle" (ψ_B). At this incidence angle, all p-polarized light is transmitted and therefore $R_p = 0$. If unpolarized light impinges with this angle on a transparent surface, all p-polarized components are transmitted and the s-polarized components are reflected [115]. For a system composed by a half-cylinder lens of refractive index $\mathrm{n}_{lens} = 1.81$ with air on top of it ($\mathrm{n}_{air} = 1$), this angle is calculated as [115]:

[3] http://www.mpip-mainz.mpg.de/knoll/soft

$$\psi_B = \arctan \frac{n_{air}}{n_{lens}} \approx 29° \tag{2.6}$$

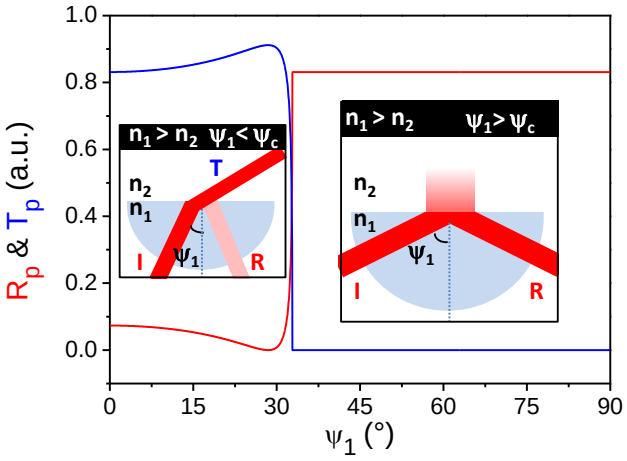

Figure 2.6: Here the reflected (red) and the transmitted (blue) beams are followed as a function of incidence angle. When R_p reaches its maximum value, T_p reaches its minimum. The sum of both is the total intensity of the incident beam, minus the effect of the reflections on the half cylinder lens wall.

2.1.2.2 Excitation of surface plasmons

Metals as *e.g.*, gold, silver, aluminum, copper, have delocalized electrons in their conduction band, which are not spatially fixed at a specific position at the metallic lattice, but can move freely (also called "free electron gas"). Due to their negative charge, electrons can suffer the effect of external electromagnetic fields. These fields can shape the distribution of the electron gas according to the properties of the field. In this way, an external electromagnetic field (as light) can modulate the electron gas at the interface between a metal and a dielectric.

When p-polarized light (for example red light, $\lambda = 632.8$ nm) impinges on a thin metallic layer (*e.g.*, for gold, depending on the dielectric above it, the thickness should be around 47 nm) in a geometry as shown in Figure 2.7 b), an evanescent wave called "surface plasmon"can be excited at an angle $\psi_1 = \psi_{SPR}$. This geometry of excitation is called "**Kretschmann-Raether**" configuration due to the work of both researchers [116]. At this resonance angle, the electromagnetic field of light matches the momentum

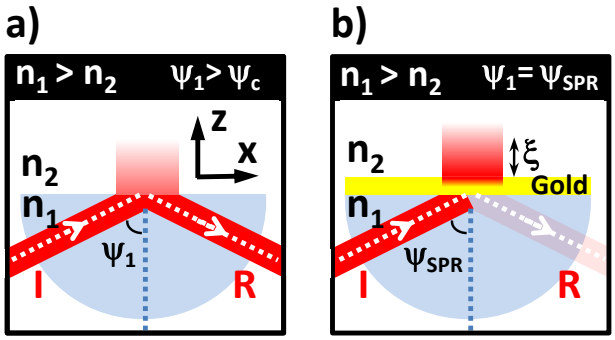

Figure 2.7: When a thin gold layer (h = 47 nm) is placed on top of the half cylinder lens (or triangular prism), it is possible at a given angle called ψ_{SPR}, to couple a p-polarized beam completely to excite a surface plasmon wave at the interface metal-dielectric. All incident beam is coupled to excite the surface plasmon wave under these conditions. Ideally, at this point $R_p = 0$. The intensity of the surface plasmon wave is therefore much stronger than that of the evanescent wave of the total internal reflection. When surface plasmons are excited in this way, it is called the "Kretschmann configuration" or "Kretschmann-Raether configuration".

and frequency of the free electron gas perfectly, entering in resonance (this momentum-frequency matching can be seen in a dispersion relation curve as conventionally shown in the literature). Surface plasmons have different names in the literature: "Surface Plasmons (SP)", "Surface Plasmon Polaritons (SPP)", "Surface Plasmon Resonance (SPR)", "non radiative surface plasmon waves". In this work it will be referred to as surface plasmon when the wave is meant and the spectroscopic technique will be mostly called "Surface Plasmon Resonance Spectroscopy" or SPR. The resonance angle is also named after this (ψ_{SPR}).

Surface plasmons have evanescent character in the z direction, and can be excited at the interface between a dielectric medium (as air or a polymer film) and the metal. The decay length into the dielectric medium depends on its dielectric properties. For air the field decay length is about $\xi \approx 200$ nm. Within the gold layer its decay reaches about 40 nm.

Surface plasmons also propagate in the x direction. The wavevector of surface plasmons in the x direction is given by:

$$k_x = k_{SP} + ik'' \approx \frac{\omega}{c} \cdot \sqrt{\frac{\epsilon'_m \cdot \epsilon_d}{\epsilon'_m + \epsilon_d}} + i \left[\frac{\omega}{c} \cdot \sqrt{\left(\frac{\epsilon'_m \cdot \epsilon_d}{\epsilon'_m + \epsilon_d} \right)^3} \cdot \frac{\epsilon''_m}{2\epsilon'^2_m} \right] \tag{2.7}$$

This propagation is hindered though, due to the energy absorption by the metallic layer due to the imaginary part ϵ''_m. Here, the surface plasmons loose energy, which is converted into heat. This means, surface plasmons are damped in the x direction, therefore are not propagating infinitely throughout the x direction. The relaxation length of the propagation of surface plasmons L_i is given by:

$$L_i = \frac{1}{2 \cdot k''_x} \tag{2.8}$$

Depending on the wavelength of light ($\lambda \approx 500$ nm to 1000 nm) on silver, the propagation length decays at about $L_i = 22$ μm to 500 μm, while on gold it is about 0.5 μm to 50 μm.

The penetration depth of surface plasmons in both, the metall (ξ_m) and in the dielectric (ξ) media are given by:

$$\xi = \frac{c}{\omega} \sqrt{\frac{\epsilon_d + \epsilon_m}{\epsilon_d^2}} \tag{2.9}$$

and

$$\xi_m = \frac{c}{\omega} \sqrt{\frac{\epsilon_d + \epsilon_m}{\epsilon_m^2}} \tag{2.10}$$

The resonance condition is shown in Figure 2.8, blue curve. In contrast, the case of total internal reflection is shown in the dashed, red curve.

There is also the possibility where on top of the gold layer, a dielectric medium in a form of thin film (instead of air), is the add-layer. This situation is shown in Figure 2.9 c).

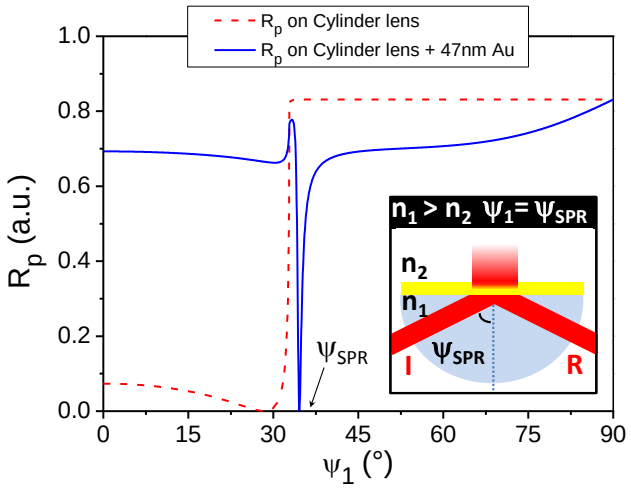

Figure 2.8: The blue curve is a commonly observed spectrum measured for a system: LaSFN9 half cylindrical lens, gold (47 nm), air. The resonance condition is shown (ψ_{SPR}). The red curve displays a simulation of total internal reflection with no gold layer on top of the half cylindrical lens.

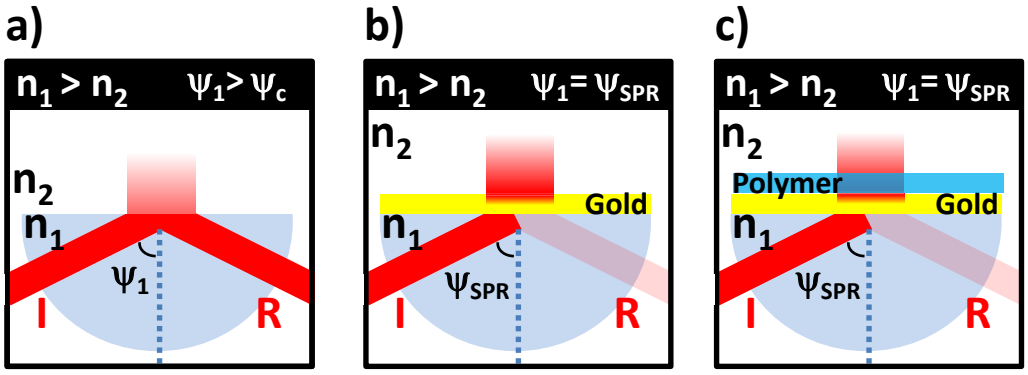

Figure 2.9: Instead of having air as add-layer (a and b) one can apply a polymer thin film on top of the gold layer (by spin-coating for example). Therefore the optical properties of the films such as refractive index and their thicknesses, will produce different reflectivity spectra. By knowing the refractive index of the polymer film, one can infer about its thickness, and vice-versa.

2.1.2.3 Surface Plasmon Resonance Spectroscopy–SPR

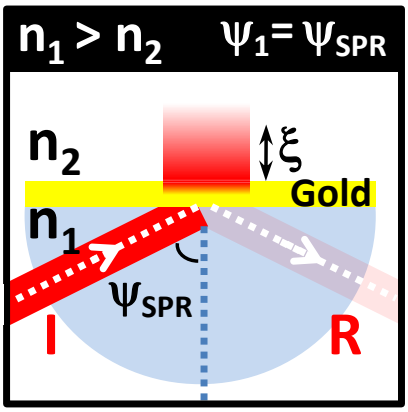

Figure 2.10: Excitation of surface plasmons with prism coupling. Throughout this work, instead of having air being the medium 2 with refractive index n_2, as in the configuration above, a polymer thin film was the add-layer as in Figure 2.9. The material used was polystyrene. Thus, polymer films were characterized by SPR.

The dielectric medium, in this work mostly a polymer with refractive index $n_{polymer}$, is the add-layer. On top of it a dry N_2 atmosphere, with refractive index $n_2 = 1$. Figure 2.10 shows these conditions. Depending on refractive index $n_{polymer}$ and film thickness h, the resonance angle ψ_{SPR} changes. In fact, by increasing one of the two values, the resonance angle shifts towards higher values.

A simulation in WinSpall for a system as: half cylinder lens (made of LaSFN9, $n_{LaSFN9} = 1.8$ for $\lambda = 632.8$ nm), gold, polystyrene (PS) and nitrogen (N_2), with varying film thickness is shown in Figure 2.11. There, one finds that the total internal reflection angle (ψ_c) keeps constant, but its intensity decreases by increasing films thickness. While shifting towards higher angles due to an increase in thickness, a broadening of the SPR spectrum is observed.

If the film thickness is further increased, the surface plasmon resonance angle increases (reaching for the half cylinder lens a plateau), while other resonance modes appear (Figure 2.12). These resonance conditions correspond to waveguide modes (for p-polarized light one excites $TM0$, $TM1$, $TM2$,..., TM_i). Here TM stands for "transverse magnetic" modes. The surface plasmon resonance itself is the TM0 mode. The thicker the film, the higher is the number of modes it supports. In Figure 2.12 the polymer was

PS ($n_{PS} \approx 1.59$, $\lambda = 632.8$ nm).

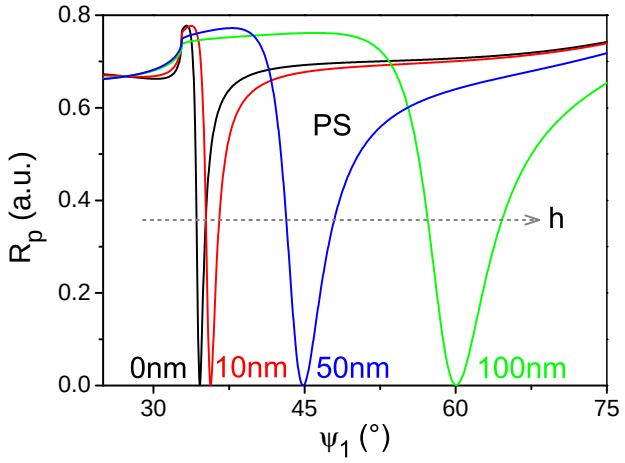

Figure 2.11: By increasing the thickness or refractive index of a polymer thin film on top of gold, the resonance angle shifts towards higher values. This case shows the evolution of resonance angle with film thickness for a fix refractive index ($n_{PS} = 1.59$). The resonance broadens as the film becomes thicker. The intensity of the total internal reflection value decreases by increasing film thickness.

The intensity of the electric field of waveguide modes throughout the film thickness depends on which mode is excited (TM_i or TE_i). The distribution of intensities is shown in Figure 2.13.

Each of these modes, (except TM0 for thick films) has a "tail" that leaks into the dielectric medium above. The higher the order of the mode, *i.e.*, the greater the value of i, the greater the penetration depth of the leaky mode into the dielectric add-layer:

$$\xi_{TM1} < \xi_{TM2} < \xi_{TM3} < ... \tag{2.11}$$

and

$$\xi_{TE1} < \xi_{TE2} < \xi_{TE3} < ... \tag{2.12}$$

These concepts presented about surface plasmon resonance spectroscopy and waveguide spectroscopy will be necessary for understanding the working mechanism of the REDLS and WEDLS techniques.

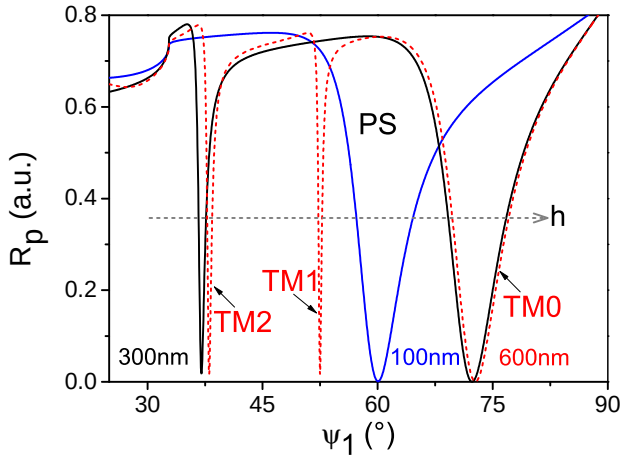

Figure 2.12: If the film thickness is continuously increased, the surface plasmon resonance angle reaches a maximum value (this just happens for the half cylindrical lens, while triangular prisms do not show an upper resonance plateau). Waveguide modes appear by increasing the film thickness. In this case, as the incident beam is p-polarized, TM modes are excited using a half cylinder lens. The thicker the film, the higher the number of modes it supports.

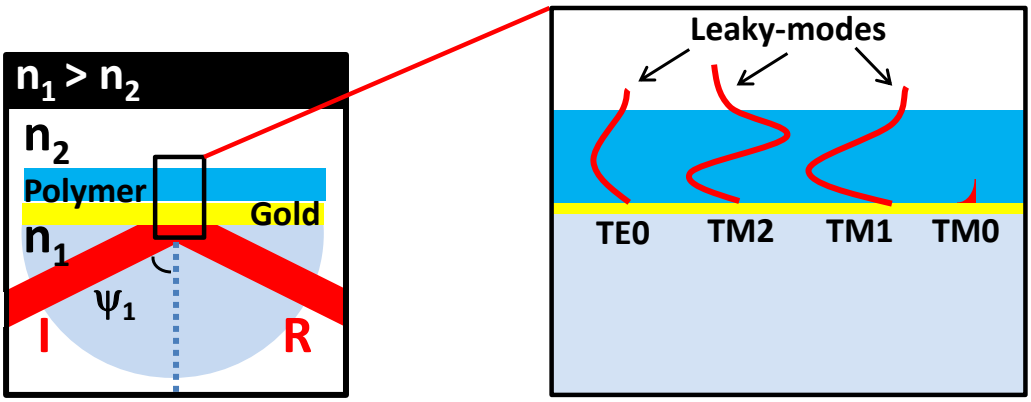

Figure 2.13: Leaky Modes and waveguide modes: according to the selected mode chosen, a different optical field distribution is found inside and outside the waveguide. By using p-polarized light, TM modes can be excited, while s-polarized light just allows TE modes. The tail of each mode inside the add-layer is called leaky-mode. The higher order modes have leaky-modes with higher penetration depth inside the add-layer. Surface plasmons (TM0) are sensitive to the polymer-solid contact in this example, and does not feel the influence of the free-surface.

2.1.2.4 Kinetic–SPR

Kinetic-SPR [4] is a powerful technique applied to detect small variations of the surface properties with time. As shown in section 2.1.2.3, an increase in the dielectric film thickness or in refractive index let the resonance minima shift towards higher angles, cf. Figure 2.11. The study of T_g from supported polymer has been experimentally addressed using such techniques [117]. When the dielectric material on top of the gold layer is heated, the thickness increases due to thermal expansion, and the refractive index decreases due to the decrease of density. The overall result can be estimated from the Lorentz-Lorenz relation (or Clausius-Mosotti model), so that the effect of expansion is greater than the refractive index decrease, and thus a shift to higher resonance angles happens, and reflectivity increases with temperature [117], Figure 2.14. In the glassy state ($T < T_g$), the expansion coefficient has an absolute value smaller than in the liquid or rubbery state ($T > T_g$), thus different slopes in the reflectivity curve with temperature can be observed in these ranges, Figure 2.14–right. T_g is defined as the temperature at which an interception of both curves occurs, Figure 2.14–right. More about thermal expansion of polymer thin films is discussed in Chapter 3.1.2.

Lorentz-Lorenz equation. The Lorentz-Lorenz equation, also known as Clausius-Mossotti equation or Maxwell's formula (equation 2.13), relates the refractive index, n, of a substance (or the real part of the dielectric constant [5], ϵ'), to its polarizability, α, and N/V is the bulk density of polarizable monomer units.

$$\frac{N\alpha}{3\epsilon_0 V} = \frac{n^2-1}{n^2+2} = \frac{\epsilon'-1}{\epsilon'+2} \tag{2.13}$$

ϵ_0 is the vacuum permittivity. Assuming that for a supported polymer film standing on a solid substrate with expansion coefficient much smaller than that of the polymer, the areal number density of monomer units, $N_A = N/A$, remains constant during thermal expansion, one can write:

$$\frac{N\alpha}{3\epsilon_0 A}\cdot\frac{1}{h} = \frac{N_A\alpha}{3\epsilon_0}\cdot\frac{1}{h} = \frac{\epsilon'-1}{\epsilon'+2} \tag{2.14}$$

with $V = A \cdot h$. Therefore:

[4] Wave guides are also used for this purpose, due to their higher resolution originated from sharp resonance minima [117].

[5] The refractive index n relates to the dielectric constant through: $n^2 = \epsilon'$

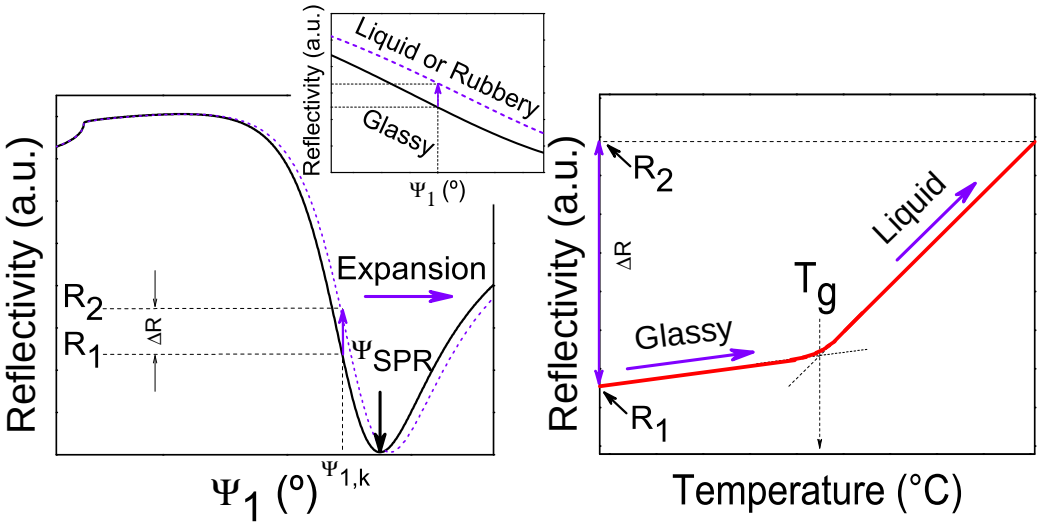

Figure 2.14: When the polymer films are heated, thermal expansion leads the SPR curve to shift towards higher resonance angles (left figure). By keeping the laser and SPR detector at a constant angle, $\psi_{1,k}$, the reflectivity increases from R_1 to R_2 during heating. As the thermal expansion coefficient in the liquid state is greater than at the glassy state, a change in slope at T_g takes place (right figure).

$$h = \left(\frac{N_A\alpha}{3\epsilon_0}\right)\cdot\frac{\epsilon' + 2}{\epsilon' - 1} \tag{2.15}$$

The derivative of thickness, h, in respect to the dielectric constant, ϵ', gives:

$$\frac{\partial h}{\partial \epsilon'} = \left(\frac{N_A\alpha}{3\epsilon_0}\right)\cdot\frac{(\epsilon' - 1) - (\epsilon' + 2)}{(\epsilon' - 1)^2} = -\left(\frac{N_A\alpha}{\epsilon_0}\right)\cdot\frac{1}{(\epsilon' - 1)^2} \tag{2.16}$$

From equation 2.14, one can write:

$$(\epsilon' - 1) = (\epsilon' + 2)\cdot\left(\frac{N_A\alpha}{3\epsilon_0}\right)\cdot\frac{1}{h} \tag{2.17}$$

Substituting the value of $(\epsilon' - 1)$ in equation 2.16 (still keeping one term $(\epsilon' - 1)$ free):

$$\frac{\partial h}{\partial \epsilon'} = -\left(\frac{N_A\alpha}{\epsilon_0}\right)\cdot\frac{1}{(\epsilon' - 1)}\cdot\frac{3\epsilon_0 h}{(\epsilon' + 2)N_A\alpha} \tag{2.18}$$

Thus:

$$\frac{\partial h}{\partial \epsilon'} = \frac{-3h}{(\epsilon' - 1)(\epsilon' + 2)} \tag{2.19}$$

or

$$\frac{\partial h}{h} = \frac{-3\partial \epsilon'}{(\epsilon' - 1)(\epsilon' + 2)} \tag{2.20}$$

By dividing both sides of the equation 2.20 by ϵ', it can be rewritten as:

$$\frac{(\epsilon' - 1)(\epsilon' + 2)}{3} \cdot \frac{1}{\epsilon'} \cdot \frac{\partial h}{h} = \frac{-\partial \epsilon'}{\epsilon'} \tag{2.21}$$

substituting the dielectric constant, ϵ', of a polymer (e.g., PS with $\epsilon' = 2.528$) in the left-hand side of equation 2.21, one gets as a good approximation:

$$0.91 \cdot \frac{\partial h}{h} \approx \frac{-\partial \epsilon'}{\epsilon'} \tag{2.22}$$

meaning that, for the case of PS, as the angular shift of a surface plasmon resonance induced by a thin dielectric coating always depends on its optical thickness, $n{\cdot}h$ [117], the negative contribution due to the decrease of dielectric constant (or refractive index) while heating is just about 91 % of the positive increase in thickness due to thermal expansion. Therefore, the SPR curve shifts towards higher resonance angles, and the reflectivity value increases at a constant angle, $\psi_{1,k}$, Figure 2.14. Naturally, the opposite affirmation is valid for cooling, *i.e.*, the reflectivity decreases while decreasing temperature. For a polymer as PMMA, in which the dielectric constant is $\epsilon' = 2.16$, the negative contribution of the dielectric constant is just 75 % of the positive contribution of thermal expansion. The lower the refractive index of the polymer film, the higher will be the difference between both contributions.

Testing the validity of the Lorentz-Lorenz equation for PS thin films. The validity of the result obtained from the Lorentz-Lorenz relation for polystyrene is not trivial, and has to be tested. To check whether or not equation 2.22 describes well the physical behavior of PS, real values of thickness and dielectric constant, based on experiments will be next used.

Assuming a PS 1821 g/mol film, with initial thickness, $h_i = 5$ nm, at the initial temperature, $T_i = 20$ °C, is heated to $T_f = 28.85$ °C, then the final thickness is, $h_f = 5.01$ nm, as the linear expansion coefficient for this

polymer at $T < T_g$ is $\alpha_L \approx 2.03{\times}10^{-4}$/K, as calculated from ref. [118]. One can calculate the dielectric constant, by using the experimentally determined relation, that can be calculated from ref. [119]:

$$n = \begin{cases} 1.5920 - 1.4 \times 10^{-4}\ T & \text{if } T < T_g \\ 1.5864 - 3.6 \times 10^{-4}\ (T - 50\ ^{\circ}C) & \text{if } T > T_g \end{cases} \tag{2.23}$$

As $T_g \approx$ 50 °C for PS 1821 g/mol, at the initial and final temperatures ones has:

$$\epsilon_i^{'} = n_i^2 = (1.5892)^2 = 2.5256 \tag{2.24}$$

$$\epsilon_f^{'} = n_f^2 = (1.5878)^2 = 2.5212 \tag{2.25}$$

therefore:

$$\frac{\Delta\epsilon^{'}}{\epsilon_i^{'}} = \frac{2.5212 - 2.5256}{2.5256} = -1.7422 \times 10^{-3} \tag{2.26}$$

and

$$\frac{\Delta h}{h_i} = \frac{5.01 - 5}{5} = 2 \times 10^{-3} \tag{2.27}$$

resulting:

$$\frac{\Delta\epsilon^{'}/\epsilon_i^{'}}{\Delta h/h_i} = \frac{-1.7422 \times 10^{-3}}{2 \times 10^{-3}} = -0.871 \tag{2.28}$$

which is in good agreement with the theoretical prediction given by equation 2.22 (error ≈ 4.3 %), confirming the validity of the Lorentz-Lorenz equation for PS 1821 g/mol.

2.1.3 Dynamic Light Scattering–DLS

2.1.3.1 Introduction to DLS

Dynamic Light Scattering (DLS) also called Photon Correlation Spectroscopy (PCS), or Quasi-Elastic Light Scattering (QELS) or even Time Domain Light Scattering (TDLS) is used in this work in combination with Surface Plasmons Resonance Spectroscopy (SPR). This combination, called Resonance Enhanced Dynamic Light Scattering (REDLS) will be further introduced. For this, the basic concepts of DLS are needed. This chapter does not intend to go deep into this topic as it has been exhaustively described in the literature as *e.g.*, in ref. [99, 120].

The basic principle of this technique is the analysis of the intensity fluctuations of scattered light from a medium, with respect to time.

The most accepted theory of light scattering is probably that given by Smoluchowski in 1908 and by Einstein in 1910. They considered the example of a continuous medium in which thermal fluctuations give rise to local inhomogeneities and therefore to density and concentration fluctuations. This theory is called "fluctuation theory of light scattering".

In other words, when light impinges in a medium in which the optical properties (refractive index, dielectric components, polarizability, etc) fluctuate from point to point in time or space, scattering happens. Contrary, when light travels through a continuous medium, where the optical properties do not fluctuate in time or space, light does not scatter. This is what happens when light travels through vacuum (momentum is not transfered and therefore the initial wavevector k_i does not change its direction).

If light passes through a real medium as *e.g.*, a polymer, density fluctuations in the material lead to fluctuations in the optical properties and therefore light scatters. The amount of scattered light (intensity) is related to the magnitude of these fluctuations. Bigger fluctuations will lead light to scatter more. The intensity of scattered light can (in principle) be calculated from the mean-square density and concentration fluctuations, which in turn can be determined from macroscopic properties such as isothermal compressibility and concentration dependence of the osmotic pressure [99].

For such an experiment a setup as shown in Figures 2.15 is normally used (Figure 2.16 is a more realistic view of the experiment on a quartz cuvette containing the sample).

For this a laser beam (throughout this work, He-Ne, $\lambda = 632.8$ nm), passes trough a polarizer, reaches the sample and scatters in all directions. A detector can be in principle placed in any of these directions (k_s, where the subscript stands for "scattered") and follow the fluctuation of the intensity of scattered light in time.

However, due to convenience, samples are placed in quartz cuvettes as the one shown in Figure 2.16. Because of its cylindrical shape, the best geometry for varying the angle of observation is the one shown in Figure 2.16. As the maximum of scattering intensity takes place in a plane orthogonal to the electric field of the incident beam [121] and considering the restricted plane of detection, the incident light is normally chosen as vertically polarized in respect to the detection plane, *i.e.*, $\vec{E}$ is parallel to the normal vector of the plane π. As the incident beam has electric field vertically polarized, it is

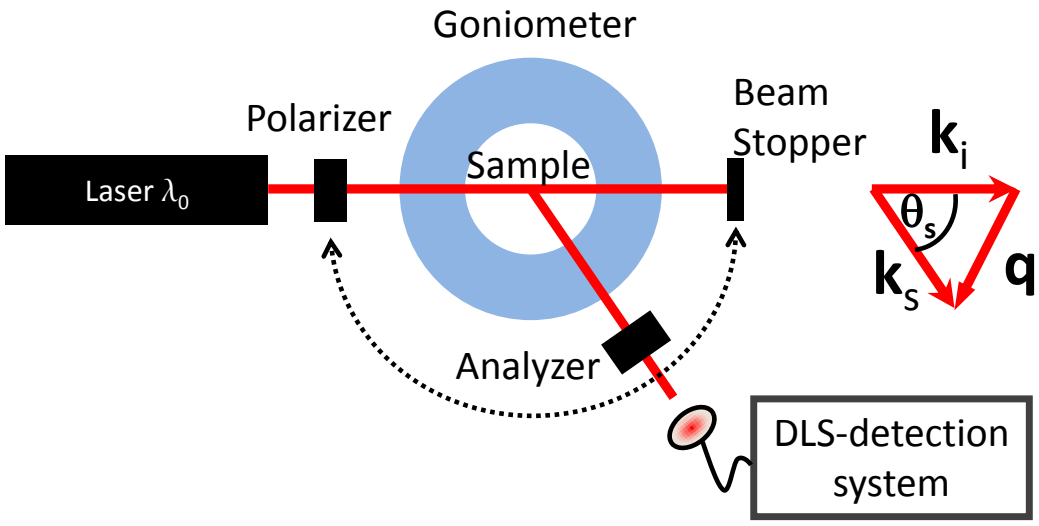

Figure 2.15: DLS- apparatus. This configuration is the most common used for bulk DLS measurements. Vertically polarized light passes through the sample and is scattered in all directions. One can place a photo-detector at any position (θ_s) allowed by the goniometer. The scattered light passes through an analyzer and then into a detection system. The detection system is normally composed by: optical fibers, photo-detectors (generally PMs or APDs), correlator and finally a PC.

denominated V-polarized.

The analyzer can be set to select vertically or horizontally scattered light (V or H polarized, respectively). In this way, one can measure DLS having V-V or a V-H configuration depending on the feature that is being studied (the incident beam is always V, just the analyzer changes to V or H). If no analizer is used, it is called V-U (vertical-unpolarized).

The incident beam has the wavevector k_i and the scattered light at the scattering angle θ_s has the wavevector k_s. Both vectors have the same modulus but different directions. The reason for having the same modulus is because both are defined in the same medium where light scatters:

$$|k_i| = |k_s| = \frac{2\pi n_i}{\lambda_0} \tag{2.29}$$

where n_i is the refractive index of the medium where light scatters and λ_0 is the wavelength of the incident beam in vacuum.

When light scatters, momentum is exchanged and therefore one can define

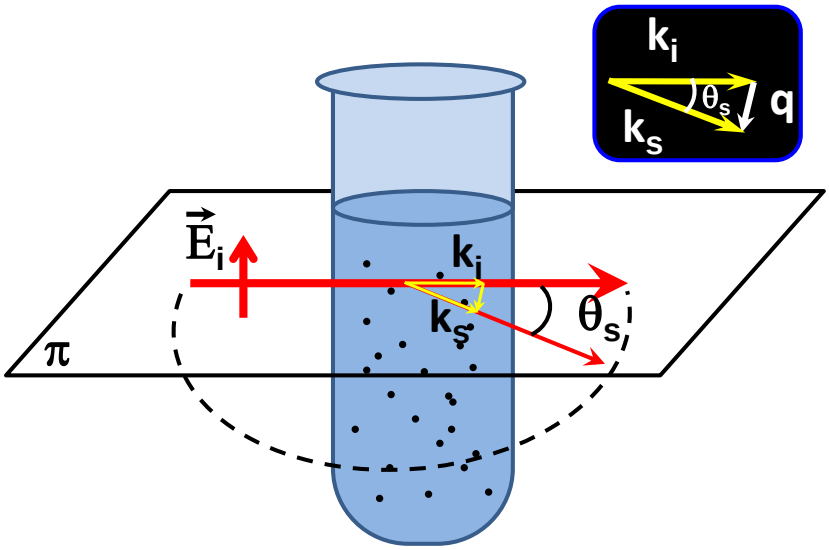

Figure 2.16: This is how a real DLS experiment on a quartz cuvette looks like. The incident field is parallel to the normal vector of the plane π. This configuration is chosen due to the higher scattering intensity obtained in the π plane in this geometry.

the scattering vector $\mathbf{q}$, *i.e.*, the difference in wavevector before and after scattering as $|k_s - k_i| = |\mathbf{q}| = q$.

As both vectors have the same size, the triangle formed by these three vectors is isosceles and therefore the modulus of $\mathbf{q}$ is given by:

$$q = |\mathbf{q}| = \frac{4\pi n_i}{\lambda_0} sin\left(\frac{\theta_s}{2}\right) \tag{2.30}$$

There are two types of detection of relevance at this point: "**homodyne**" and "**heterodyne**". If only the scattered light from the sample impinges on the detector, then this is named "homodyne detection". On the other hand, if a small portion of the initial beam is deviated and impinges on the detector together with the scattered light from the sample, then this is called "heterodyne detection". In heterodyne detection it is important that both coherent beams are in phase in order to have a successful positive interference.

The intensity fluctuation in time around an average intensity ($I_{average}$) of a heterodyne experiment is shown in Figure 2.17 (right). An autocorrelator is a physical device able to extract an autocorrelation function out of these fluctuations (Figure 2.17, left).

The intensity autocorrelation function $G_2(q,t)$ is calculated as:

$$G_2(q,t) = \frac{\lim_{T\to+\infty} \frac{1}{2T} \int_{-T}^{T} I(q,t')I(q,t'+t)\,dt'}{\langle I(q,t')\rangle^2} \tag{2.31}$$

where, $\langle I(q,t')\rangle$ is the average time intensity and T is the total experiment time.

The field autocorrelation function $G_1(q,t)$ can be calculated by the Siegert-relation:

$$G_2(q,t) = 1 + f \cdot G_1(q,t)^2 \tag{2.32}$$

this relation between both autocorrelation functions is derived from the dynamic light scattering theory. A heterodyne experiment measures $G_1(q,t)$ directly [99]. f is a contrast factor.

Such correlation functions can generally be fit by a single exponential or by a streched exponential decay, such as equation 1.51, in a variety of systems. In this way a relaxation time can be directly extracted from the experiments at given experimental conditions of temperature, **q**, pressure, etc (Figure 2.17, left).

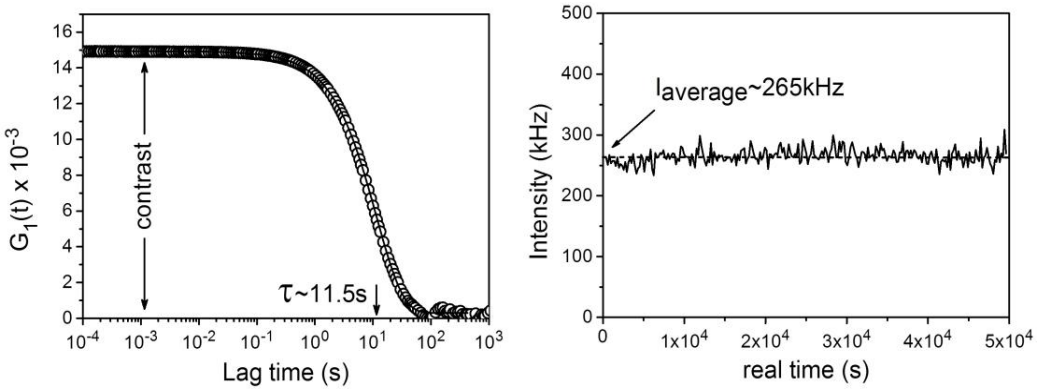

Figure 2.17: Autocorrelation function (left) and time intensity fluctuation (right). During a DLS experiment, intensity as a function of time is monitored and, from this an autocorrelation function (left) is computed. Such a curve can be fit by a function such as a single or stretched exponential, delivering a relaxation time (11.5 s in this example). The intensity fluctuates around an average value $I_{average}$ (265 kHz in this example).

2.1.4 Resonance Enhanced Dynamic Light Scattering–REDLS

Combining the surface sensitivity of SPR with the time resolution of DLS, a powerful technique able to resolve interfacial dynamics was developed [122–124]. This technique is named Resonance Enhanced Dynamic Light Scattering (REDLS) and showed to be suitable for the study of dynamics of polymer ultrathin films at solid surfaces. A schematic REDLS setup is shown in Figure 2.18.

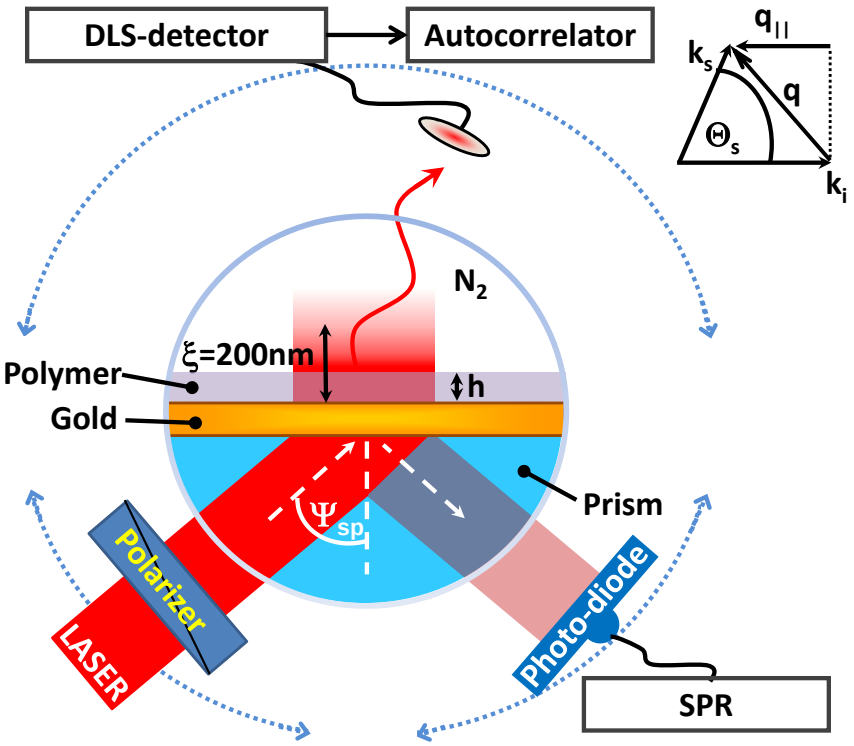

Figure 2.18: REDLS configuration: here the incident beam is the surface plasmon wave. Therefore, light will scatter solely at the vicinities of a solid interface (gold in this case), within the evanescent field. The scattered light is collected by an optical fiber and the fluctuations in intensity are followed. The nitrogen chamber allows keeping the thin films in an inert atmosphere during the whole experiment, avoiding polymer degradation and contamination.

The scattering geometry is basically given by the properties of the surface plasmon wave and the choice of the experimental **q**-vector. As the surface

plasmon wave propagates parallel to the gold surface, k_i is also parallel to the surface. Since the light scattering process takes place at the polymer thin film, k_s has the same modulus as k_i. As the incident beam of the dynamic light scattering experiment is the surface plasmon wave, the incident and scattered beams are both p-polarized. This means, the maximum scattering intensity is obtained in a plane parallel to the sample plane. However, this experimental geometry is not favorable and therefore light is collected at the plane made by both vectors k_s and k_i. This intensity level however was highly satisfactory for most of the experiments.

Due to the evanescent character of surface plasmons in the z direction (cf. 2.1.2.2), if a very thick polymer film is the add-layer (h >> 200 nm), solely the solid-polymer interface, and the first 200 nm close to it, will contribute to the scattering signal. The free-surface will not contribute to the scattering signal, as it is out of the surface plasmon optical field if the film thickness is much greater than the relaxation length of the surface plasmons. On the other hand, if the film has thickness similar to the decay length of surface plasmons, or even h << ξ, the whole film thickness will be included in the scattering volume and will contribute to the scattering signal. Here, the scattering volume is defined by the overlapping between the polymer film and the surface plasmon wave. Fluctuations of optical properties within this scattering volume will lead light to scatter and mix with the statically scattered light (originated due to surface roughness, defects, etc) in the detector. If the intensity of these scattering processes is big enough, and the relaxation times are within the DLS window, then REDLS is able to resolve such dynamical process.

2.1.4.1 Advantages of REDLS over X-PCS

The surface dynamics of supported entangled polymer ultrathin films has been thoroughly studied by means of X-PCS [98, 125–132]. This technique however, is relatively expensive for the study of the surface dynamics since high energy photon density is required (actual values are $\approx 10^9$ photons/second). For this very same reason the samples cannot be exposed to the radiation for excessively long times at the same spot, otherwise chain scission may take place, increasing polydispersity and finally leading to an irreversible sample damage [98].

Thus, REDLS has tremendous advantages over other experimental techniques concerning the study of capillary waves in ultrathin films, for being practically non-expensive compared to X-PCS, non-invasive and having the

feature of enabling the study of thin films as a whole (X-PCS just allows the investigation of the first ≈ 10 nm of the free surface).

2.2 REDLS-Setup

The approach to study dynamics of supported polymer thin films required the combination of two well established techniques: Surface Plasmon Resonance (SPR) and Dynamic Light Scattering (DLS). A new setup configuration was designed to fulfill the needs to perform Resonance Enhanced Dynamic Light Scattering (REDLS) measurements in thin films having thicknesses down to some few nanometers (≈ 17 nm so far) under controlled atmosphere (filtered and dry nitrogen) and controlled temperature in the range of approximately 22 °C to 200 °C. This section describes the technical characteristics of the REDLS setup, as optics used, light scattering detection system and the controlled environment for the realization of the experiments.

2.2.1 REDLS configuration

Surface Plasmon Resonance Spectroscopy as well as Dynamic Light Scattering setups have been extensively described in the literature [99, 115, 120, 133–135]. The first successful REDLS setup was built in 2008 by Plum *et al.* [122]. REDLS technique was first applied to resolve the diffusive characteristics of polystyrene colloidal particles in water at the vicinity of gold covered glass surfaces and was able to reveal the changes in the Brownian diffusion coefficients (parallel and perpendicular) close to the solid interface for particles as small as ≈ 10 nm in radius. It enables to investigate interface induced dynamics, *e.g.*, diffusion of particles or small molecules through membranes, the hindering of diffusion and rotation close to solid surfaces and many others. The present project aimed to understand how solid and free-surfaces influence the dynamics of polymer melts, according to the type of polymer, strength of interaction between polymer and substrate, polymer molecular weight, film thickness, roughness of the solid surface, composition of the atmosphere on the "free-surface", etc.

To systematically tackle these issues, a novel configuration for the REDLS setup was needed since the project required well controlled experimental conditions: an insulated gas chamber that enables measurements under inert atmosphere; a heating system with controlled temperature stability as well as *in situ* sample temperature determination, humidity control during the mea-

surements and optical matching liquids that are stable even under extreme temperature ranges. Apart from these issues, to reach a resolution to be able to resolve dynamics of supported polymer films showing very low contrasts was also a technical challenge. The next sections will treat stepwise these topics and show how the technical difficulties were overcome.

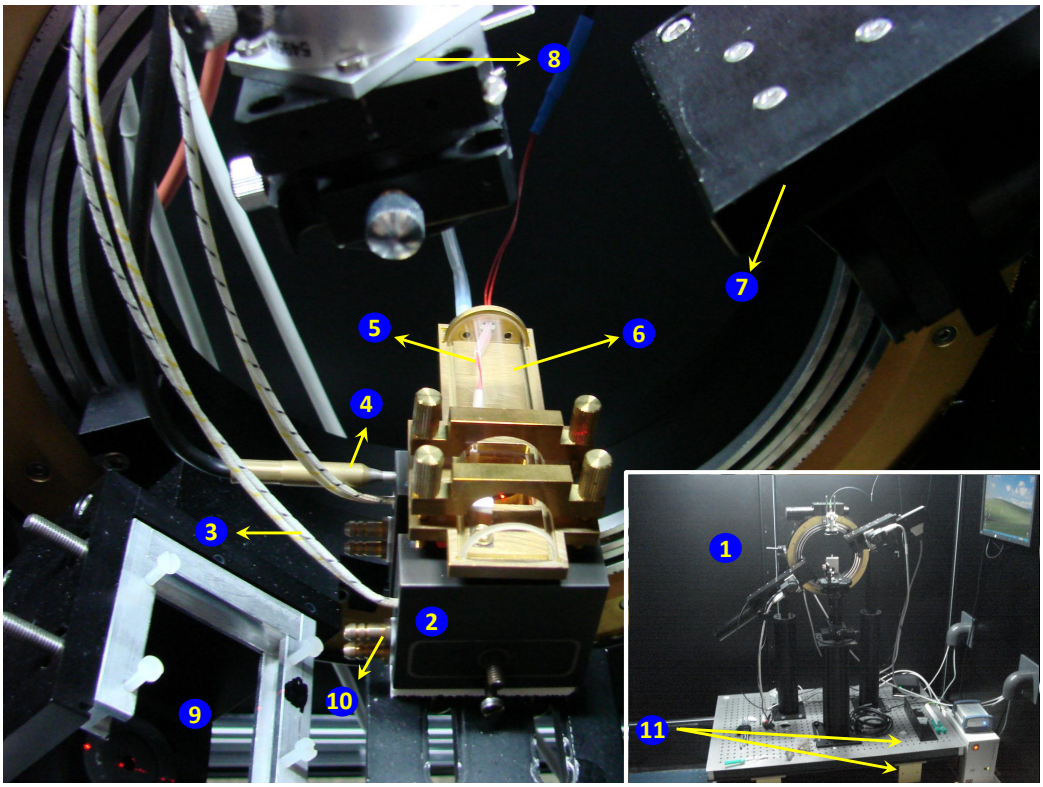

Figure 2.19: 1) REDLS setup including all parts assembled on the goniometer from Optrel (Multiskop). 2) Sample/prism holder. 3) heater cartridges (2 pieces), heating the sample holder. 4) A thermo-sensor unit (PT100) for heating control. 5) flat PT100 directly on top of the sample, close to the illuminated volume. 6) quartz cell. 7) Photo-diode detector for SPR. 8) holder for optical fiber with alignment system. 9) He-Ne laser $\lambda = 632.8$ nm with lens for focusing on the sample and polarizers (both are not shown). 10) input/output of coolants into the body of the holder. 11) anti-vibration system. The sample is placed on top of the half cylinder lens.

2.2.2 Double Goniometer–Multiskop

The setup was built on the basis of a commercial setup from the company Optrel GmbH called Multiskop, which is normally used for reflectivity based measurements as SPR, Ellipsometry, Brewster angle microscopy and others. The primary configuration consists of:

- A double wheel goniometer on which the laser source and the photo-detector as well as the optical pieces needed are implemented. Instead of step motors as in conventional setups, Multiskop contains a continuous angle scanning system.

- He-Ne red laser ($\lambda = 632.8$ nm).

- Detector for reflectivity–photo-diode.

- Software for computer control (Multi).

Multiskop from Optrel has several advantages over the conventional setups. Some of them are: i) it is able to perform the reflectivity scan in some few seconds (approximately 10 s against something like 30 min for the same resolution in conventional setups). ii) it does not need a "lock-in amplifier" normally required in conventional systems, what makes the setup more efficient, therefore the proper option for this application.

Another main aspect of Multiskop is its configuration: laser and photodiode work in a $\Psi - \Psi$ geometry, allowing the use of half cylinder lenses. This brings a tremendous advantage when the DLS detector has to be adjusted. In this configuration the point where the laser beam reflects can be aligned to the center of the goniometer, an impossible task when triangular prisms are used. The plane of the liquid film is horizontally oriented. This allows studies in liquid systems where flow has to be avoided.

2.2.2.1 Anti-vibration table

Dynamic light scattering is an extremely sensitive technique and any external correlated signal can result in an undesired correlation function. These external signals have different possible sources as the intrinsic vibration modes of the building itself or an air flow produced by the air conditioning system,

people walking in the laboratory or even an external source of light that reaches the photo-detector, etc. In order to avoid these spurious signals, an insulation system was built: the setup was placed on the top of an anti-vibration table and, the whole construction was enclosed in a "dark-box". This anti-vibration table consists of three main parts: directly on the laboratory ground a rigid and massive stone platform was set to decrease the effect of the harmonic vibration modes from the building on the setup. On top of it, an active vibration insulation system (AVI-350/LP) consisting of a combined piezo-coil damping mechanism from "Table Stable" was used. This active insulation is effective on the range of frequencies starting from approximately 1 Hz and is dynamic up to about 200 Hz (beyond this value the insulation will be passive). A stiff honeycomb breadboard was placed on the top of the active system and together with the bottom stone, it is responsible for the absorption of vibrations of higher frequencies.

2.2.2.2 DLS detection system

Fluctuations of the dielectric properties of the polymer thin films in time cause the scattering of the surface plasmons optical field (cf. section 2.1.3). The roughness of the metallic or polymer film surface, crystalline defects (in the case of the metal layer) or medium discontinuity also lead light to scatter from the surface. This scattered light is captured by an optical fiber (that can be a single-mode or a multi-mode fiber).

For having correlations showing higher contrast level, single-mode fibers are normally indicated. Unfortunately this type of fiber produces undesired self-correlations normally having decay times at ≈ 0.1-100 s with contrasts on the order of 10^{-4} or higher [124]. This occurs because a single-mode fiber works as a Fabry-Perot interferometer and due to unavoidable thermal fluctuations that are correlated in time, a self-correlation appears [124]. To avoid this self-correlation, a mode scrambler was previously used ("ALV-static and dynamic enhancer"–SDE–ALV GmbH, Langen). With this device the contrast level of the self correlations were dropped down to ≈ 2×10^{-5} or even 10^{-6} depending on its efficiency [124].

In this project multi-mode fibers were used due to the good baseline achieved with this type of optical fiber, being even better than the one obtained by using the SDE. The collected light is then split into two photon detectors, normally an "Avalanche Photo Diode" (APD) or a "Photomultiplier" (PM) is used in DLS. In this project PMs were used (MP-973 (6606-P-079)–Perkin Elmer). These detectors are single photon counters and transfer the

counts fluctuations to a "multi-tau correlator" (ALV7004/fast multiple tau digital correlator, ALV GmbH). For this project PMs were a good option due to their relative low prices and good quantum efficiency/dark counts relation.

2.2.2.3 Optical fibers: the baseline

The multi-mode fibers combined with the pseudo-cross correlation detection deliver the best baseline in DLS. In Figure 2.20 three cases are compared: the conventional single-mode fiber detection, a single-mode fiber with the "Static and Dynamic Enhancer" and the use of a multi-mode fiber.

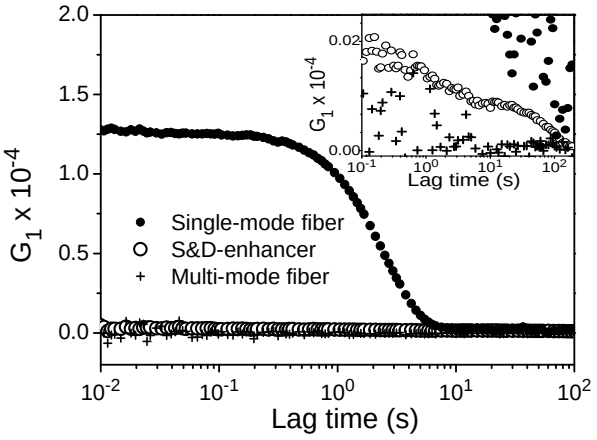

Figure 2.20: Baseline for REDLS. Multi-Mode *vs.* Single-Mode fibers were tested on bare-gold. The commonly used single-mode fibers show a self-correlation with contrast 1.25×10^{-4} with decay time of the order of 1 s. The inset is a zoom showing that multi-mode fibers deliver the best baseline.

2.2.2.4 Pseudo cross-correlation

Pseudo cross-correlation is a method for generating cross-correlation functions free of spurious contributions from each photon detector individually. It is based on splitting the incoming signal into two photon detectors and then their outputs into a correlator. As it is statistically impossible for both detectors to have the same self-correlation, these undesired signals can be eliminated. A sketch of the pseudo cross-correlation is given in Figure 2.21.

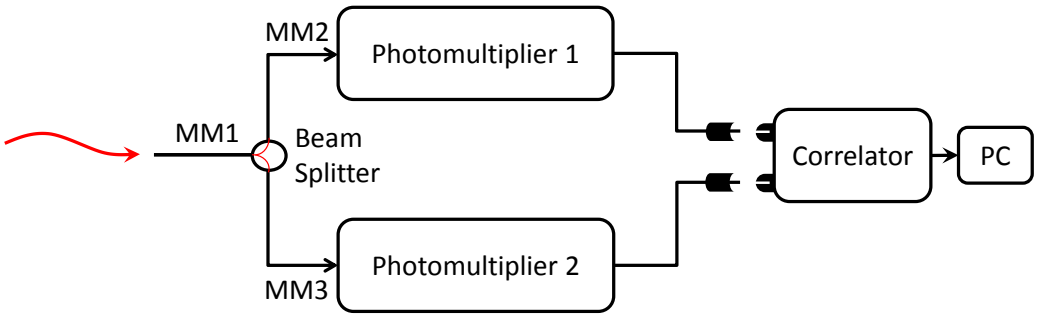

Figure 2.21: Pseudo Cross-Correlation: the scattered light is captured by a multi-mode fiber, passes through a beam splitter and it is directed towards two different single-photon detectors. The signal is sent to the multi-tau correlator and finally the autocorrelation function is displayed in a computer.

2.2.2.5 Environment control (nitrogen chamber, heating system and temperature measurement)

It has been shown that polymers such as polystyrene suffer strong oxidation and chain scissions (others can suffer cross-linking) if kept in relatively high temperatures (some few Kelvin above its T_g) for some hours under ambient air atmosphere, due to the exposure to oxygen [18]. In fact a whitening and further complete degradation of PS thin films on gold surfaces can be observed for samples kept in ambient air over few days ($\approx$ 2 days). On the other hand, no degradation was observed on the samples as in comparison to the ones measured in air after performing the same measurements under dry and filtered nitrogen atmosphere. This led to the decision of having an inert, filtered and dry atmosphere for all the experiments investigating the dynamics of supported thin films.

The gas-chamber consists of a half cylindrical quartz cell highly polished (roughness lower than $\frac{\lambda}{10}$ to avoid diffraction) normally used for light scattering experiments. A half cylinder was cut from the original cuvette piece and covers the sample completely.

Conventional polymers have a rather small range of relevant dynamical processes that can be observed within the DLS spectrum (processes as Brillouin or Raman scattering are out of the DLS time frame). Therefore a heating system for such setup should be able to bring the sample to approximately +200 °C in order to allow the investigation of the α-relaxation or processes related to the α-relaxation in a quite large family of polymers. On the other hand polymers such as polybutadiene (PB) or polyisoprene (PI)

need lower experimental working temperatures (≈ -100 °C) if one wants to observe the "glass-rubber transition" range.

For matching these requirements, a sample holder that heats the half cylinder lens and thus, the sample on top of it, was built. Heating takes place using heating cartridges. The temperature on the sample surface is monitored *in situ* by using a flat thermocouple type PT100 pressed directly onto the top of the thin films, close to the illuminated volume. The controlling system allows effective heating rates on the sample lower than 0.1 K/min. This is essential if a quasi-static temperature increase is required.

Cooling to temperatures much lower than ≈ 14 °C is in the present setup not possible, due to the condensation of water on the sample and on the quartz window. This procedure could be done by different means,*e.g.*, the use of a "Peltier cooler" or any kind of coolant as liquid nitrogen or a mixture of specific coolant substances that circulate the holder. Here, a circulation cavity inside the sample holder was built, which allows the future use of cooling fluids. The condensation of water vapor on the sample can be avoided by using an inert and dried atmosphere as dry and filtered nitrogen. In this case water could just condensate on the chamber window if its temperature goes lower than the condensation temperature of water. Here one could think about two solutions: to build a double window glass chamber and produce vacuum between both windows or a simpler choice, that is to heat up the glass window by blowing a hot gas on it (as nitrogen for instance) or even electrically (by means of resistors). These measurements in low temperatures were not done in the present work, but for future studies the latter option seems to be the ideal one since pumping a fluid trough the sample holder could produce undesired vibrations.

2.2.2.6 Index matching

Surface plasmons are excited at the interface between a metal layer (normally gold or silver) and a dielectric layer, which in our case is the polymer film. Smooth, thin films were obtained by spin-coating of dilute solutions on gold covered glass substrates. These gold covered glass substrates are finally optically index matched to the prisms. Optical matching is conventionally obtained by using a so-called "index matching oil" with well defined value of refractive index. However, for this application these kind of index matching cannot be used due to the thermo-instability of these materials and the heating induced expansion of the oil between the glass substrate and the prism (or half cylinder lens). This leads to "dewetting" of the index matching oil

and discontinuity of optical path.

A simple way to overcome this problem is to evaporate the metal layer directly onto the glass prism and then spin-coat the polymer film on top of it. However, this procedure is not recommended because the cleaning procedure to remove the polymer film and the gold layer causes the roughening of the glass surface, leading to a much lower quality of the layers in the next cycles. As high refractive index prisms are required for this study, the matching liquid has to have high refractive index (normally around 1.8 at 632.8 nm wavelength) in order to be used with *e.g.*, LaSFN9 prisms (n = 1.81 for λ = 632.8 nm).

This means the matching liquid has to be transparent, thermally stable, should not suffer dewetting due to thermal expansion and have high value of refractive index (polymers in general show refractive indexes between n = 1.4 and n = 1.6).

The only class of materials found that could match most of these needs are some special high refractive index ionic liquids that can be sometimes even mixed with others to precisely match the refractive index of the prism. However, to achieve simultaneously thermal stability and transparency in the desired wavelength is generally not feasible.

Another solution, for the case of studying ultrathin films, is the use of polymers as PDMS (polydimethylsiloxane) or any polymer from the silicone family for showing at room temperature low viscosity and refractive indexes that allow the measurement of reflectivity of ultrathin films. Thicker films however cannot be measured using this type of matching oil. This limitation comes from the fact that, the total internal reflection between PDMS and a LaSFN9 glass happens at incidence angle of approximately 50°, disabling the excitation of surface plasmons in high resonance angles, as it happens for thicker films.

Short chain materials as oligomers or some ionic liquids when used as index matching liquids have the advantage of improved mechanical properties due to their relatively high viscosity in comparison to the conventional matching oils. This avoids dewetting and keeps the continuity of the optical path. For this reason and also due to its relatively high refractive index (n ≈ 1.58), oligomer PS (M_w = 400 g/mol) was applied as index matching liquid. A consequence of the use of matching liquids having refractive indexes lower than both glasses (substrate and prism) is a set of undesired multiple reflections at the glass-matching liquid interfaces, Figure 2.22.

Multiple reflections are extremely prejudicial to SPR measurements: the

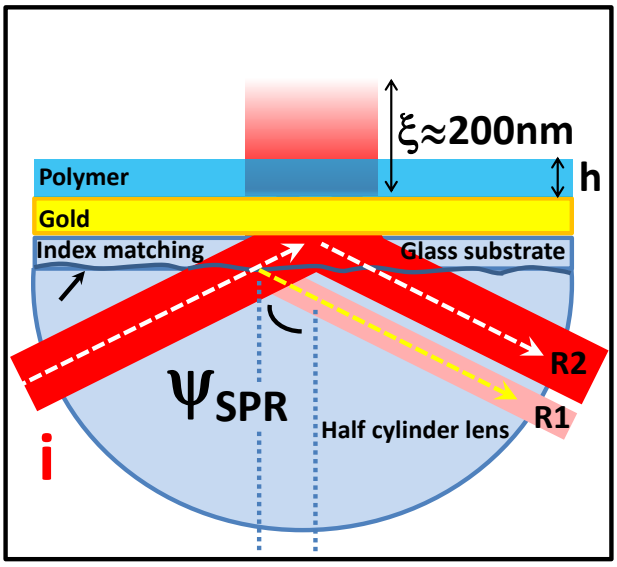

Figure 2.22: The incident beam (**i**) passes through the index matching liquid (PS 400 g/mol in this case) and reflects at each interface. Here just the relevant beams **R1** and **R2** are shown. **R1** happens due to the lower refractive index of the matching liquid in comparison to the glasses, $n_{matching} = 1.58$ and $n_{LaSFN9} = 1.81$ respectively (if the matching is perfect R1 does not exist).

photo-diode placed in **R2** is not collecting the proper amount of signal that would come out at a give incident angle (part of the intensity is lost in multiple-reflections); at high incidence angles, total internal reflection happens at the interface between the matching liquid and the prism, not allowing the beam to reach the gold surface and therefore avoiding the surface plasmon excitation.

The total internal reflection between PS 400 g/mol and LaSFN9 is shown in Figure 2.23. The curves are a simulation (done in WinSpall) showing the evolution of the reflectivity **R1** by increasing the incident angle. For a half cylinder lens made of LaSFN9 for example, at about 50° **R1** > 0, *i.e.*, interference fringes start being detected by the photo-diode. Therefore, to perform measurements at resonance angles $\Psi > 50°$ under these conditions turns out to be impossible (the same happens to triangular prisms at about 55°). Naturally, after the total internal reflection angles (Ψ_c) no light reaches the gold surface, *i.e.* **R2** is completely turned into **R1**.

Figure 2.23 shows that high resonance angles are impossible to be achieved

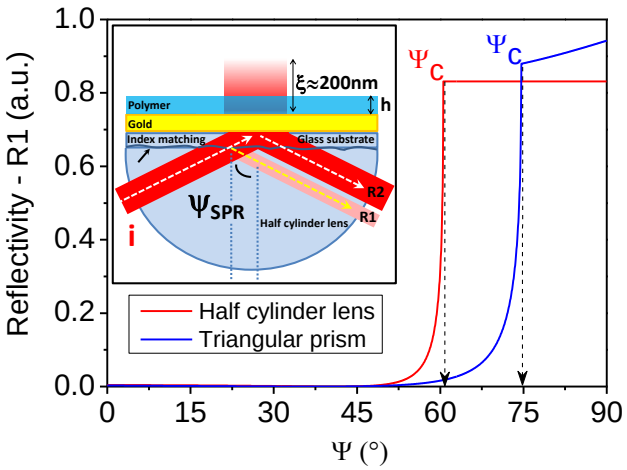

Figure 2.23: Reflectivity **R1** *vs.* incident angle. The red curve shows that by using PS 400 g/mol as index matching for LaSFN9 glass substrate and LaSFN9 half cylinder lens, the maximum resonance angle that can be exited without great problems is about 50°, while for a triangular prims it could be a bit higher, 55°. For angles higher than that, **R1** increases rapidly.

due to the scarce availability of matching liquids. A way to overcome this problem is to play with the prism geometry. As a conclusion, to shift the resonance angles to the lowest possible values is always wished. This can be achieved by:

- decreasing the film thickness. However, one could wish to study thicker films as well;
- measuring films of low refractive indexes. This restricts the number of materials that can be studied;
- using very high refractive index prisms. Unfortunately, there is a lack of materials with refractive indexes much higher than n = 2. These materials are generally extremely expensive in relation to normal glasses, and often brittle. Some of them are even birefringent, what is completely undesired in these measurements;

With these arguments, it seems that there are just two options when thicker films are the add-layer: to play with the geometry of the prism or evaporate gold directly on the top of the prism.

2.2.2.7 Prisms

SPR measurements are conventionally done by using prism coupling in the Kretschmann-Raether configuration (cf. section 2.1.2.2). In general 90° triangular prims are the main choice due to the easiness of aligning the SPR setup to the back reflection on the prism wall that takes place at exactly 45°, and therefore it enables an absolute alignment taking this angle as a reference point.

For the REDLS setup configuration used in this work, this kind of prism is not a good choice. Half cylinder lenses (Figure 2.24 - left) have the geometrical advantage that the spot **C** where light undergoes reflection coincides with the center of the goniometer. This makes the positioning of the photon detection (optical fiber) relatively simple. Once it is aligned, it remains fairly good positioned for a subsequent measurement in another scattering angle.

In the case of triangular prisms (Figure 2.24 - right) the same does not happen: the beam leaving the goniometer (pointing towards **C**), suffers refraction when it reaches the wall of the prism and meets an "off-Center" spot, **oC**. In this way, it is easy to show with a simple geometrical argument that there is no way to align a triangular prism so that the central spot on the prism coincides with the center of the goniometer **C** at all incident angles. In order to use such prisms one has to realign the optical fiber for each scattering angle.

Another issue concerning the prism geometry is that the surface plasmon resonance angles are different for different prism geometries (Figure 2.25). This is of fundamental importance due to the matching oil needed as mentioned before (to avoid multiple reflections and total internal reflection on the matching liquid layer) and the lack of materials with high refractive indexes for prisms (above $n = 2$ just some few materials are available but they are comparatively very expensive, and besides they are normally brittle).

Figure 2.25 shows that for PS films thicker than ≈ 50 nm the resonance angles are lower if one uses half cylinder lenses instead of triangular prisms. The advantage of triangular prisms for thinner films is fully irrelevant if one takes all facts into account.

As a conclusion, considering the total internal reflection and the resonance angles of different configurations, to measure films thicker than 60 nm with PS 400 g/mol as matching liquid, cannot be done. Instead, the gold layer should be directly evaporated on top of the prims (preferentially half cylinder lenses due to their lower resonance conditions, allowing a broader

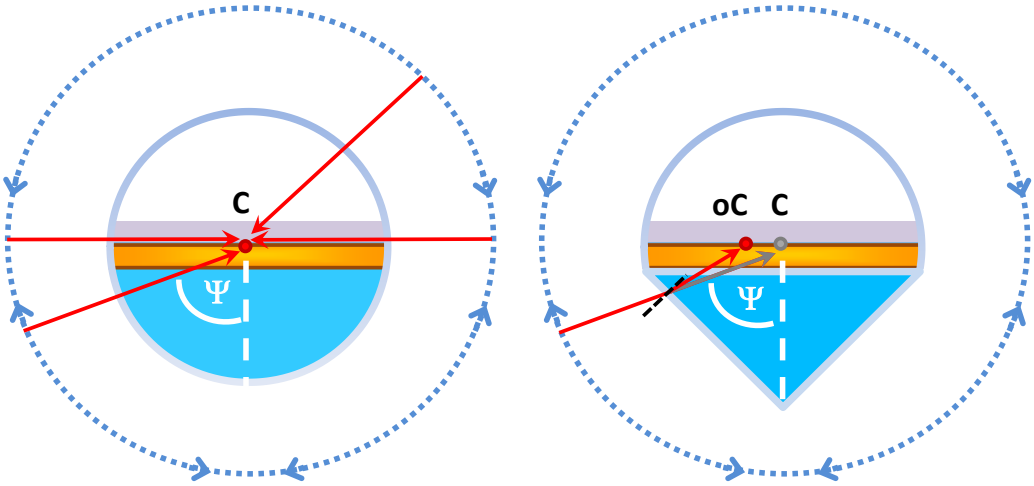

Figure 2.24: Half cylinder lenses *vs.* triangular prims: half cylinder lenses (left) allow the center of the prism to be concentric with the center of the goniometer. In this way the alignment procedure for DLS becomes simple as the optical fiber can be adjusted to the point **C** and stay at this position for any scattering angle. If the usual 90° prisms are used (right), it is geometrically simple to show that the center of the goniometer and the point C cannot coincide. The refracted beam reaches the off center spot **oC**.

range of thicknesses). Finally, half cylinder lenses show better performance than conventional triangular prisms concerning DLS alignment.

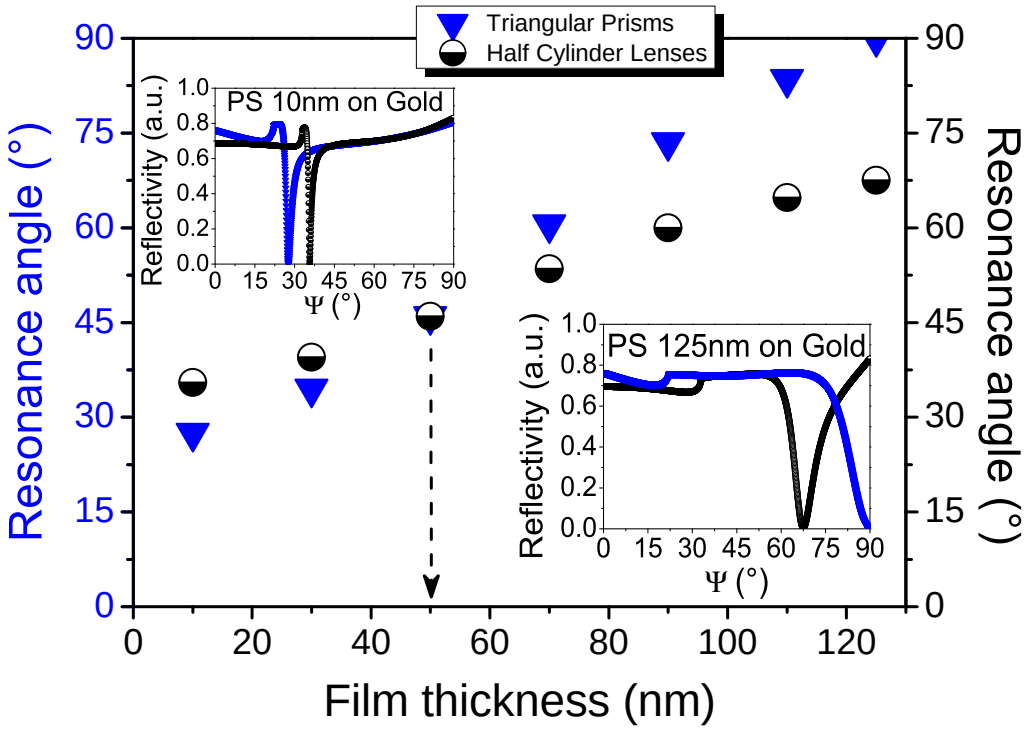

Figure 2.25: The resonance angle of different PS film thickness are plotted for a triangular prism and for a half cylinder lens. For films thicker than about 50 nm, half cylinder lenses deliver significantly lower resonance angles than the triangular prisms. The simulations take into account the gold layer, N_2 on top of PS, the prism and lens are made of LaSFN9 ($n_{LaSFN9} = 1.8$ for $\lambda = 632.8$ nm). The insets show simulations for the thicknesses of 10 nm and 125 nm. It can be seen that even by evaporating gold directly on top of the triangular prism (without the need of matching liquids) a maximum thickness of 125 nm can be studied. Half cylinder lenses afford basically any thickness for PS (the resonance angle goes asymptotically to 76.8° as revealed by simulations in WinSpall).

Chapter 3

Results & Discussion

REDLS has proven to be sensitive to the dynamics of polymer ultrathin films, specially at the polymer free-surface. The dynamics of the region is governed by the spectrum of surface waves, specifically thermally activated capillary waves. The central region of ultrathin films, defined as the space between the free-surface and the polymer-solid contact, delivers small but sufficient contrast in DLS, and therefore it was possible to resolve part of the dynamical processes from this region by REDLS. Dynamics of capillary waves are rich in valuable information about intrinsic properties of polymer ultrathin films, such as viscosity (η), shear modulus ($G'(\omega_{c.w.}, T)$), surface tension (γ), density (ρ), etc. Due to the extremely long accumulation time for a correlation function in such ultrathin film at a constant temperature, q, etc, only discrete curves of q-dependence, and activation plots were possible. This chapter treats the spectrum of relaxations experimentally observed by REDLS in polymer ultrathin films, showing a parallel to bulk polymer physics, and the theory of thermally activated capillary waves as described in Chapter 1.

3.1 Thin film dynamics by REDLS

3.1.1 Thin film T_g *vs.* bulk T_g

The T_g of bulk polymers can be determined by a number of techniques, such as *e.g.*, DSC, BDS, Rheology and many others. Here, the bulk T_g was determined by DSC for different heating rates and these values were compared to the T_g values obtained by kinetic-SPR from the polymer ultrathin films,

at corresponding heating rates. Kinetik-SPR is explained in Chapter 2.1.2.4. These experiments showed no deviations of the T_g of thin films in comparison to the bulk T_g value even for extremely thin films as of h = 8 nm thickness (PS M_w = 1821 g/mol), and h = 4 nm (PS M_w = 350 000 g/mol). These results for entangled PS are in perfect agreement with the work published in the literature [18–21, 23, 65]. The results on oligomers of styrene (PS 1821 g/mol) published in the present dissertation have no parallel in the literature due to the experimental difficulty in preparing such films with high surface quality and stability as the ones presented in this work.

Figure 3.1 shows the discontinuity in slope of a curve reflectivity *versus* temperature obtained by kinetic SPR. The dynamic T_g, *i.e.*, the T_g as a function of heating or cooling rate, takes place precisely at the same temperature than the T_g measured in bulk by DCS at those corresponding heating rates, as shown in the inset. The full red lines are linear fits in the glassy and liquid range of temperatures. The cross-over point is considered to be T_g. The estimated error bars in the inset are about the size of the symbols.

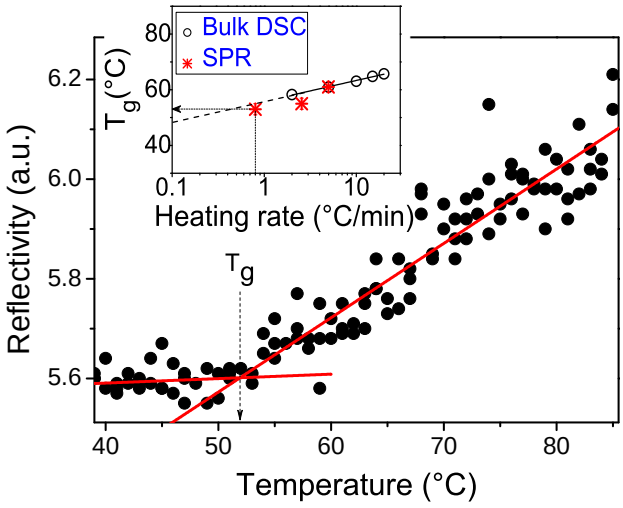

Figure 3.1: Reflectivity of a PS film (1821 g/mol, h = 8 nm) *versus* temperature. Constant heating rate of 0.8 K/min was used during the entire kinetic SPR experiment. T_g is considered to be the temperature at which the kink in the reflectivity curve appears. This kink reflects the change in expansion coefficient between glassy and liquid state. No shifts in T_g of thin films were observed when compared to the bulk calorimetric values at corresponding heating rates. Inset: ◯ - T_g by DSC in bulk; ✳ - SPR in a h = 8 nm PS 1821 g/mol.

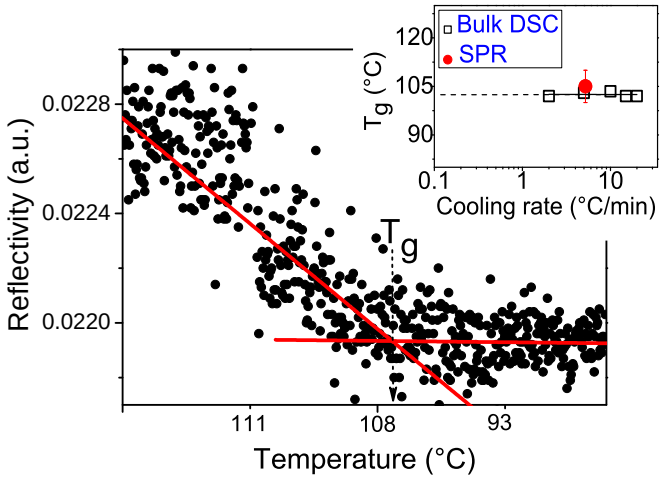

Figure 3.2: Reflectivity of a PS film (350 000 g/mol, h = 4 nm) *versus* temperature. Constant cooling rate of 5.2 K/min was used during the entire kinetic-SPR experiment. T_g is considered to be the temperature at which the kink in the reflectivity curve appears. This kink reflects the change in expansion coefficient between liquid and glassy state. No shifts in T_g of thin films were observed when compared to the bulk calorimetric values at corresponding cooling rates within the experimental error. Inset: □ - T_g by DSC in bulk; • - T_g kinetic-SPR in a h = 4 nm PS 350 000 g/mol.

3.1.2 Thermal expansion: thin films *vs.* bulk

When one plots volume *versus* temperature for a glass former material, regarding a range of temperatures from the glassy to the rubbery state, *i.e.*, from temperatures below T_g to temperatures above T_g, a change in behavior can be observed [25]. In both ranges, volume is a linear function of temperature, and a change in slope takes place at T_g. This finding is valid for a constant heating or cooling rate. The slope of such a curve in respect to the initial volume is the expansion coefficient β_V of the material being tested [136, 137]:

$$\beta_V = \frac{1}{V_0}\left(\frac{\partial V}{\partial T}\right)_p \tag{3.1}$$

This value represents how much a material expands when submitted to a certain increment in temperature, in comparison to the initial volume V_0. Another way of determining a one-dimensional or linear expansion coefficient (α_L) is to take the derivative of a curve thickness *versus* temperature, and compare to the initial thickness:

$$\alpha_L = \frac{1}{h_0}\left(\frac{\partial h}{\partial T}\right)_p \tag{3.2}$$

where $\beta_V = 3 \cdot \alpha_L$ for a cubic material [136].

From the Maxwell relations [138], it follows:

$$\beta_V = -\frac{1}{V}\left(\frac{\partial S}{\partial p}\right)_T \tag{3.3}$$

where V is the volume, S is the entropy and p the pressure. The index T indicates that the expansion coefficient is given at a constant temperature. Another form is:

$$\beta_V = \frac{1}{p}\left(\frac{\partial S}{\partial V}\right)_T \tag{3.4}$$

where $1/P = K$ is the volume compressibility. Finally one can extract [136]:

$$\beta_V = \frac{1}{V_0}\left(\frac{\partial V}{\partial T}\right)_p = K\left(\frac{\partial p}{\partial T}\right)_V = K\left(\frac{\partial S}{\partial V}\right)_T \tag{3.5}$$

When the material is cooled down, it suffers volume contraction.

What happens to the expansion coefficient of a supported polymer ultrathin film, is an important question kinetic-SPR might be able to answer. In principle the solid surface could hinder somehow the linear expansion, leading to values other than those of bulk material. On the other hand, one could suppose that ultrathin films show lower density than bulk material and therefore a change in thermal expansion is eventually possible.

However, some materials show negative expansion coefficients. An example is an oriented polymer film that suffers contraction when submitted to heating. This phenomenon happens due to entropic reasons [139]. Another reason why supported films could possess an expansion coefficient different from that of bulk, lays in the spin-coating method used to prepare the films. Films prepared by this method could show some degree of orientation despite annealing. It is well known and widely used in polymer engineering the negative thermal expansion (NTE) [136, 139, 140] of polymeric films as bi-oriented polypropylene among others. One explanation for the contraction during heating is that the polymer chains initially oriented are in a low entropy state, thus the chains are favored to relax towards a more "desorganized" state (of higher entropy) of smaller volume, due to the energetic increment [136, 139]. This can be explained by means of equation 3.4 [136, 139].

In this work, the linear expansion coefficient (α_L) of annealed PS ultrathin films (relaxed) were measured by kinetic SPR. The experimental value of the bulk volumetric expansion coefficient for PS 1821 g/mol, estimated at 25 °C ($T < T_g$), is about $\beta_V = 6.1\times10^{-4}$ K^{-1} [118]. The heating or cooling rate used were not specified in their publication. Considering that the linear expansion coefficient α_L is about one third of the volumetric expansion coefficient, β_V, then $\alpha_L = 2.03\times10^{-4}$ K^{-1}. In the present work, kinetic SPR experiments on PS 1821 g/mol, h = 8 nm, revealed linear expansion coefficient at $T < T_g$, $\alpha_L = 2.0\times10^{-4}$ K^{-1}, which is in perfect agreement with the bulk literature value at this range of temperatures. Therefore no variations of expansion coefficients were observed for long term annealed films within the experimental accuracy. The calculation of the thermal expansion coefficient is performed as follows:

Equation 3.2 gives the linear expansion coefficient. To calculate the variation of thickness, over a given range of temperatures, can be done by using equation 2.22, but instead of the theoretical proportionality term 0.91, one should use the experimental value 0.871, calculated in section 2.1.2.4. Therefore:

$$0.871 \cdot \frac{\partial h}{h} \approx \frac{-\partial \epsilon'}{\epsilon'} \tag{3.6}$$

From the reflectivity curve shown in Figure 3.1, four temperatures are selected, *i.e.*, two in the glassy and two in the liquid state: $T_1 = 39.01$ °C, $T_2 = 51.97$ °C, $T_3 = 62.47$ °C, $T_4 = 85.45$ °C. At these specific temperatures, by using equation 2.23, the refractive index and thus, the dielectric constants at the corresponding temperatures can be calculated here for $T<T_g$:

$$\epsilon_1' = n_1^2 = (1.5865)^2 = 2.5171 \quad for \quad T_1 = 39.01\ ^\circ C \tag{3.7}$$

$$\epsilon_2' = n_2^2 = (1.5847)^2 = 2.5114 \quad for \quad T_2 = 51.97\ ^\circ C \tag{3.8}$$

Thus:

$$\frac{\Delta\epsilon'}{\epsilon_1'} = \frac{2.5114 - 2.5171}{2.5171} = -2.26 \times 10^{-3} = -0.87 \cdot \frac{\Delta h}{h_1} \tag{3.9}$$

$$\frac{\Delta h}{h_1} = 2.6 \times 10^{-3} \tag{3.10}$$

The theoretical expansion coefficient for a PS 1821 g/mol for T<T_g (approaching the quasi-static value) becomes:

$$\alpha_L = \frac{1}{(51.97\ ^\circ C - 39.01\ ^\circ C)} \frac{\Delta h}{h_1} = 2.0 \times 10^{-4}\ K^{-1} \tag{3.11}$$

in good agreement with the experimental bulk value for the same polymer. Performing Fresnell calculations with WinsPall, allows to calculate the values of reflectivity, R_p at different temperatures as the values of thickness and dielectric constant can be calculated in each temperature. With this, the theoretical value of reflectivity change gives $\Delta R = 1.3{\times}10^{-3}$ a.u., while the experimental value gives ΔR =0.5602-0.5589= $1.3{\times}10^{-3}$ a.u., which is in perfect agreement with the experimental value within the error. Thus, one can confirm that in the glassy state, *i.e.*, T > T_g, no changes in thermal expansion coefficient due to chain orientation or confinement effects happened.

If the expansion coefficients are calculated from kinetic SPR without considering the contribution of the refractive index changes while heating, *i.e.*, by keeping $\Delta\epsilon' = 0$, then an error of about factor two takes place, cf. Table 3.1. The theoretical calculations of expansion coefficients based on the previous calculation procedure could not be performed for T > T_g due to scarce information about expansion coefficients in oligomeric melts.

Table 3.1: Expansion coefficients of PS 1.8 kg/mol, h = 8 nm. These values were calculated considering a constant refractive index while heating. This brings an error of about a factor 2. [a]The proper calculated value considering the variation of refractive index, n(T), during expansion is $2.0{\times}10^{-4}$ K^{-1}.

	$\alpha_L = \frac{1}{h_0} \cdot \frac{\Delta h}{\Delta T}(K^{-1})$	
Heating rate ($K{\cdot}min^{-1}$)	$T < T_g$ ($\times 10^{-4}$)	$T > T_g$ ($\times 10^{-3}$)
0.8	1.05[a]	1.97
4.9	1.3	9.5

3.1.3 The dynamical spectrum by REDLS

REDLS was applied to non-entangled and entangled polystyrene ultrathin films. The used molecular weights were: PS 1821 g/mol (PDI=1.078), PS 4389 g/mol (PDI=1.046), PS 9800 g/mol (PDI=1.057), PS 17690 g/mol

(PDI=1.03), PS 189 680 g/mol (PDI=1.05) and PS 350 000 g/mol (PDI=1.05). Most of the exhibited results however, are from PS 1821 g/mol. By means of REDLS, it was possible to test the theoretical predictions for capillary wave dynamics in such films and, therefore, verify the impact of solid surfaces on the dynamics of polymer ultrathin films. The spectrum of relaxations, *i.e.*, the heterodyne autocorrelation function G_1 (cf. equation 1.51), revealed two main processes:

(a) a slow-mode that follows the VFT behavior of the bulk viscosity (which is the same as the α-relaxation);

(b) a fast-mode with an Arrhenius temperature dependence of the relaxation-times.

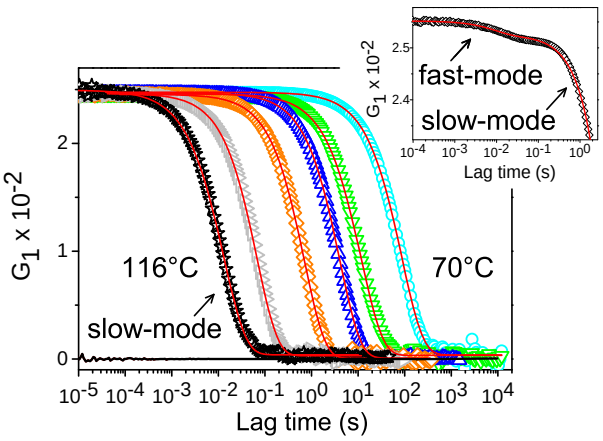

Figure 3.3: Characteristic heterodyne autocorrelation functions (G_1) for polymer ultrathin films. In this example, PS 1821 g/mol, h = 45 nm, showing the fast- and the slow-mode. By increasing temperature, both modes become faster, cf. section 3.1.4.3 and 3.1.6.3.

The labels "slow-mode" and "fast-mode" were given due to the different time scales at which these modes relax. The next sections deal with the characterization of these two modes, intending to define what each of them represent and how to extract valuable information from them. For this purpose, the following tests were performed:

1) **Total intensity of the scattered light *vs.* film thickness:**

This test allows to infer about the origin of the signals throughout the entire thickness, *i.e.*, if the mode is originated at the free-surface, at the central region of the film or at the polymer-solid interface. If the mode is originated throughout the whole thickness, then thick films should have higher signals than thin ones. On the other hand, if the mode is originated at the free-surface, thin films would have stronger signals than thick ones. This is due to the evanescent character of the optical field of surface plasmons. The intensity of the incident field decreases exponentially with distance to the solid surface. Finally, if a signal originates at the polymer-solid interface, then its intensity should be independent of the thickness, cf. Figure 3.5.

2) **Temperature dependence at a constant experimental q value and constant thickness:**

This tests if the temperature dependence of the relaxation times for a given mode follows an Arrhenius- or a VFT-type.

3) **Temperature dependence of the relaxation times performed for several thicknesses:**

This tests if there is thickness dependence of the relaxation times and, if yes, the functional law behind it.

4) **q-dependence of the relaxation times at constant temperature and thickness:**

The q-dependence gives important information about the physics of motion and helps to direct the interpretation about the physical nature of a given mode.

5) **q-dependence of the relaxation times for several thicknesses:**

This helps to understand the impact of thickness on the q-dependence, and therefore if the physics of motion suffers the effect of thickness.

6) **These experiments were performed, when possible, for all molecular weights mentioned at the beginning of this section:**

This test intends to verify scaling laws of the molecular weight.

This set of tests was performed for both, the slow and the fast-mode. Next these tests will be shown first for the slow-mode followed by the results from the fast-mode.

3.1.4 The slow-mode

3.1.4.1 Total intensity *vs.* film thickness

Figure 3.4 shows that I_{total} decreases three orders of magnitude by increasing the film thickness, h, from 17 nm to 440 nm. This confirms that the scattered signal that gives rise to the slow-mode is originated at the top free-surface since the surface plasmon shows an exponential decay throughout the film thickness.

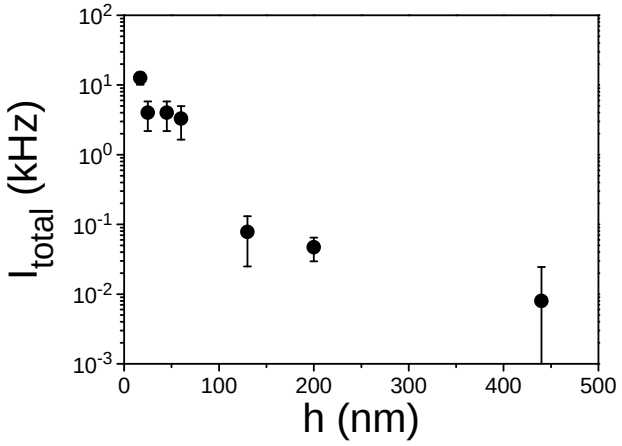

Figure 3.4: By increasing film thickness from 17 nm to 440 nm, the total scattered intensity decays over many decades. This implies that the slow-mode is originated at the polymer free-surface.

Figure 3.5 pictures the prediction that the free-surface of thinner films would scatter more than those of thicker films. In fact, if the film thickness, h, is much greater than the penetration depth of the surface plasmon wave (about 200 nm) the total scattered intensity should vanish (Figure 3.5-b).

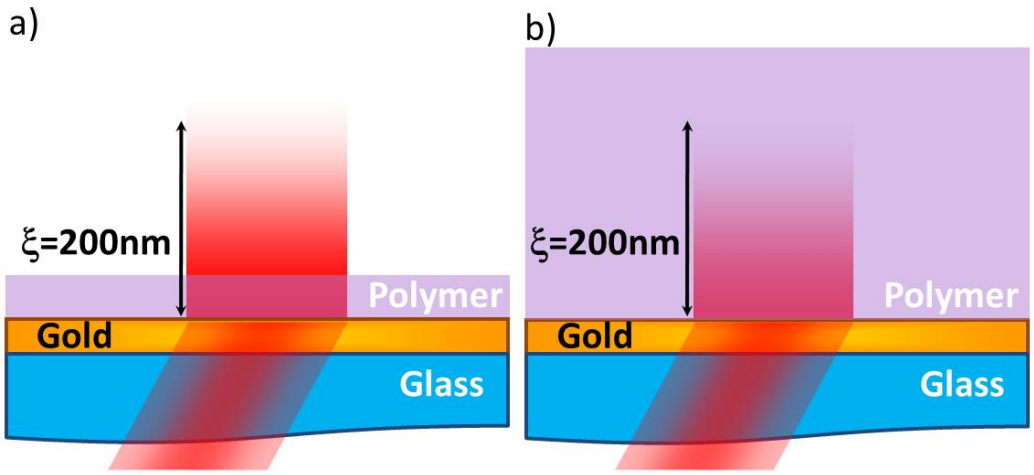

Figure 3.5: Thin *vs.* thick films: the evancescent character of the surface plasmons reveals that in the case of a free-surface mode, thinner films will scatter more than thicker ones. Intensity *vs.* thickness should follow approximately an exponential decay since the intensity or field of the surface plasmons decay exponentially with distance to the gold surface. That is exactly what happens in the case of the slow-mode.

3.1.4.2 Total intensity *vs.* modulus of scattering vector (q)

The aim of this experiment is not to characterize the static properties of the free-surface, by measuring the total scattered intensity as a function of q, but important informations can be extracted from such measurements, such as to get an idea about the size of the scattering centers in respect to the wavelength of light [121], cf. section 3.1.6.2. In Figure 3.6, the characteristic total scattered intensity of the slow-mode, against modulus of the scattering vector, I_{total} *vs.* q, delivers the information that the scattering centers responsible for the slow-mode do not behave as isolated localized scatterers as it is the case for the fast-mode (cf. section 3.1.6.2).

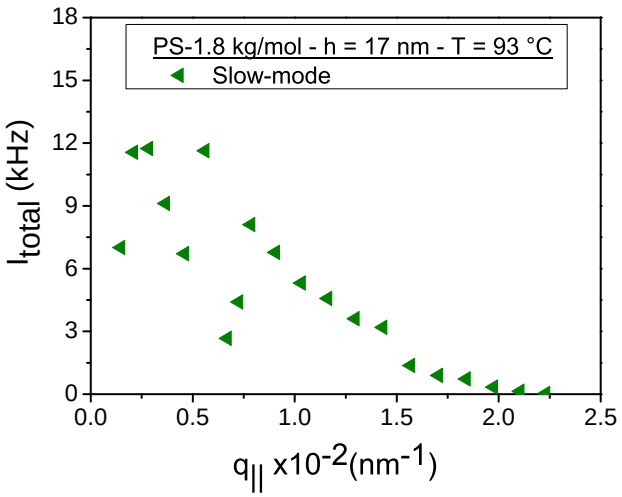

Figure 3.6: The total scattering intensity decreases by increasing the modulus of scattering vector.

3.1.4.3 Temperature-dependence

The heterodyne autocorrelation function, G_1, obtained by REDLS from the slow-mode is a single exponential decay (sometimes a β_{KWW} slightly different from the unity is needed to fit the data). Such a curve is shown in Figure 3.7. The temperature evolution of G_1 for the slow-mode is characterized by faster relaxation times at higher temperatures.

This type of curves were obtained from the small molecular weight polymers. In this example, they refer to the PS M_w = 1821 g/mol, h = 45 nm. It is hard to observe the slow-mode fully correlated in very high molecular weight polymers because the relaxation times become very long rendering the experiments unfeasible to be done. This is a first sight to the effect of viscosity on the slow-mode. As it will be further shown in section 3.1.5, the relaxation times of the slow-mode scale with the viscosity.

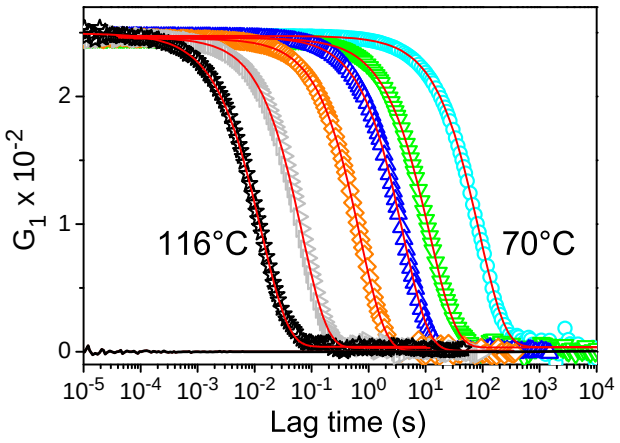

Figure 3.7: Evolution of the autocorrelation functions with increasing temperature in PS 1821 g/mol - h = 45 nm on gold. ◯ 70°C, ▽ 76 °C, △ 81 °C, ◇ 87 °C, ▷ 99 °C, ☆ 116°C. At 70 °C, the slow-mode shows relaxation times of the order of 10^2 s while at 116 °C, it becomes much faster and relaxes at times of the order of 10^{-2} s. The curves were collected at the scattering angle $\theta_s = 60°$ ($q_{||} = 1.57{\times}10^{-2}$ nm^{-1}). The bottom black full line is the baseline measured on bare gold.

3.1.4.4 Activation plot

The relaxation functions delivered by REDLS (Figure 3.7) can be fitted by equation 1.51, which requires ω_p = 0, and therefore, they are reduced to single-exponential functions. The relaxation times, τ, obtained in different temperatures at a constant q value (Figure 3.7), are plotted as a function of temperature in what is called "activation plot", Figure 3.8. For any film thickness, the activation plots for the slow-mode in PS 1821 g/mol display an approximate VFT temperature dependence of the relaxation times, cf. Figure 3.9.

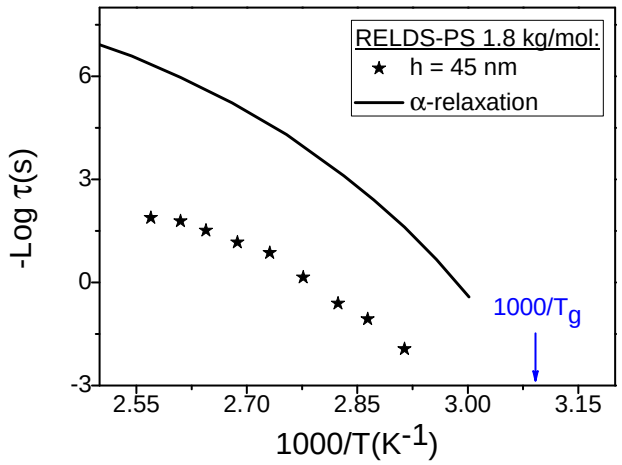

Figure 3.8: The relaxation time obtained in each temperature can be displayed in an Arrhenius plot, also called "activation plot". The slow-mode shows approximately a VFT behavior just as the bulk α-relaxation or bulk viscosity obtained by rheology.

3.1.4.5 Thickness-dependence

By decreasing the film thickness of a PS 1821 g/mol from h = 440 nm down to h = 25 nm, the relaxation times increase by about four orders of magnitude (Figure 3.9). An approximate parallel shift downwards from the bulk α-relaxation times (τ_α) measured by rheology means that the slow-mode on a h = 25 nm film relaxes about 10 000 times slower than on a film with thickness of h = 440 nm.

The total scattered intensity (I_{total}) decreases by about three orders of magnitude when the thickness is increased to 440 nm (Figure 3.4). This is the reason why just four data points are displayed in the graph for the thickness h = 440 nm. In fact, the correlation functions for this thickness show extremely small contrast, and therefore they could hardly be resolved.

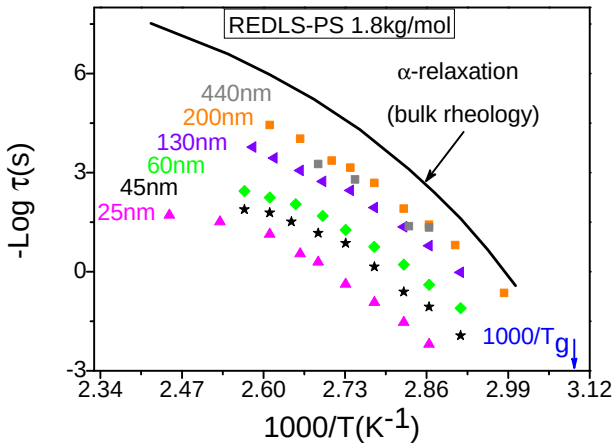

Figure 3.9: The slow-mode becomes slower by decreasing the film thickness (at a given constant temperature) starting from 440 nm down to 25 nm. The curves show the slow-mode in PS 1821 g/mol captured at the constant scattering angle $\theta_M = 60°$. The slow-mode has almost a parallel shift of the bulk viscosity (in this specific case not the viscosity but the bulk α-relaxation from rheology is displayed). For all thicknesses an approximate VFT behavior was observed.

3.1.4.6 q-dependence

As shown before, the intensity of scattered light detected in REDLS is originated at the free-surface of the thin films. Therefore, two possibilities for the calculation of the scattering vector $\mathbf{q}$ arise:

(a) the plasmonic field scatters at the last few nanometers close to the free-surface, suffers refraction, and finally reaches the detector that is placed at θ_M. In this case the "real" scattering angle is θ_P and therefore the scattering vector should be calculated based on the projection of the $\mathbf{q}^P$ vector parallel to the surface. This case is shown in figure 3.10a;

(b) the plasmonic field scatters exactly at the contour of the free-surface in all directions and the detector that is placed at θ_M captures the "real" scattering angle, *i.e.*, θ_M itself. Again the component of the scattering vector $\mathbf{q}^M$ parallel to the surface is taken. This is shown in 3.10b.

Experimental results have to be compared to the component of q parallel ($q_{\|}$) to the surface, as the theory of capillary waves is derived in these terms [47].

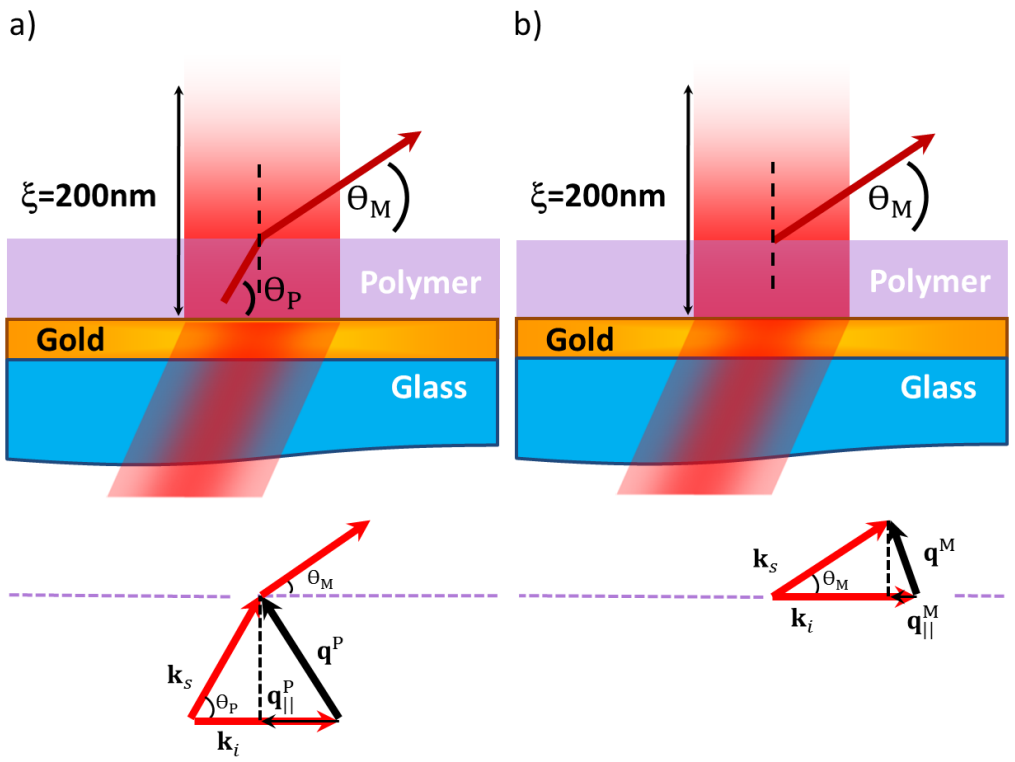

Figure 3.10: Scattering configuration. Two situations are possible: a) light scatters at the last few nanometers close to the free-surface, suffers refraction and the detector placed at θ_M actually observes light coming from θ_P. Case b) light scatters at the film contour in all directions, and the detector placed at θ_M captures signal coming from the actual scattering angle θ_M without the need of refraction to be considered.

Case a)

As the three vectors $\mathbf{k}_i, \mathbf{k}_s$ and $\mathbf{q}^M$ constitute an isosceles triangle:

$$|\mathbf{q}_{||}^P| = |\mathbf{q}^P| \cdot \cos\left(\frac{180° - \theta_P}{2}\right) = \frac{4\pi n_P}{\lambda_0} \cdot \sin^2\left(\frac{\theta_P}{2}\right) \tag{3.12}$$

where θ_P is calculate from the Snell-Descartes law:

$$n_P \cdot \sin(90° - \theta_P) = n_{N_2} \cdot \sin(90° - \theta_M) \tag{3.13}$$

therefore:

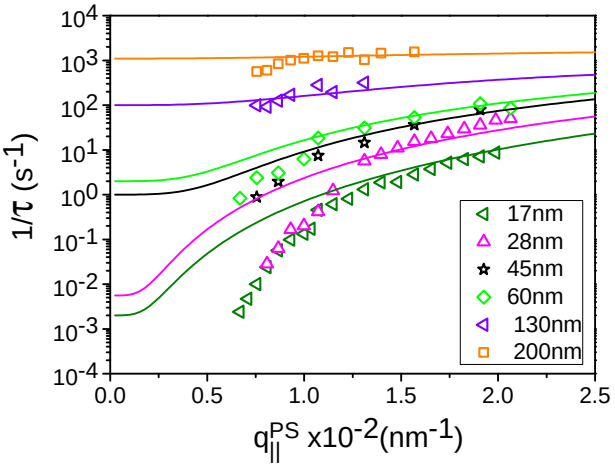

Figure 3.11: When one plots the q-dependence of the scattered light considering the theory of capillary waves, the parallel component of q has to be taken since the theory is derived for this case. A disagreement of the experimental data with the theory is observed when refraction is considered, cf.–case a) of Figure 3.10.

$$\theta_P = \arccos\left(\frac{n_{N_2} \cdot \cos(\theta_M)}{n_P}\right) \tag{3.14}$$

Case b)

The experimental $|\mathbf{q}^M|$ is defined as:

$$|\mathbf{q}^M| = |\mathbf{k}_s - \mathbf{k}_i| = \frac{4\pi n_P}{\lambda_0} \cdot \sin\left(\frac{\theta_M}{2}\right) \tag{3.15}$$

$$|\mathbf{q}_{||}^M| = |\mathbf{q}^M| \cdot \cos\left(\frac{180° - \theta_M}{2}\right) = \frac{4\pi n_P}{\lambda_0} \cdot \sin^2\left(\frac{\theta_M}{2}\right) \tag{3.16}$$

Experimental results show an agreement with the $q_{||}$-dependence predicted by the theory of thermally activated capillary waves when it is considered that light scatters at the contour of the film, *i.e.*, at the very last molecular layers (Figure 3.12). This is an even stronger argument supporting the fact that the slow-mode is originated at the polymer free-surface.

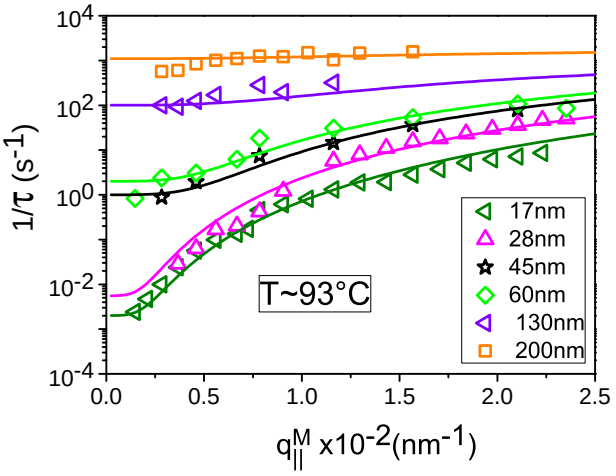

Figure 3.12: If the case b) is considered, *i.e.*, that light scatters exactly at the contour in all directions and the detector placed at θ_M captures light at the real scattering angle, the theory of capillary waves in viscoelastic media of arbitrary thickness is able to describe the experimental curve with good accuracy. The full curves are fits of the experimental data using the theoretical predictions for capillary waves at the corresponding thicknesses obtained at 93 °C.

3.1.4.7 M_w-dependence

In order to determine the M_w-dependence of the relaxation times in polystyrene thin films, several molecular weights were specifically selected in order to have a broad view of both, entangled and non-entangled polystyrene. The thickness was kept constant at h = 45 ± 1 nm for all molecular weights. The molecular weights selected for this study were: 1 821 g/mol, 4 389 g/mol, 7 669 g/mol, 9 800 g/mol, 17 690 g/mol, 189 680 g/mol and 350 000 g/mol.

The entanglement molecular weight for polystyrene is $M_e \approx 13500$ g/mol [44] and therefore the PS 17 690 g/mol is already within the transition range towards full entangled regime. The higher molecular weight polymers with molecular weight much greater than M_e (189 680 g/mol and 350 000 g/mol) showed a slow-mode with high relaxation times in the accessible range of temperatures. These modes were too slow to be resolved. Extremely high temperatures can lead to the destruction of the films, due to dewetting or even molecular degradation if the necessary thermal energy is given to the system.

This type of experiment is way more convenient for the determination

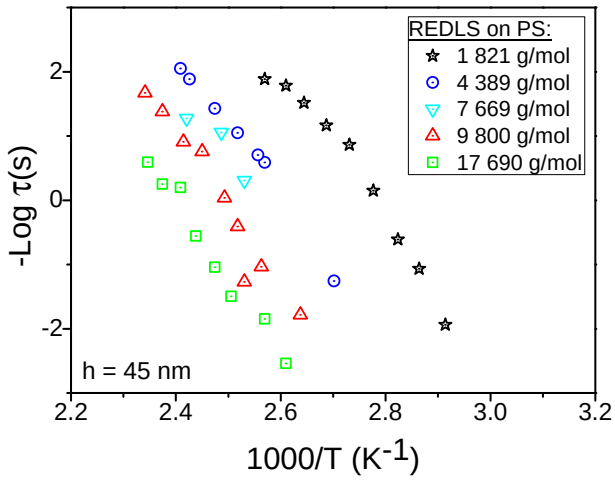

Figure 3.13: Slow-mode in PS, h = 45 nm: different molecular weights were tested. Higher molecular weights show slower relaxation times. This is an indication that the slow-mode scales with viscosity.

of the scaling laws in polymer ultrathin films than by plotting the viscosity as a function of molecular weight (Log η *vs.* Log M_w) for a huge number of molecular weights and taking the slope before and after the entanglement molecular weight for finally comparing to bulk values. Ideally this should deliver slope 1 and 3.4 before and after M_e respectively (equation 1.2 and equation 1.4).

The question whether or not under confinements or close to interfaces, the reptation or the Rouse diffusion of a polymer chain represented by the normal-mode changes, is also important. One could imagine that due to the influence of the solid surface, the chain reptation could change its dynamical behavior and therefore expand this changed property towards the whole film thickness. The present experiments lead to conclude that such a phenomenon does not take place down to h = 45 nm, as it will be further shown by comparing these experimental results with the theory of capillary waves, cf. Figure 3.16. If at all, just the extreme vicinity near the solid surface would be affected, considering that even films as thin as 17 nm do not show deviations from the bulk behavior, as shall be shown.

3.1.5 Capillary Waves *vs.* slow-mode

The slow-mode was revealed to be a free-surface mode. A single exponential function is required to fit the autocorrelation functions G_1 obtained by

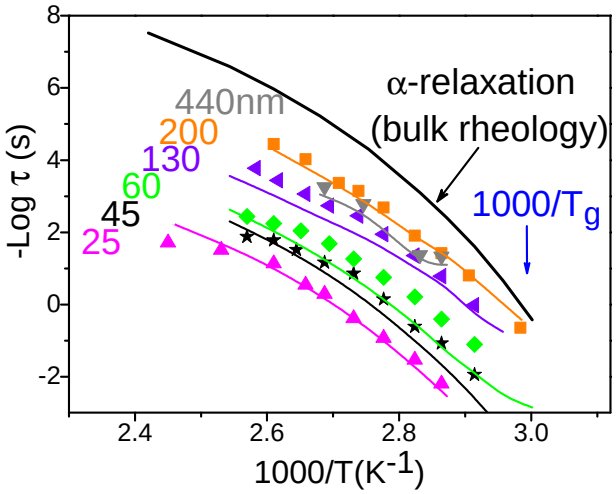

Figure 3.14: Temperature dependence of the slow-mode for several thicknesses: thinner films show relaxation times much greater than thick ones. A VFT-like behavior is observed for all thicknesses. Thick films show small contrast, therefore the slow-mode becomes barely indistinguishable above h = 200 nm. Bulk values of viscosity and storage shear modulus are required to describe the experimental data. Films that were not thoroughly annealed are faster than the theoretical predictions using bulk values of viscosity and shear modulus. Examples of this type are the 45 nm, 60 nm and 130 nm films.

REDLS. By increasing temperature, the relaxation times become smaller (*i.e.*, faster) following an approximate VFT temperature dependence. This mode suffers strong slowing down by decreasing film thickness. The corresponding VFT curve for each thickness is approximately a parallel shift of the bulk α-relaxation (or bulk viscosity) that depends on the thickness h, viscosity η, and storage shear modulus G'. Bulk viscosity and storage shear modulus values from rheology are required to interpret the data, using the theory of capillary waves given by equation 1.48.

$$\frac{1}{\tau(q_{\|})} \approx \frac{1}{\tau_0(q_{\|})} + \frac{G'(\omega,T)}{\eta(T)}$$

Thickness dependence is also obtained from capillary wave dynamics, with no-slip boundary conditions at the solid surface. The $q_{\|}$-dependence of the slow-mode ($1/\tau$ *vs.* $q_{\|}$) is well described by the $q_{\|}$-dependence of capillary waves dynamics, equation 1.48. From this test it comes out that

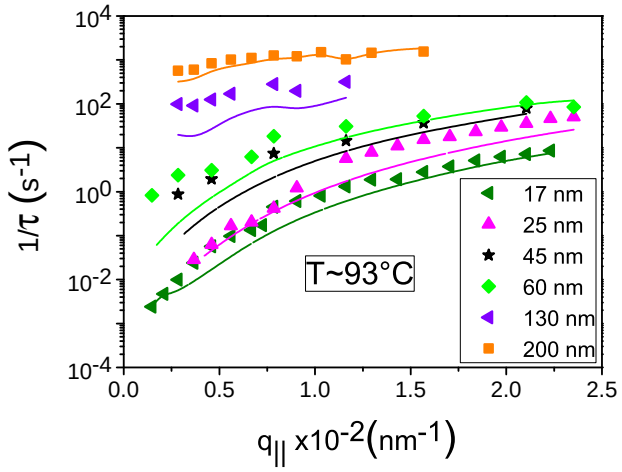

Figure 3.15: $q_{||}$-dependence of the slow-mode at T ≈ 93 °C: the physics of motion of this relaxation can be well described by the dispersion relations of capillary waves, equation 1.48. Again, bulk values of viscosity and storage shear modulus are necessary to describe the data. Films with remaining solvent show a decreased viscosity and therefore are faster than theoretical predictions. Even down to h = 17 nm, no deviations of the bulk properties were found, within the experimental error of REDLS. Films that were not thoroughly annealed, show decreased viscosity and shear modulus, being therefore faster than the theoretical expectations using bulk values for the physical properties at the corresponding temperature and frequencies. Examples of this type are the 45 nm, 60 nm, and 130 nm films. As the experimental frequency of the slow-mode is used to obtain the value of $G'(\omega, T)$, the theoretical full lines follow the shape of the experimental data, as *e.g.*, h = 130 nm.

apart of following the physics of capillary waves, just the very last molecular layers of the free-surface are involved in the scattering of light. High molecular weight polymers show a slow-mode with relaxation times greater than small molecular weight ones. For entangled PS (M_w = 189 680 g/mol and M_w = 350 000 g/mol), the autocorrelation functions obtained (even in very high temperatures, T ≈ 200 °C) were not fully correlated due to their extremely long relaxation times.

As a result of these comparisons between the behavior of the slow-mode and the dynamics of thermally activated capillary waves, it becomes evident that the slow-mode here observed is the manifestation of capillary waves on PS ultrathin films. Finally, as bulk values of viscosity and storage shear modulus described the experiments successfully, it is confirmed that the scaling

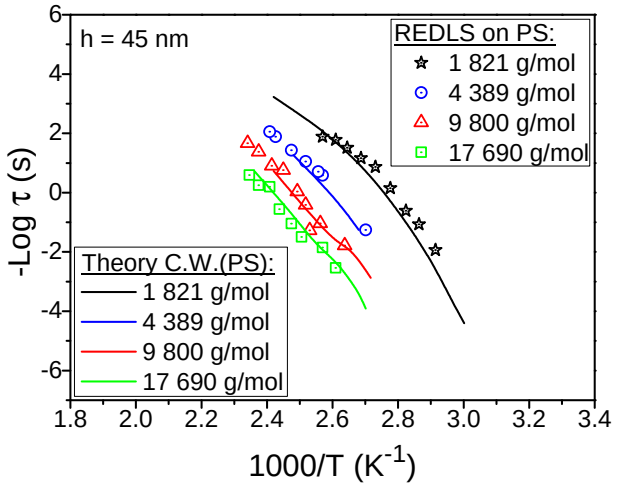

Figure 3.16: Slow-mode in PS: different molecular weights were tested. The theory of capillary waves describes accurately the slow-mode, when bulk values of viscosity, surface tension and shear modulus are considered. The higher the molecular weight, the higher the thermal stability of the film against dewetting. Therefore, high molecular weight polymer films can be submitted to more efficient annealing conditions.

laws valid for bulk material are also valid for supported polymer ultrathin films.

The behavior of shear modulus at the free-surface of polymer films: In this section, it was pointed out that bulk values of viscosity (η) and storage shear modulus ($G'(\omega$,T)) were necessary to describe the dynamical behavior of capillary waves on polystyrene ultrathin films. However, at exactly the same experimental physical conditions (temperature, pressure, material, etc), thinner films show capillary waves slower than thicker ones, up to a certain maximum frequency value, cf. Figure 1.4. The thickness dependence of capillary waves dynamics, $\omega_{c.w.}(h)$, is given by the term τ_0 in equation 1.48. Therefore, the probing frequencies, $\omega_{c.w.}(h)$, in thinner films are smaller than those in thicker films, leading to a thickness dependence of the observed storage shear modulus at the free-surface, $G'(\omega_{c.w.}(h), T)$. Thus, capillary waves when at the free-surface of thinner films feel storage modulus smaller than when at thicker films, cf. right-hand side of Figure 3.17. This must not be confused with the existence of anomalous storage shear moduli, due to confinement effects. The left-hand side of Figure 3.17 shows that the storage moduli, $G'(\omega$,T), of PS 1821 g/mol films of different thicknesses, are not

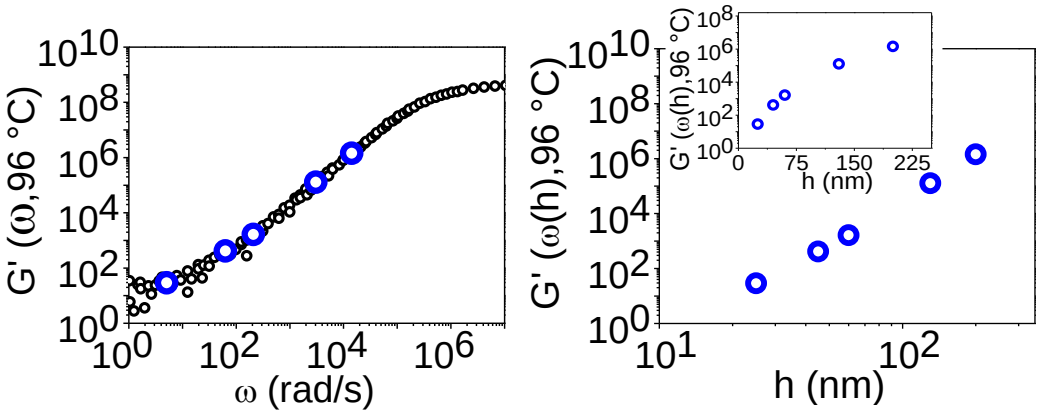

Figure 3.17: Left-hand side: frequency dependence of the storage shear modulus in bulk PS 1821 g/mol, measured by rheology (black open circles), and in PS 1821 g/mol thin films of different thicknesses (blue open circles). The film thickness increases with the frequency from h = 25 nm to h = 440 nm, corresponding to the right-hand side picture. A perfect agreement between bulk and thin films is found when the slow-mode is described by capillary waves dynamics. Right-hand side: thickness-dependence of the storage shear modulus in PS 1821 g/mol thin films at T = 96 °C.

anomalous, but exactly the same as the bulk values of storage shear modulus measured by rheology in bulk PS 1821 g/mol, *i.e.*, the frequency and temperature dependence of the shear modulus in bulk material is kept in ultrathin films. This result also confirms that the time-temperature superposition principle is valid in polystyrene ultrathin films.

A not commonly observed feature of the storage shear modulus appears at the free-surface when the film thickness is kept constant and the temperature varies. Figure 3.14, shows the activation plot for different film thicknesses of PS 1821 g/mol. What happens if one keeps the film thickness constant, *e.g.*, 25 nm or 45 nm, and watches the behavior of $G'(\omega, T)$ over the corresponding VFT curve? By increasing temperature, $G'(\omega, T)$ **decreases**, but at the same time, the capillary wave frequency increases, therefore $G'(\omega, T)$ **increases**. The total effect of temperature on storage shear modulus is a sum of both contributions, so that the temperature term wins, and thus $G'(\omega, T)$ decreases by increasing temperature at constant thickness. This behavior is shown in Figure 3.18.

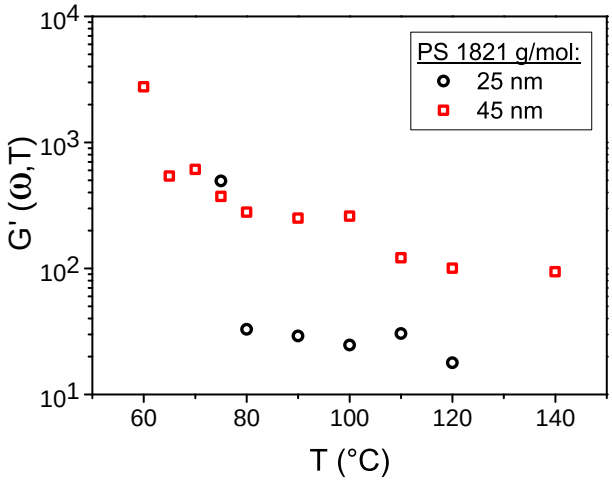

Figure 3.18: Temperature-dependence of the storage modulus, $G^{'}(\omega(T),T)$, in PS 1821 g/mol. As the temperature increases, $G^{'}(\omega(T),T)$ decreases. When the temperature approaches $T_g \approx 50$ °C, $G^{'}(\omega(T),T)$ approaches the glassy shear modulus.

3.1.6 The fast-mode

3.1.6.1 Total intensity *vs.* film thickness

Figure 3.19 shows that I_{total} increases with increasing film thickness h. This confirms that the scattered signal that gives rise to the fast-mode is originated across the entire film thickness, because the signal gets higher when the volume of material is increased. This is a signature of a bulk mode. Another confirmation is that one would expect from the signal of a bulk mode to decay to zero when the amount of material vanishes. This can also be observed as in Figure 3.19.

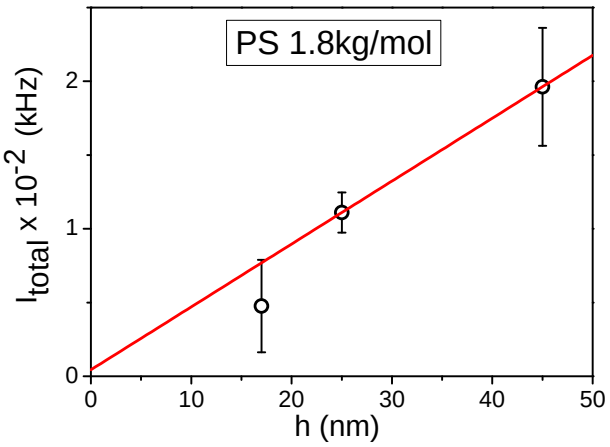

Figure 3.19: I_{total} of the fast-mode increases by increasing film thickness – the signature of a bulk mode. I_{total} is proportional to h and in this specific case is given by: $I_{total} = 4.3 \cdot 10^{-4} h$.

3.1.6.2 Total intensity *vs.* modulus of scattering vector (q)

In static light scattering, when the scattering centers are much smaller than the wavelength of light ($<< \lambda/20$), the total scattered intensity against the modulus of scattering vector, I_{total} *vs.* q, is a constant, *i.e.*, it does not depend on q [121]. The fast-mode shows q-independent scattered intensities, therefore it can be assumed to be a localized process.

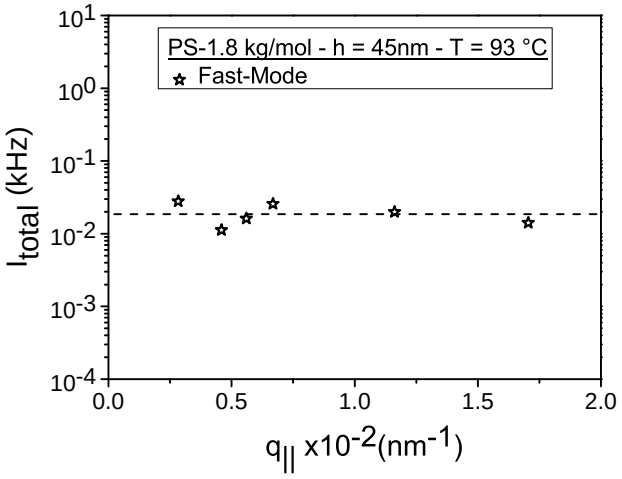

Figure 3.20: The total intensity against the scattering vector is, within the experimental error, constant in the studied q-range. This is the signature of a localized process.

3.1.6.3 Temperature-dependence

The fast-mode can be observed in temperatures much lower than T_g as shown in Figure 3.21 and Figure 3.23, where the bulk T_g of PS 350 000 g/mol is $T_g \approx 105$ °C and the fast-mode can be already detected at the temperature of approximately 30 °C.

For the non-entangled PS 1821 g/mol, the correlation function corresponding to the fast-mode is found on top of the one from the slow-mode, Figure 3.22. To avoid the overlapping of the correlation functions from both modes, the fast-mode of small molecular weight PS was mostly characterized at small scattering angles ($\theta_s = 35°$). Under these conditions the slow-mode is much slower due to its q-dependence, allowing the study of the fast-mode at low scattering angles.

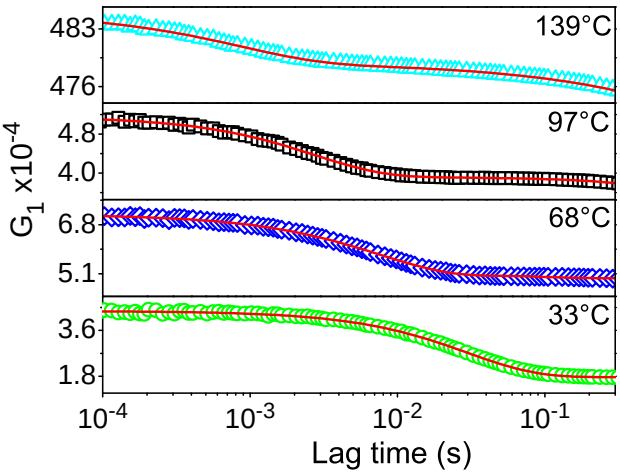

Figure 3.21: Fast-mode on PS 350 000 g/mol: even under the thin film T_g value (T_g = 105 °C), the fast-mode can be well detected. The initial decay of the slow-mode for this polymer can be seen in the right corner at T = 139 °C. The slow-mode, however, cannot be fully resolved due to its enormous relaxation times in PS 350 000 g/mol. Full red lines are single exponential fits.

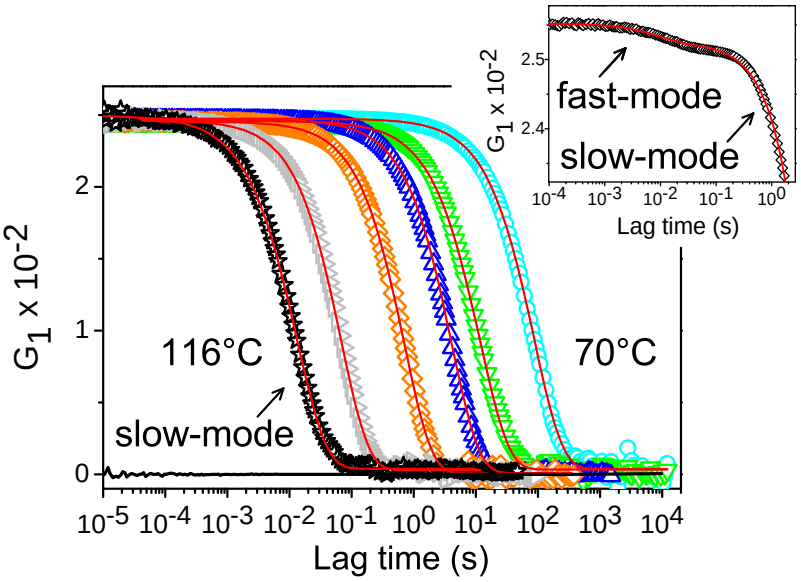

Figure 3.22: Fast-mode on the top of the slow-mode: the inset shows the typical form of the fast-mode showing a very small contrast in comparison to the slow-mode (main figure). This reflects the tiny amount of scattered light originated from the scatterers responsible for the fast-mode. The slow-mode was taken at $\theta_s = 60°$, and the fast-mode at $\theta_s = 35°$. Full red lines single exponential fits.

3.1.6.4 Activation plot

An activation plot of the fast-mode shows an Arrhenius temperature dependence of the relaxation times. The Arrhenius curve crosses the bulk α-relaxation without merging. Even at temperatures much smaller than T_g mobility related to this mode can be already detected.

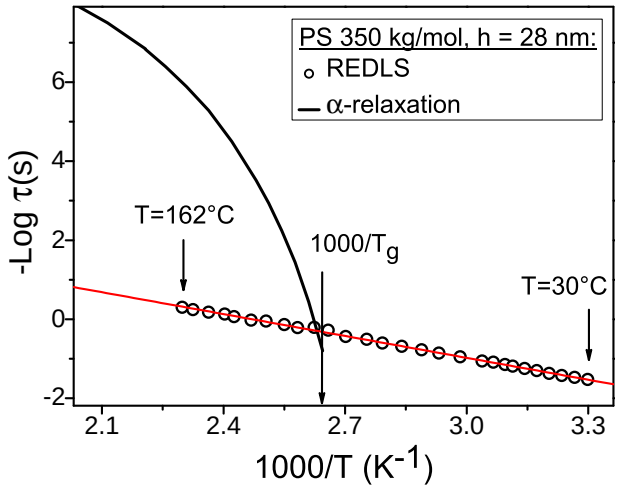

Figure 3.23: The activation plot of the fast-mode reveals its Arrhenius character. It crosses the bulk α-relaxation without merging (not showing the $\alpha-\beta$ bifurcation). At temperatures $T << T_g$, this process shows already mobility, confirming that it is a very localized process, as mobility is observed despite the small free-volume under T_g ($f_V \approx 2.5$ % at T_g, as calculated by Williams, Landel and Ferry after the evaluation of Doolittle's data [25].)

When the fast-mode crosses the bulk α-relaxation, a deviation from the Arrhenius behavior is observed, manifesting as a small bump at this crossover point. This happens due to the coupling of the fast-mode to the mobility of the α-relaxation. This effect can be observed better in Figure D.15, appendix D.2. This is another confirmation that the α-relaxation in thin ultrathin film gains mobility exactly at the same point as it does in bulk material, *i.e.*, T_g does not change in thin films.

3.1.6.5 Thickness-dependence

In order to determine if there is a thickness dependence of the fast-mode, one should perform a systematic series of experiments on this mode for several film thicknesses.With the annealing procedure performed in this work at the

time these films were prepared, the fast-mode could be observed solely for a few samples.

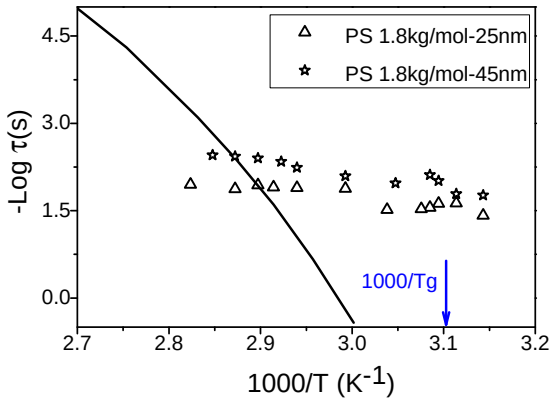

Figure 3.24: Fast-mode in PS 1821 g/mol, △–25 nm and ☆–45 nm). The fast-mode in oligomers also shows mobility at $T < T_g$ and no $\alpha-\beta$-bifurcation can be observed. The black line is the bulk α-relaxation, given by rheology measurements.

An apparent slowing down of the fast-mode by decreasing film thickness can be observed in Figure 3.24. However, instead of using confinement effects to explain this mode, another more convincing explanation for the general behavior of the fast-mode will be further given in section 3.1.10, where the self-diffusion characteristics of toluene in polystyrene is treated.

3.1.6.6 q-dependence

The q-dependence of the fast-mode can be approximated by a square power-law. This type of q-dependence is also observed for diffusive modes. However, deviations from a perfect square power-law implies that the physics of motion is not perfectly described by these diffusive laws, Figure 3.25.

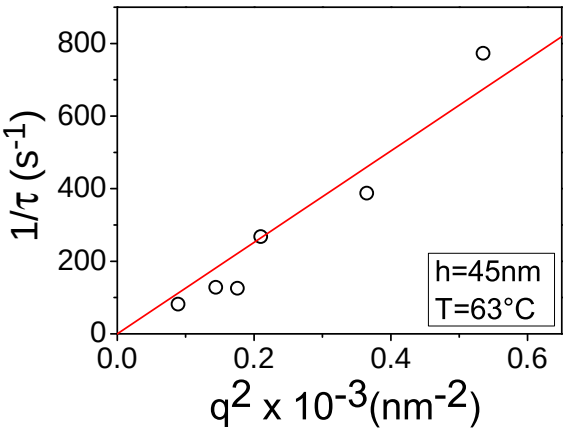

Figure 3.25: The q-dependence of the fast-mode in PS 1821 g/mol, h = 45 nm at T = 63 °C. A square power-law describes the data for low q values, within the experimental error.

3.1.6.7 M_w-dependence

Figure 3.26 shows the fast-mode for non-entangled (PS 1821 g/mol) and entangled (PS 350 000 g/mol) molecular weights. At a first sight, the fast-mode apparently suffers slowing down by increasing molecular weight. However, the non-annealed PS 189 680 g/mol also reveals relaxation times for the fast-mode at the same order of magnitude as the ones shown in PS 1821 g/mol, cp. Figure 3.27. Therefore, no systematic molecular weight dependence can be extracted from these few data points. In section 3.1.10 an explanation for the general behavior of the fast-mode will be given.

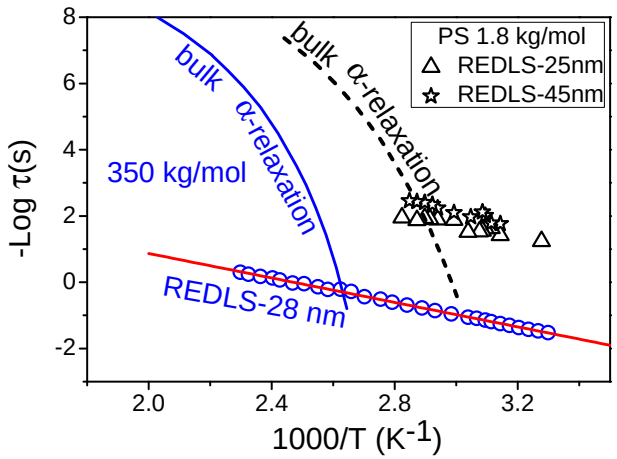

Figure 3.26: M_w-dependence of the fast-mode for different molecular weights. Arrhenius behavior is observed for all molecular weights. The fast-mode crosses the α-relaxation without merging in both molecular weights. The bulk α-relaxation was measured by rheology.

3.1.7 Effect of annealing on the fast-mode

The importance of annealing has been mentioned in Chapter 1. If no annealing is performed, T_g deviations (as other properties, *e.g.*, viscosity, elastic modulus, etc) will take place. However, oligomeric films such as PS 1821 g/mol, are sensitive to extreme annealing conditions, involving high temperatures and ultra-low vacuum. Therefore, to completely remove remaining solvent from such oligomeric films is extremely difficult. On the other hand, high molecular weight polymers tend to be more stable under these experimental conditions, allowing to achieve better annealed samples. Although complete solvent removal from oligomeric samples might not be possible, the amount of remaining solvent can be decreased to levels at which no T_g deviations can be observed, as shown in section 3.1.1.

Samples of entangled PS (M_w = 189 680 g/mol), thickness h = 50 nm, were annealed under vacuum (p < 1 mbar) at 150 °C for 36 hours. These annealed samples were compared to films prepared exactly under the same conditions, but without performing annealing. The final result is that, after annealing under these conditions, the fast-mode is no longer present in the REDLS spectra. Films that were not annealed showed a pronounced correlation function for the fast-mode, Figure 3.27. For non-annealed samples, instead of a single exponential autocorrelation function, stretched exponentials with $0.43 < \beta_{KWW} < 0.55$ were needed to describe the data.

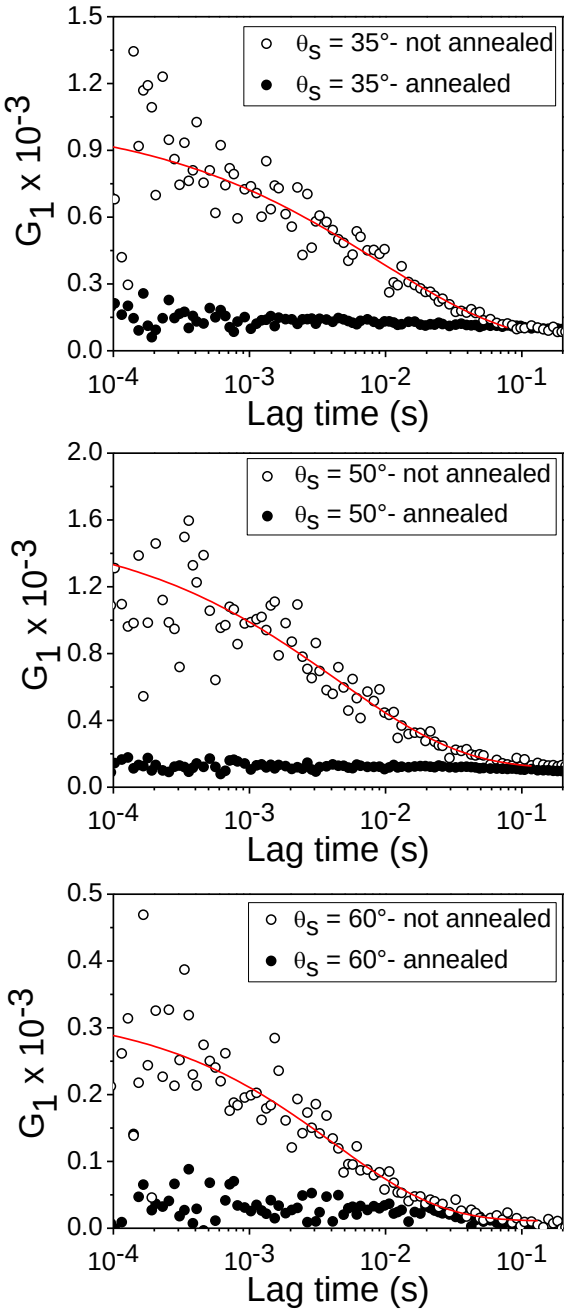

Figure 3.27: Annealed *vs.* not annealed samples of PS 189 680 g/mol, h = 50 nm. Thoroughly annealed samples do not show a fast-mode in their REDLS spectra. The red lines are KWW fits, with $0.43 < \beta_{KWW} < 0.55$, increasing with θ_s.

3.1.8 β-relaxation in polystyrene *vs.* fast-mode

The β- together with the γ- and δ-relaxation in polystyrene were earlier studied in the bulk material by several authors [25] using mechanical techniques as the torsion pendulum. The amplitudes, or strength levels of these peaks, are much smaller than the α-relaxation peak.

Illers *et al.* [141, 142] showed that the β-relaxation in polystyrene is only resolved at low frequencies. At frequencies higher than 40 cycles/s, the peak is merged into the α region. This kind of observation has led to the idea of an α-β-bifurcation, where both relaxations merge in high temperatures or high frequencies. They found apparent activation energies in the range of 146.5 to 167.5 kJ/(mol K) for the β-relaxation and suggested that this process is due to the motion of parts of the polymer chain in which the phenyl groups have less hindrance than that related to the whole chain.

Buchdahl and Nielsen [143] however, noted that the β peak would appear in the dynamical spectrum if the chain ends had bulky substituents or if low molecular weight polymers were present. Takayanagi [144] proposed that the β peak was due to the local relaxation mode of the twisting of main chains. Lee *et al.* [49] measured by DLS the β-relaxation in polystyrene and reported activation energy $E_a = 62.8$ kJ/(mol K). Boyer [145] noted a similar value for the crazing process in polystyrene and attributed the β-relaxation to be a stress-induced additional process. Lee, however, argued that the β-relaxation cannot be attributed to stress, because if this would be the case, this relaxation would not appear in his experiments.

Cavaille *et al.* [146] measured activation energy in polystyrene by dynamical mechanical thermal analysis (DMTA) and the activation energy obtained was given as 93.4 kJ/(mol K). **It was shown that the strength and even the presence of the β-peak in polystyrene depends upon its physical aging below T_g [147]**. It is important to note that in all these reports, the β-relaxation as well as the faster modes, shows Arrhenius-like temperature dependence.

More recently, Lupascu *et al.* [148], observed by BDS Arrhenius processes that show activation energies of the order of 80 kJ/(mol K), which cross the α-relaxation without merging in the so-called α-β-bifurcation point. They attributed these modes to the dynamics of T_2G_2 (trans-trans-gauche-gauche) helixes of different sizes in s-PS, and **noted that polymers that were not prepared from solvent casting did not show these modes**. They related this fact to the capability of solvents of inducing microstructures

in syndiotactic segments, therefore forming helix-like structures, which they claimed to be the responsible for the Arrhenius processes. More about this issue will be discussed in further sections.

From all these controversial values of activation energy, and inconsistent findings reported for the β-relaxation in polystyrene and to what this mode has been attributed to, it becomes clear that there is no well founded argumentation based on strong theoretical predictions to explain this mode. The inconsistency of the data reported also brings mistrust towards these types of relaxations. This opens up new questions regarding the nature of this relaxation as well as for the faster modes such as γ, δ, in polymers in general. Therefore it is useful to inquire and propose new ideas on this topic.

Based on the Arrhenius character and magnitude of relaxation times, just as on the activation energies, one could argue that the fast-mode detected by REDLS is the manifestation of the β-relaxation in polystyrene ultrathin films. The fast-mode shows in fact activation energies in the range 35-47 kJ/(mol K) in annealed samples, roughly half of the values normally reported for the β-relaxation in bulk material. Furthermore, different annealing conditions can modify the behavior of the fast-mode. **Thoroughly annealed samples do not show the fast-mode at all. It is as this mode could be completely erased from the REDLS spectra after being submitted to harsh annealing conditions**, *i.e.*, samples submitted to temperatures as high as $T_g + 50$ °C, under vacuum (p < 1 mbar) for more than 24 h. Samples that were annealed under less effective conditions show a fast-mode with shorter relaxation times (faster), cf. Figure 3.26. Even entangled polymers can show fast-mode having relaxation times as fast as for the case of oligomers, if no annealing was performed or if non-effective annealing conditions took place, cp. Figures 3.27 and 3.26. Finally, the fast-mode crosses the α-relaxation without merging.

In fact, as annealing conditions could change the behavior of the fast-mode or even delete it from the spectra when thoroughly annealed samples were investigated, a narrow similarity of both fast-mode and β-relaxation can be drawn, providing strong evidence that the observations earlier reported for the β-relaxation concerning its aging dependent behavior [147] are actually related to annealing as in our samples. Hence, it follows from the experiments presented herein that the β-relaxation can be deleted from the dynamical spectra of polystyrene through annealing just as the fast-mode. If this proves to be correct, this process does not refer to a hydrodynamic mode of polystyrene, and is not an intrinsic property of this material. Here stays the question: What is the nature of both, the fast-mode and the β-relaxation

in polystyrene?

3.1.9 T_2G_2 helix dynamics in polystyrene *vs.* fast-mode

Polystyrene can be synthesized using different polymerization conditions, as free-radical or anionic polymerization, so that its polydispersity and tacticity can be controlled [25]. The most commonly studied form of polystyrene is the atactic (or a-PS), that is taken for granted as the "amorph" polystyrene (Szwarc, 1960) due to the absence of crystalline peaks in X-ray diffraction experiments performed on this polymer. By using an organometallic (stereospecific) catalyst, isotactic polystyrene (i-PS) can be obtained, being a semi-crystalline polymer, with $T_m \approx 245$ °C (Sorensen and Campbell, 1961). The syndiotactic form of polystyrene can also be obtained, showing some degree of crystallinity as well.

Although it has being shown by NMR that a-PS contains a high fraction of syndiotactic sequences in its molecule [149], the localized semi-crystalline nature of a-PS is normally completely ignored or even not known by the majority of the authors studying a-PS. It was proposed that a-PS is better described by a prevailing syndiotactic configuration of at least eight aliphatic bonds in the trans conformation [150]. Apart from that it is also well known that solvents induce microstructures in s-PS in solution, which is naturally also true for the syndiotactic regions present in a-PS [148, 151].

In s-PS and a-PS T_2G_2 helices have been observed by MIR FTIR [148]. In the same work, dielectric losses revealed two extra Arrhenius processes apart of the main α-relaxation. These relaxations were attributed to the dynamics of helixes of different sizes and were labelled β_1 and β_2, being a faster and a slower activated process, respectively. Their activation energies were of the order of ≈ 80 kJ/(mol K) in all cases, but the β_1 process was about three orders of magnitude faster than β_2. **From the sample preparation procedures detailed in ref. [148], it is clear that different solvents remained in the sample, because annealing took place under T_g for short periods. The only sample that did not enter in contact with solvent, *i.e.*, it was molded by compression of the melt, did not show any Arrhenius process.**

Some reported values for the activation energy of the β-relaxation in bulk polystyrene show considerable agreement with these results obtained in ref. [148], which were also measured in relatively thick films (all h > 1 μm). The experimental dynamic loss data obtained by BDS in ref. [148] were fit by

the empirical Havriliak-Negami relaxation function. For this, the conduction-free dielectric loss was taken in order to eliminate the Ohmic conduction in the loss spectra [148]. Due to fit-dependent relaxation times, quite noisy Arrhenius processes were obtained in all cases.

Figure 3.28 is a collection of Arrhenius processes found in polystyrene in the literature including the ones measured by REDLS in entangled a-PS 350 000 g/mol–h = 28 nm and the non-entangled a-PS 1821 g/mol h = 25 nm and h = 45 nm. The Arrhenius processes found in these polymers by REDLS in ultrathin films show activation processes of about 35-47 kJ/mol, values that are around half of the activation energies reported for the β-relaxation in bulk material.

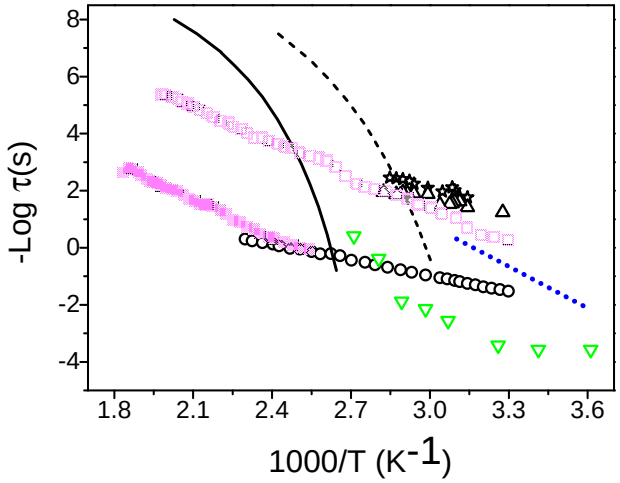

Figure 3.28: This picture is a collection of some of the Arrhenius processes in polystyrene found in the literature throughout the years. The VFT curves correspond to the bulk α-relaxation from PS 350 000 g/mol (–) and PS 1821 g/mol (- - -). The black Arrhenius curves are REDLS measurements for entangled and non-entangled polystyrene (PS 350 000 g/mol: ◯–h = 28 nm and PS 1821 g/mol: △–h = 25 nm, ☆–h = 45 nm). □–β_1-relaxation, ■–β_2-relaxation found by Lupascu et al. [148]. The common β-relaxation found in polystyrene [146] (• • •) is well in agreement with β_1, and both seem to be the manifestation of the same relaxation. ▽: free-surface dynamics reported by Fakhraai et al. [16].

In the work from Lupascu *et al.* [148], it is proposed that the Arrhenius modes β_1 and β_2 are due to the relaxation dynamics of T_2G_2 helical segments. If this was really the case, then it should be possible to erase both modes by heating the samples above the melting point of those crystalline regions.

This would require temperatures around 275 °C [148,152,153], which is about 1000/T = 1.82 in Figure 3.28.

From Figure 3.28 it becomes evident that the β_1-relaxation reported in ref. [148] is exactly the same common β-relaxation measured by DMTA in polystyrene. Therefore it should possible to delete the β_1-relaxation by heating the sample to values much lower than T_m, as reported by Cavaille *et al.* [146]. Lupascu *et al.* [148] reported however that, the samples were molded at temperatures up to 270 °C and the "helixes" were not destroyed. They gave two reasons for that: 1) the samples were not annealed for a long time at this temperature; 2) the films were clamped between two aluminium electrodes in a sandwich configuration, what they claimed to avoid the complete transformation of polymer chains into the all-trans conformation (expected at such temperatures) [148].

The activation energies for the fast-mode in PS 1821 g/mol, just as the magnitude of the relaxation times at specific temperatures relates well with the β_1-relaxation, Figure 3.28. One could argue that both modes are the expressions of the same entity behaving similarly in different molecular weight polystyrenes. If this is the case, than it should be possible to delete the β_1 and β_2 modes from the dynamical spectra, just as it is possible for the fast-mode, in temperatures not higher than 150 °C, much below the melting point of the crystalline region in s-PS. This would imply that the β_1 and β_2 modes are not due to the dynamics of T_2G_2-helixes, but in fact it shows the thermal behavior of the fast-mode and the β-relaxation in PS, and can be erased at temperatures much lower than T_m.

3.1.10 Self diffusion of toluene in polystyrene *vs.* fast-mode

Considering that most of the polystyrene samples treated in the literature were prepared starting from a solution, it is important to look at possible remaining solvents present in these samples and their possible effects. As toluene is by far the most used solvent for polystyrene in these studies, let us focus attention to this specific case.

Good solvents are required for preparing samples in general, therefore one can also expect that solvent removal is a hard task, taking into account the strong interactions between polymer and solvent. The complete solvent removal may even be unlikely. If so, one has to ask whether or not and to which degree the remaining solvent changes the properties of polymers. It

is well known that remaining solvents work as plasticizers [25], decreasing T_g values in comparison to the bulk homopolymer. If a negligible amount of solvent is remaining in the polymeric mass, these effects might not be so evident.

Throughout the literature of thin polymer films (including recently published articles), one can find several examples where no annealing was performed [17, 72]. In bulk materials, the situation becomes even more critical, as it is expectable that trying to remove solvent of the inner part of a large polymeric mass by applying vacuum and high temperatures is even naive. Assuming that remaining solvent is likely to be present, even in tiny quantities, one should know what to expect from it.

Thermal diffusion of solvent is likely to take place. The behavior of toluene self-diffusion in polystyrene has been theoretically and experimentally regarded [154–157]. The free-volume theory of Vrentas and Duda (V&D) [154] was experimentally tested in ref. [156] by means of pulsed gradient spin echo nuclear magnetic resonance (PGSE) NMR. Different temperatures and polymer concentrations were studied. The temperature range tested was 25-115 °C and the concentration range 0.04-0.90 polymer weight fraction (*i.e.*, from dilute solutions to high polymer concentrations). Entangled polystyrene with M_w = 270 000 g/mol was used. Arrhenius behavior with activation energies ranging from 10.9-67.8 kJ/(mol K), were found for these different concentrations. Higher polymer concentrations showed higher activation energies and smaller values of diffusion coefficient. The following theoretical expression was compared with the data:

$$D = D^* exp\left(-\frac{E_a}{RT}\right) \cdot exp\left(-\frac{\gamma(\omega_1 V_1^* + \omega_2 \xi V_2^*)}{V_{FH}}\right) \tag{3.17}$$

where D^* is a fit parameter, E_a^* is the activation energy for moving the diffusing molecule from its initial environment to its destination (this is not the Arrhenius activation energy), R is the gas constant, T is the temperature, γ accounts for the fact that the same free volume is available to more than one molecule for diffusion and may take values ranging from 1/2 to 1, V^* is a critical volume (the volume of the diffusing species) of the solvent or polymer at 0 K, V_{FH} is the average free-volume available for diffusion in the mixture, ξ is the ratio of the solvent critical free-volume to that of the polymer jumping unit, ω is the mass fraction, and the subscripts 1 and 2 refer to the solvent and polymer, respectively. The ratio γ/V_{FH} can be determined from available free-volume parameters as follows:

$$\frac{V_{FH}}{\gamma} = \left(\frac{K_{11}}{\gamma}\right)\omega_1(K_{21} + T - T_{g1}) + \left(\frac{K_{12}}{\gamma}\right)\omega_2(K_{22} + T - T_{g2}) \tag{3.18}$$

where T is the temperature, T_g is the glass transition temperature, ω is the weight fraction and the subscripts 1 and 2 relate to the solvent and to the polymer, respectively. The K_{ij} constants are given by:

$$\frac{K_{11}}{\gamma} = 2V_1^\circ \alpha_1 \tag{3.19}$$

$$\frac{K_{12}}{\gamma} = \frac{V_2^*}{2.303 C_1 C_2} \tag{3.20}$$

$$K_{22} = C_2 \tag{3.21}$$

where V_1° is the molar volume of the solvent at the glass transition temperature, α_1 is the expansion coefficient of the solvent, C_1 and C_2 are the WLF constants. This theory showed good predictive capacity even for the higher polymer concentrations, after some parameters were optimized [156]. Solvent concentrations, as low as it might be the case in the present study, were not experimentally regarded though.

Table 3.2: values for the free volume parameters V&D

Constants	Values
K_{11}/γ	$1.57 \cdot 10^{-3} cm^3/(g\ K)$
K_{12}/γ	$5.82 \cdot 10^{-4} cm^3/(g\ K)$
$K_{21} - T_{g1}$	-90.5 K
$K_{22} - T_{g2}$	-327 K
V_1^*	0.917 cm^3/g
V_2^*	0.850 cm^3/g
E_a	0
ξ	0.536
D^*	$3.85 \cdot 10^{-4}\ cm^2/s$

Using equation 3.17 one can infer about the concentration of toluene in polystyrene if the diffusion coefficient D is known. This value can be estimated with some care, from the slope obtained in a curve $1/\tau$ *vs.* q^2, *i.e.*, from the q-dependence of the fast-mode. As an example, for a diffusion coefficient of about D $\approx 10^{-15}$ m^2/s, toluene concentrations of C $\approx$ 0.3 ppm are expected.

The free-volume theory of Vrentas and Duda [154, 157] predicts that high polymer concentrations will give higher Arrhenius activation energies and

lower diffusion coefficient values. From T_{g2}, one can also infer the toluene diffusion behavior in different molecular weights polymers. Small molecular weight polymers ($M<M_e$) show T_g values lower than the entangled T_g value, and also have higher free-volume [25]. Therefore, if two different molecular weight polymers have exactly the same solvent concentration, one should expect faster diffusion processes in smaller molecular weights.

One can summarize some characteristics of solvent diffusion:

- it is Arrhenius-like [157];
- times-scales depend on the polymer free-volume [157];
- Activation energies and time-scales depend on solvent concentration [157].

In summary, the diffusion characteristics of solvents in polymers can explain well the fast-mode and even the β-relaxation behavior in polystyrene samples. Better annealed samples would lead to lower solvent concentrations. This also explains why the fast-mode vanishes after thorough annealing is performed. Different activation energies reported for Arrhenius processes, would result from different remaining solvent concentrations. The dynamics found by Lupascu *et al.* is also well explained by self diffusion of toluene in PS rather than due to the dynamics of T_2G_2 helixes. The possibility of changing the dynamic behavior of the β-relaxation in bulk polystyrene by annealing, even enabling to erase this mode from dynamical spectra, as reported in ref. [146], can also be explained as being the diffusion of remaining solvent.

3.1.11 "Highly mobile" free-surface in polystyrene: fact or fiction?

One of the most referred reasons for T_g anomalies in polymer ultrathin films is a high mobility of the free-surface, expanding its enhanced mobility towards the central region of the thin films, decreasing T_g (cf. section 1.1.2.2). The theory of capillary waves describes precisely the slow-mode in well annealed samples, using bulk values of viscosity and shear modulus, as can be observed in Figure 3.16. Considering the perfect agreement between the theory and experiments, it is possible to affirm that the dynamics of the free-surface is not Arrhenius-like as claimed by many authors [16, 17], but VFT, and is

not enhanced in comparison to bulk material, since bulk values were used to theoretically calculate the free-surface dynamics. On the other hand, films that could not be thoroughly annealed due to their intrinsic thermal instability, such as some oligomeric films, presented enhanced free-surface mobility, as can be seen in the PS 1821 g/mol, h = 45, 60, and 130 nm, Figure 3.14 and 3.15. Thinner films, submitted to better annealing conditions as the PS 1821 g/mol, h = 17 and 25 nm, were well in agreement with the theory within the experimental error, Figures 3.14 and 3.15. If the enhanced mobility was a real physical change, it should be seen in the thinner films as well, having even a stronger effect than in thick ones. The reason for a better agreement with the theory for higher molecular weight polymers, as in Figure 3.16, is that these films show higher temperature stability and therefore they could be annealed under better conditions (T_g+50 °C, under vacuum –p<1 mbar–, for about 36 hours).

A highly mobile free-surface, which expands its mobility to the central region of the film, decreasing T_g can be therefore discarded. On the other hand, the existence of a free-surface with a little higher mobility, without impacting on the films T_g, cannot be completely excluded on the basis of the statistical accuracy of REDLS and the mathematical model used to describe the experimental data. In case of existence of a more mobile free-surface in polymer ultrathin films, this region cannot exceed the very last molecular layers (monomers), considering the length scale of capillary waves and the good agreement of theory and experiments. This enhanced mobility cannot also be completely discrepant in comparison to the capillary waves dynamics.

3.1.12 Other relaxations found

Two main relaxations were found in REDLS spectra, the slow and the fast-mode. However, under specific physical conditions, other relaxations appear. When thin films are measured at temperatures much lower than their T_g, as the case shown in Figure 3.29, an extremely slow propagating wave with frequency $\omega_p \approx 0.12$ rad/s, *i.e.*, $f \approx 0.019$ Hz, can be observed, as revealed in the REDLS spectrum. This type of relaxation was found in several molecular weights, but its full characterization was not possible, because this mode suddenly fades away by increasing temperature. The q-dependence characterization of this mode is also not simple, as the mode is not present for all values of scattering vector observed, vanishing in a non-systematic way.

It is important to point out that the relaxation shown in Figure 3.29 cannot be, in any case, the manifestation of propagating capillary waves.

At temperatures much lower than T_g, the viscosity is infinitely high and, therefore, all capillary waves are expected to be overdamped, cf. Chapter 1. Propagating waves are expected to appear in the q-range accessible to the REDLS experiment when the viscosity becomes too low, *i.e.*, by increasing temperature above T_g, they should first manifest as overdamped waves, and when the viscosity becomes small enough, then propagating capillary waves may appear, cf. section 1.2.3.2.

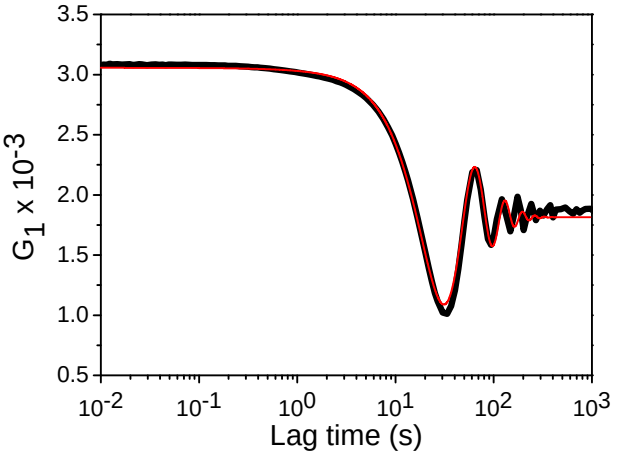

Figure 3.29: Black curve: relaxation observed in PS 4 389 g/mol, h = 45 nm at T = 24 °C, $\theta_s = 60°$. The red line is a fit function with the type of equation 1.50.

In contrast to capillary waves, surface waves such as sound waves, become slower by increasing temperature, due to diminishing stiffness, as predicted by the Newton-Laplace equation [158]:

$$c_L = \sqrt{\frac{E(1-\psi)}{\rho(1+\psi)(1-2\psi)}} \tag{3.22}$$

where, c_L is the longitudinal velocity of propagation of sound waves in a medium of Young modulus (or stiffness) E, density ρ, and ψ the Poisson's ratio. The transversal velocity component is given by:

$$c_T = \sqrt{\frac{G}{\rho}} \tag{3.23}$$

where G is the shear modulus. By substituting the glassy modulus of polystyrene

($G'_g \approx 1.5$ GPa) and the density $\rho = 1050$ kg/m^3, ones finds [159]:

$$c_T \approx \sqrt{\frac{1.5\ GPa}{1.05 \times 10^3\ kg/m^3}} \approx 1200\ m/s \tag{3.24}$$

With $c = \lambda f$, where f is frequency in the range of GHz, the wavelength of such elastic waves should be in the nm range. Considering the low apparent propagating frequency, f = 0.019 Hz, one gets a wavelength $c_T/\mathrm{f} = \lambda \approx 63$ km ! Therefore, it is not possible that this type of relaxation observed is the manifestation of such elastic waves. A conclusive answer about the nature of such waves cannot be driven so far, as the full characterization of this mode was not possible.

Another type of relaxation that is found in some REDLS spectra is shown in the right side of the dashed line in Figure 3.30. The q-dependence of this mode revealed to be non-systematic. This relaxation seems to appear often in high viscous and relatively stiff materials, as it can be observed in PS 189 680 g/mol and 350 000 g/mol and not often in PS 1821 g/mol. The shape of the curves cannot be fitted by a stretched exponential. The slow-mode appears in these polymers at longer times than this mode shows, *i.e.*, this undefined mode, from now on labeled as "x-mode", has in general relaxation times between the fast and the slow-mode, but at high temperatures the slow-mode can overlap with the x-mode, cf. 3.31. The x-mode is temperature independent, and it should not be confused with the α-relaxation just due to the apparent q-independence of the relaxation times, because it does not fulfill the features of the α-relaxation, as for example the VFT temperature-dependence of the relaxation times, and to show relaxations described by a stretched exponential with $\beta_{KWW} = 0.4$, cf. section 3.1.13.

As the x-mode seems to behave similarly in different molecular weight polystyrene samples, different thicknesses, temperatures and scattering vectors, one can imagine that the x-mode is not a polymer film mode, but some external excitations that are not absorbed by the insulation system. An explanation why it appears in high viscous systems, and not in low viscous ones, is possibly because low viscosity systems are able to absorb and damp these external excitations, while high viscous materials couple with the external fluctuations. The x-mode relaxes at about $\tau \approx 1$ s, which is likely to be due to vibrations of the building or laboratory. The x-mode is not due to the intrinsic self-correlation generated by single-mode optical fibers, due to the Fabry-Perot effect, cf. Chapter 2.2.2.2. Throughout this entire work, multi-mode fibers were used to avoid this effect, and the base-line for this configuration is shown in Figure 2.20.

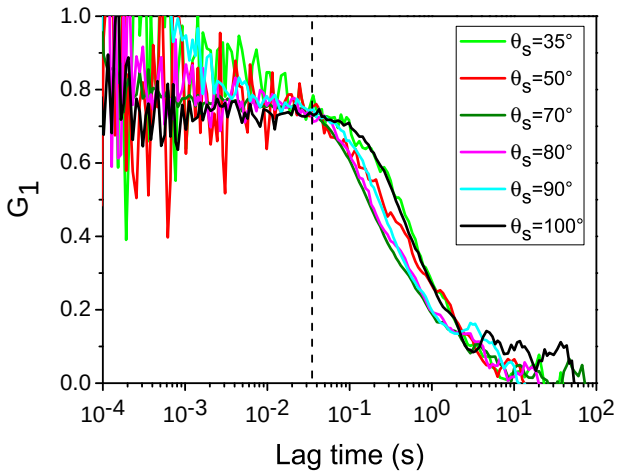

Figure 3.30: This relaxation appears in higher times-scales than the fast-mode. For non-annealed films of PS 189 680 g/mol, h = 50 nm, T = 63 °C, the fast-mode appears in the left side of the dashed line.

All these low frequency relaxations are possibly originated by external sources, which cannot be absorbed by the active anti-vibration table as this insulation system starts its insulation activity at frequencies around 1 Hz and higher, cf. Chapter 2.2.2.1.

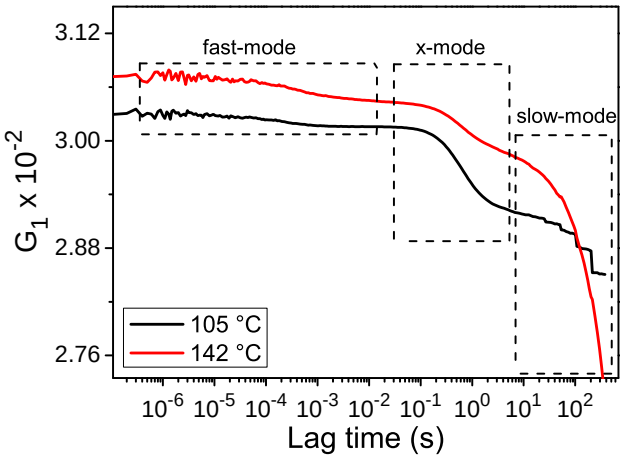

Figure 3.31: PS 350 000 g/mol, h = 28 nm, $\theta_s = 60°$. Between the fast and the slow-mode, one can observe the x-mode, which is temperature independent. The slow-mode becomes faster in higher temperatures and overlaps with the x-mode in high temperatures. The slow-mode in PS 350 000 g/mol could not be fully resolved even in high temperatures due to the high viscosity of this polymer.

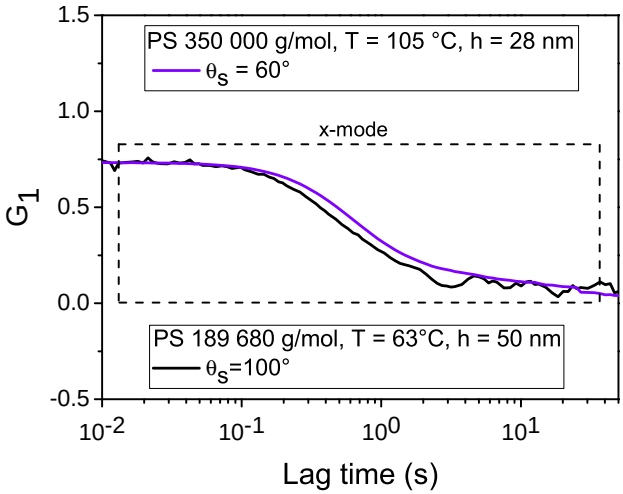

Figure 3.32: Here the x-mode is compared in two polymers at completely different physical conditions. Even though, in both cases this mode behaves similarly, being independent of q, thickness, molecular weight and temperature.

3.1.13 The α-relaxation in polystyrene

The α-relaxation could not be directly identified in any correlation function obtained by REDLS. Such a relaxation in PS would deliver a stretched exponential with $\beta_{KWW} = 0.4$, it should be q-independent in the range of DLS and the relaxation times against temperature in an activation plot would deliver a VFT curve [54]. These characteristics exclude the slow-mode and fast-mode to be the manifestation of the α-relaxation in polystyrene ultrathin-films.

A reason why the α-relaxation does not appear in the REDLS spectra of thin films is that the scattering volumes studied as well as the scattering intensities expected from this mode are too small to be resolved in this configuration. This relaxation is attributed to the reorientational motion of chain segments, what explains why the contrast levels observed by REDLS are expected to be so small. The glass transition however, could be studied at different cooling or heating rates down to h = 4 nm in PS by means of thermal expansion determined by kinetic SPR. This is an indirect way of studying the α-relaxation behavior in such systems.

3.1.14 REDLS *vs.* X-PCS

X-PCS is a well established technique and has been for many years successfully applied to study the dynamics of capillary waves. The theoretical advantages of REDLS over X-PCS were mentioned in 2.1.4.1.

REDLS proved experimentally to deliver the same type of dynamic information as X-PCS does, with an extra advantage of being sensitive to the dynamics of the central region of the film and possibly to the polymer-solid contact in some systems. REDLS does not lead to sample destruction as the latter does, and does not have all the inconvenience of using a technique that requires a considerably high infra-structure level, as X-PCS does. Therefore, REDLS shows definitely a higher performance over X-PCS regarding these studies. One could, however, argue that the length-scales probed in the q range by X-PCS and by REDLS are not equivalent. This is actually a wrong idea influenced by analyzing solely the wavelengths of both techniques without caring about the different physical geometries involved. X-PCS requires total external reflection configurations, what implies in an upper limit for the q value, and one should keep in mind that very low scattering vectors lead to extremely large relaxation times, implying in a lower limit for the q value. This restricts considerably the absolute value of q-vectors probed, *i.e.*, practically, both techniques work in the similar range

of $q_{\parallel}$ in dynamic experiments (actually the REDLS window is a bit larger) – REDLS: 1.4×10^{-3} nm$^{-1} < q_{\parallel} < 2.5 \times 10^{-2}$ nm^{-1}, while X-PCS measures dynamics in the range: 3×10^{-3} nm$^{-1} < q_{\parallel} < 1 \times 10^{-2}$ nm^{-1}, as can be seen in refs. [82, 98].

3.1.15 Glass transition, surface tension, shear modulus and viscosity measurements by REDLS

It is important to be able to fully characterize polymer ultrathin films. The glass transition (T_g), viscosity (η), elastic moduli (G, E, K, etc) and the surface tension (γ) are of main interest. Nowadays, few techniques can deliver such informations in the length scales studied in the present work (starting from h = 17 nm to h = 440 nm). Using waveguides in the WEDLS configuration (cf. Chapter 4.1) even thicker films can be characterized. As mentioned in section 3.1.14, X-PCS is able to deliver some informations about these properties, but the technique is rather expensive, requires facilities not easily available, and is a destructive technique. AFM is able to deliver some information about these properties, but the experiments are mostly model dependent and the error bars involved are quite large. Thus, REDLS is a powerful technological tool to characterize supported polymer ultrathin films. Next, it will be summarized how the characterization of such properties by REDLS is made possible.

The dynamic glass transition temperature can be characterized as described in section 3.1.1. The absolute value of surface tension does not play a strong role on the dynamics as shown in Chapter 1.2.4.4. Therefore, the characterization of this property in thin films can be conventionally performed (*e.g.*, as described in ref. [102]). From equation 1.48, it can be observed that three unknown parameters, $\eta(\omega, T)$, $G'(\omega, T)$, and the thickness h, have to be determined. The thickness h is directly delivered by SPR, which is a technique coupled to REDLS anyhow. Two parameters remain unknown ($\eta(\omega, T)$ and $G'(\omega, T)$), therefore one of both have to be determined in order to achieve the proper values of the other. For materials where the viscosity is practically frequency independent in the range of frequencies tested, as the case of low molecular weight polymers, a simple trick can be applied: as the dynamics in thinner films become slower (*i.e.*, low frequencies), the thickness can be chosen to be small enough so that the shear modulus $G'(\omega = 0, T) \approx 0$. This happens because at very low frequencies, the shear modulus goes to zero, for any temperature in the liquid state. Therefore, in an ultrathin film of oligomers, just the effect of the viscosity ($\eta(T)$, the zero-shear viscosity)

plays a role. For thicker films, the zero shear viscosity dependence on temperature, $\eta(T)$, is exactly the same as for ultrathin films, as shown in this work. This allows the determination of $G'(\omega, T)$. Following these steps, any oligomeric film in the liquid state can be fully characterized by REDLS. For the case of entangled polymers, where the viscosity is also frequency dependent and decreases with increasing frequency, the situation is more complex but valuable information can be extracted by measuring ultrathin films and thick films. Ultrathin films will show capillary waves with low frequencies, therefore, the shear modulus goes to zero, while the viscosity goes to the zero shear viscosity. By measuring a thick film, the opposite situation happens, and the shear modulus at high frequencies can be determined, since the viscosity decreases to zero at high frequencies. The ability of determining these properties at such tiny volumes with the REDLS precision, was never achieved by any other experimental technique so far.

3.1.16 Overview on polymer ultrathin films dynamics

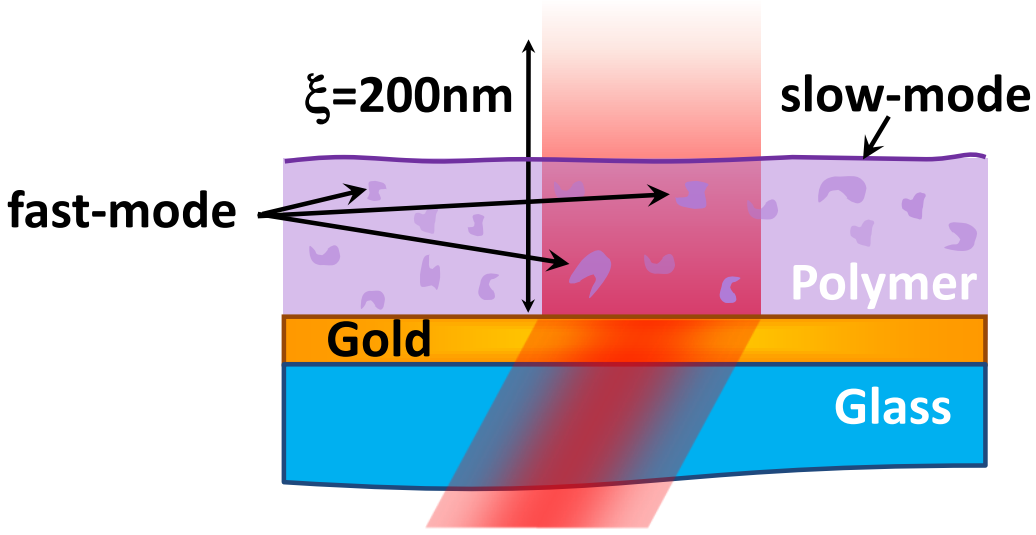

Figure 3.33: Schematic representation of the slow-mode originated at the free-surface and, the fast-mode at the central region of the film. The chart does not necessarily represents the reality in terms of sizes of the density fluctuations in the central region of the film corresponding to the fast-mode and length scales of the slow-mode.

Figure 3.34 is a collection containing the main aspects of the relaxation spectra related to the slow- and fast-mode, found in supported polystyrene

thin films measured by REDLS. Next, a description summarizing all of the results in Figure 3.34, corresponding to the previous sections, is given.

REDLS experiments were performed on PS with M_w = 1821 g/mol (in **D** also M_w = 350 000 g/mol and inset of **B** 189 680 g/mol) varying temperature (T), film thickness (h), and scattering angle (θ_s). **A**: T-dependence (◯ 70°C, ▽ 76 °C, △ 81 °C, ◇ 87 °C, ▷ 99 °C, ☆ 116°C) of $G_1(q,T,t)$ at θ_s = 60° (q = 1.57×10^{-2} nm^{-1}), h = 45 nm. Black line: baseline on bare gold. Red lines: single exponential fits. **B**: G_1 magnified to highlight the fast-mode at θ_s = 35° (q = 9.44×10 3 nm^{-1}), T = 48 °C, and h = 45 nm. Red line: fit of sum of two single exponentials. Inset of **B**: PS Mw = 189 680 g/mol, h = 50 nm, T = 63 °C, $G_1(q,T,t)$ at θ_s = 60°, (q = 1.57×10^{-2} nm^{-1}) thoroughly annealed (▲) compared to non-annealed sample (•). **C**: -Log(τ_{cw}) obtained for the slow-mode *versus* 1000/T for films of different thicknesses. The corresponding lines are theoretical predictions for capillary wave dynamics given by equation 1.48. **D**: Fast-mode (Arrhenius-like) in entangled and non-entangled films with E_a = 35 and 47 kJ/(mol K) respectively, crossing the bulk α-relaxation without merging. Mobility can be already detected at $T << T_g$. **E**: Total scattered intensity (I_{total}) of the slow-mode *versus* film thickness reveals its origin at the free-surface. **F**: In this case, I_{total} is proportional to h: I_{total} = 4.3×$10^{-4}h$. I_{total} of the fast-mode increases by increasing film thickness – the signature of a bulk mode. **G**: q-dependence of the slow-mode at T = 92 °C. The lines are theoretical descriptions of capillary wave dynamics given by equation 1.48. **H**: q-dependence of the fast-mode h = 45 nm, T = 63 °C.

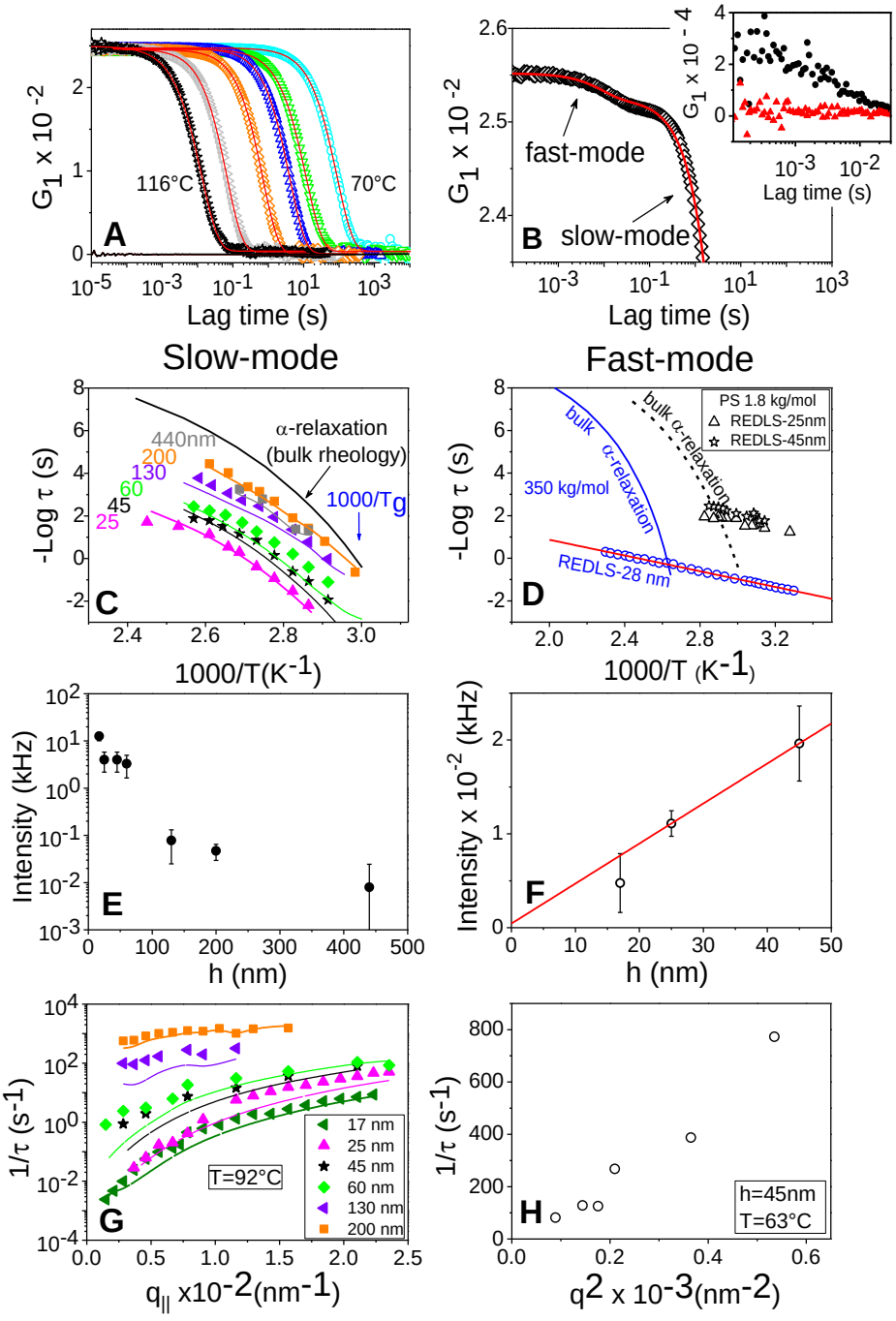

Figure 3.34: This picture is a summary of the most important aspects of the main relaxations found in polymer ultrathin films.

Chapter 4

Final Conclusions & Remarks

Polymer ultrathin films, both supported and free standing have gained tremendous industrial and scientific importance in the last decades. Nano-devices, membranes, coatings, nanocomposites, foams, and a variety of other systems, where interfaces and confinements play a relevant role, are on focus of interest. Polymer physics at the interfacial level, as well as under confinement geometries is a relatively new field within the context of condensed matter physics. To understand the relations between structure, morphology, processing, and their impact on the final properties of materials, is the basis of materials sciences. Therefore, new tools that are able to characterize efficiently different properties of materials, in these resolution levels, are necessary and welcome. REDLS was successfully applied to resolve dynamical processes of the three characteristic regions of supported polymer ultrathin films: the free-surface, the polymer-solid interface and the central region of the films.

The slow-mode is originated at the free-surface and shows VFT temperature dependence of the relaxation times. It is attributed to overdamped, thermally activated capillary waves and is fully described by the theory derived by Jäckle [47], with a form similar to the one proposed by Jiang *et al.* [82], which is analogous to the theory derived by Herminghaus [81]. These theories were here corrected though, by taking the storage shear modulus, $G'(\omega, T)$, instead of the Young modulus, E, as proposed by Herminghaus [81], or the real, frequency independent storage shear modulus, μ, as proposed by Jiang *et al.* [82]. The latter theory had to be adapted to describe the data: the frequency independent shear modulus μ is substituted by the storage modulus $G'(\omega, T)$. Bulk values of viscosity, and storage modulus directly obtained by rheology from the here used polymers were needed to describe the dynamics

of thoroughly annealed thin films.

Based on the sub-nanometer length scale of the amplitudes of capillary waves for these systems, and the full agreement between theory and experiment revealing a VFT free-surface dynamics, the possible existence of an anomalous high mobility at the free-surface becomes restricted and cannot extend to more than a few monomers, if at all. Consequently, these results ultimately drop the old idea of a "liquid-like" free-surface, having Arrhenius behavior, normally used to explain the T_g anomalies found in polymer ultrathin films. The concept developed by Herminghaus [81], that capillary wave dynamics would penetrate towards the central region of polymer ultrathin films enhancing the mobility of this region, thus decreasing T_g, also turns out to be equivocated.

The fast-mode showing Arrhenius-like behavior is related to the relaxation dynamics of localized processes as proven by the q-independent total intensities from this mode. This is confirmed by the fact that relaxation times are not coupled to the viscosity η, meaning that it should take place in regions smaller than the CRRs (in PS $\approx$ 1-2 nm). The fast-mode is originated at the central region, *i.e.*, it exists throughout the whole film thickness and, it is not a surface mode as proposed by many authors [16, 17]. This information was obtained by evaluating total intensities from samples annealed under the same conditions. For thoroughly annealed films, the fast-mode could be completely erased from the REDLS spectra, reinforcing the idea that its origin is related to the presence of remaining solvent in the thin films, despite annealing. The full removal of solvent from samples made of oligomers, as PS 1821 g/mol, is probably not doable due to the necessary high temperatures and vacuum levels needed, which would lead to sample destruction. However, the amount of remaining solvent can be brought to relatively small values, so that it no longer has a significant plasticizer effect on the films, decreasing T_g.

As shown by means of kinetic SPR, the dynamic T_g of supported polystyrene films does not change for film thicknesses down to 4 nm as measured for PS 350 000 g/mol and down to at least 8 nm for the oligomer PS 1821 g/mol. As the T_g does not change down to such length scales, it reinforces the idea that both, the microscopic events responsible for the glass transition and consequently the α-relaxation, take place at length scales much smaller than that of the film thicknesses studied. Another consequence is that the radius of gyration, R_g, normally attributed as a length scale for confinement in polymer ultrathin films, is ultimately disregarded to be so, as $R_g \approx 16$ nm for PS 350 000 g/mol, four times larger than the thickness of

4 nm studied. Oligomeric ultrathin films such as the ones of PS 1821 g/mol here studied, with high surface quality and T_g values in agreement with the bulk material, have no parallel in the literature.

The previous state-of-the-art on polymer ultrathin film dynamics, recently put forward by the group of Friedrich Kremer [5, 18–22, 65], states that the α-relaxation and, therefore, the T_g, does not suffer any confinement effect down to about h = 5 nm. Their final conclusion was that no dynamical differences can be observed in polymer ultrathin films, if a careful sample preparation is obeyed. However, another complex side of the coin was presented in detail in this dissertation: even though the dynamic T_g, the α-relaxation, the viscosity, and the shear modulus remain unaltered in respect to bulk material, the final dynamical state of the free-surface of polymeric films is strongly affected by the film thickness, not due to any confinement effects of the polymer chains, but purely due to the hydrodynamic conditions super-imposed by the polymer-solid contact, *i.e.*, due to the non-slip boundary conditions at the solid surface. These boundary conditions alter the dynamic state of the polymer free-surface when the film thickness becomes small enough. Therefore, the free-surface probes a thickness dependent shear modulus. The effect of the film thickness on the dynamics of the free-surface is included in the term τ_0 of equation 1.48, which was derived in Chapter 1.2.

In summary, it is legitimate to state that the present work ultimately answered most of the long term standing controversies in the field of supported polymer ultrathin films, regarding their structure and dynamics. Furthermore, it puts forward new ideas about other "forgotten" old problems as the β-relaxation and other faster processes in glass forming materials, bringing even possible answers for the $\alpha - \beta$-bifurcation in some polymers. This phenomenon likely relates to the coupling of the remaining solvent dynamics to the α-relaxation in high temperatures or frequencies, whith the β-relaxation vanishing or not, depending on the physical conditions of the material and the resolution of the specific technique.

This work impacts directly on the industrial application of polymer ultrathin films, and related topics such as, *e.g.*, the use and processing of nano-composites, membranes, supported and free-standing films, etc.

4.1 Outlook: the future of REDLS & WEDLS

Concerning the REDLS technique, future studies related to both, the slow and the fast-mode are enabled. As the slow-mode is the manifestation of

capillary waves dynamics on polymer films, and its dynamical behavior is governed by the intrinsic property of the material, REDLS will prove useful to study different situations in which the intrinsic properties of the materials are changed on purpose. For example, polymer films with different degrees of cross-linking would have different viscosities and elastic properties, leading to changes in the capillary waves dynamics. Different cross-linking times (*e.g.*, PMMA under UV light) would deliver different properties. A certain plateau should be achieved when the cross-linking activity reaches a maximum. This type of knowledge is industrially important since cross-linked films are widely used as coatings. Another possibility is to study the effect of plasticizers in different concentrations on polymer ultrathin films. The controlled addition of plasticizers would decrease T_g, viscosity and moduli, so that a systematic understanding of the impact of such substances on the dynamics of polymer ultrathin films can be achieved. The processing of nanocomposites is also related to the interfacial properties. The roughness of polymeric films can be decreased to a certain minimum that is naturally controlled by the amplitude of capillary waves. As the amplitude of these waves is a function of temperature, different roughness can be induced on the film surfaces when different annealing conditions are applied: a polymer film at very high temperature, *e.g.*, 200 °C, would be rougher than the same film at lower temperature, let us say 120 °C, so that when both are quenched to room temperature at very high cooling rates, different surface roughness are kept frozen. However, the film intrinsic roughness can be tuned by controlling the cooling rate: slowly cooled samples would show intrinsic roughness smaller than fast cooled samples. Roughness is an important issue when concerning friction, abrasion and optical quality of films. Multi-layered systems have different interfacial properties in each interface, just depending on the properties of both materials. In this way one could study the impact of capillary wave dynamics in multi-layered media, stress generation, etc. The stability of membranes or thin films, both, supported and free-standing, is related to the shearing the free-surface is submitted. Therefore capillary wave dynamics might be intrinsically correlated to the maximum thermal stability of such thin films. When a liquid surface wets another surface, capillary waves are inevitably present, and one could study deeper how the momentum transfer is impacted by capillary waves. This type of phenomenon has been studied in colloidal systems in ref. [90], but they did not mention the possibility of understanding the dynamics of wetting as a whole.

An idea about changing the properties of the slow-mode by tuning surface tension is given next.

Tuning surface tension with colloidal systems. It is possible to promote considerable tuning of surface tension in colloidal systems, by changing the radius of the colloidal particles. The surface tension in colloidal systems is given by [90]:

$$\gamma \sim \frac{k_B T}{d^2} \tag{4.1}$$

where d is the particle radius. This enables to achieve systems with ultra-low values for γ, ($\gamma \sim 1$ μN/m and below !) [90]. In these systems it is possible to observe capillary waves with huge amplitude and very small capillary lengths (equations 1.26 and 1.27).

The fast-mode is related to the existence of remaining solvent in the polymer ultrathin films. Therefore, different annealing conditions, as time, pressure, temperature, etc, and their impact on the fast-mode still require deeper understanding. These effects impact directly the slow-mode dynamics as well. Therefore, annealing as a whole, can be better understood. If it would finally turn out that the fast-mode is the diffusion of remaining solvents in polymer ultrathin films, then one could study diffusion of different solvents under different concentrations and physical conditions in such films. This understanding has a tremendous impact on the diffusion of solvents in polymeric membranes, coatings, etc. Chemical reactions in such systems is also an important issue, since the kinetics of reactions depend on the mobility (or diffusivity) of molecules in these media. The stability and mobility of pigments in gels, membranes or coatings can also be studied in detail, since diffusivity plays a main role in these issues.

Waveguide Enhanced Dynamic Light Scattering–WEDLS. Waveguide Enhanced Dynamic Light Scattering (WEDLS) [109] was developed within the framework of the present thesis but was not used in the scope of this work for resolving polymer dynamics in thin films. However, its development puts forward new possibilities for analyzing the dynamics of polymer ultrathin films as well as thicker films (when h $>$ 200 nm).

It is based on the scattering of light on polymer films, where the incident beam is a given waveguide mode (TM or TE) (Figure 2.13, right). As the intensity of the optical field throughout the polymer film depends on the order, i, of the mode (TE_i or TM_i), by selecting the proper mode, different regions of the polymer film can be studied independently.

By applying a s-polarized beam, one could use the TE0 mode and there-

fore achieve a maximum sensitivity at the central region of the film (Figure 2.13, right), *i.e.*, bulk information in the case of thick films. Using a p-polarized beam however, one excites the TM2 mode and extracts more informations about the contributions of both interfaces, the free-surface and the polymer-solid contact. For a thick film, the surface plasmon wave (TM0) just probes the polymer-solid contact and has no influence from the free-surface (bulk contribution provenient from the first $\approx$ 200 nm will also be present).

In this configuration, by exciting the TM0 mode, the polymer film can be used as a spacer in order to avoid the dynamics of the add-layer on top of the polymer film to be resolved. An example is, to study the forced diffusion of magnetic nanoparticles through membranes. One can apply a magnetic field, in a system where these magnetic particles are dissolved in a liquid add-layer (as water), forcing a particle to diffusive towards the polymer-solid contact. While the magnetic particles are driven towards the interfacial region, they would start to scatter light when they reach the optical field of the surface plasmons. This type of investigation is important for understanding how magnetic nanoparticles diffuse through membranes, such as the walls of human cells, a relevant aspect in cancer treatment nowadays.

The work done using this technique regards the diffusion of polystyrene colloidal particles in water (add-layer) on top of the waveguide [109]. From Figure 2.13 - right side, it can be seen that a tail "leaks" from the waveguide film towards the add-layer (water for example). Each waveguide mode has a different penetration depth into the water, being able to resolve dynamics of particle diffusion at different distances from the soft wall. The higher the order of the mode, the higher the penetration depth of the leaky-mode. Therefore, high order modes capture diffusion similar to bulk diffusion, while low order ones trace the diffusion close to the soft wall. The hindering of diffusion and the effects of the wall on the diffusion of colloidal particles could, in this way, be resolved.

Acknowledgements

Either write something worth reading
or do something worth writing.

Benjamin Franklin

As I focused most of the time on the second part, I decided to concentrate here on the first, for those who deserve it. For me, this part is the most relevant of this entire thesis.

By rapidly browsing this PhD thesis, it is easy to realize that this work would not be feasible without different types of help I got from so many people. Some of them contributed with fundamental scientific discussions, others with a pleasant everyday lunch time, others with building up setups, others patiently listened my crazy new ideas that usually come up every half an hour, including issues about science, technology, philosophy, love and life. All this people effectively contributed not just for an amazing and inspiring time, but also for a period of deep personal development and professional success in my life.

I would like to thank Prof. Hans-Jürgen Butt for giving me the unique opportunity to join his group, which allowed me to live science in its deepest meaning of the word. To work at the Max Planck Institute means to be part of one of the greatest active sources of knowledge the human kind has seen, and this is a great honor for me. In our regular meetings, Prof. Hans-Jürgen Butt always inspired fruitful ideas and asks questions with profound meaning. He thinks a lot before saying a word, and I think that is why his words are so precious. He gave me the freedom I needed to develop my own ideas in this work, the way it is. The freedom that made me judge hard situations, take important decisions alone, and grow from this. I also want to acknowledge the "DFG SPP1369 Priority Program" for funding this scientific project and for giving to so many other people equal opportunities as I had.

Prof. Florian Müller-Plathe, Prof. Bernd Stühn and Prof. Markus Biesalski, kindly accepted to be referees of my doctoral thesis. The group of Prof. Florian Müller-Plathe expresses impressive affection towards my person, which is surely reciprocal. They are all very lovely people and received me as an external member of their group.

I am deeply indebted with Prof. Werner Steffen, who was a great supervisor and patiently introduced me to the beautiful art of Light Scattering, a topic that illuminates my thoughts everyday. We used to discuss deeply the fantastic and non-understood aspects of glass former materials and the glass transition phenomenon. His experience and knowledge on these topics, and his ability of transmitting ideas, always made me to go for more and more informations, which finally resulted to be crucial for the success of applying REDLS to characterize polymer ultrathin films. These productive discussions certainly roused my "abnormal" interest in surface sciences, polymer physics and dynamics in general. Prof. Werner Steffen understands a lot about the many aspects of human behavior and psychology. I think, that is the reason why he always gave me freedom to do what should be done, and develop myself in the same way as a chrysalis should develop: without continuous and active help. Otherwise, the butterfly has no strength to fly by itself and dies. He acts as a sort of invisible hand, many times present when I was about to go out of the rail, and make irreversible mistakes. I learned to recognize mistakes that can be made, and the ones that should be completely avoided. He was always available for listening new ideas and open for discussions, from which I am sure, both of us gained a lot.

Prof. Hatice Duran (TOBB Univ. of Economics and Technology-Turkey), recently left the MPI-P and became an external member of our group. She always trusted my work, and gave me enthusiasm for so many times to keep going on the direction of my goals. Actually, she started this project within the context of DFG SPP1369 Priority Program, Polymer-Solid Contacts: Interfaces and Interphases, together with Dr. Vagelis Harmandaris (Univ. of Crete-Greece), with whom I also have had several productive scientific discussions.

When I start my PhD at the MPI-P, there was a young fellow, Dr. Markus A. Plum, who actively helped me with Surface Plasmon Resonance Spectroscopy and Dynamic Light Scattering. We had uncountable exciting and productive discussions about physics and surface sciences, which culminated to the development of the powerful WEDLS technique. I still remember the happiness I felt when I saw the successful result of a strong collaboration, the step by step of developing a completely new thing. That was great! our

discussions also led me to think about how to improve REDLS and extract its maximum power, with the least possible.

I acknowledge the fruitful cooperation with the group of Prof. Friedrich Kremer, specially to Martin Tress, Dr. E.U. Mapesa and Dr. Serghei Anatoly. They were the ones that made me believe my own results about the controversial topic: T_g in polymer ultrathin films. At that time (beginning of 2009), this issue was discussed with knives and swords in the scientific community. We were part of the few groups telling that the "apple should fall down", not trying to publish "amazing papers" on wrong-but-easy-to-sell ideas. Because of the serious work provided by the group of Prof. Friedrich Kremer, the world is a better place. At least for me. I hope to see in the future, other groups doing the same type of revealing work as these people have done. Unfortunately, nowadays science is contaminated and full of bad faith people and publications, surely not just in polymer physics and surface sciences. Science should be more than indexes and ratings, it is the highest proof it is worth it to be a human, it is a legate from our ancestors that worked so hard to help nature to understand herself. Let's keep it clean!

I enjoyed a lot to get to know Prof. Kurt Binder, an alive authority in polymer sciences. We had great time together in schools organized by his group, where I had the opportunity to discuss important scientific issues relevant to my work.

I thank the group of Prof. Matthias Rehahn for synthesizing and suppling some polymers, specially Katrin Sondergeld. I also exchanged samples and performed some work in a good collaboration with the group of Prof. Dr. Klaus Rätzke (Univ. Kiel).

Prof. George Fytas, an external member of our institute, told me some few wise words at the beginning of my work in 2009, which were crucial for the success of this project: "I am sorry for telling you it like this, but I have more than 20 years experience on this topic, and I tell you something...IT IS NOT GOING TO WORK !!!". At that time, he knew already that this project could not work the way it was proposed to be done. He was completely right on his statement! What he probably did not expect, was that his words would make me to work hard to reach the goal and make it possible, no matter how. Because of his words, I got impulse to take this work as a challenge and dig deep to find a solution. When I was digging deep, the answer came from the very top surface, where nature postulated that capillary waves would start saving my life, instead of making me drown.

I enjoyed very much to get to know people I include in my box of "great

scientists", as Dr. Benoit Loppinet (IESL-FORTH-Greece). He is a kind of "walking Wikipedia" as some other people would agree. At the very beginning of my PhD he also told me important things about my project, and put me in contact with Prof. Friedrich Kremer for the very first time. He told me some words I will never forget: "at the end of your PhD, you will put one more brick on top of the huge wall of science". I am happy that he was right. Benoit became a good friend, and we have great time together always when it is possible.

I would like to deeply thank my diploma supervisor, the Brazilian Prof. Edgar Dutra Zanotto, who supported me in many important situations. His office room at UFSCar is surely one of the most pleasant places to be on Earth. Not just because of his fantastic ability of making everything to look beautiful, but also for his presence. In my opinion, the alive definition of a human being.

I am deeply indebted to technical support of MPI-P: Achim Gerstenberg and his team (Feinmechanik) for helping me intensively during 9 months with the building of my setup, and even afterwards, for their excellent work, and for the nice atmosphere every morning when I pass by to have breakfast together with them. Andreas Best, for the amazing technical support and great scientific discussions. His family name is really proper. Andreas Hanewald for performing several rheological measurements for me. Gabi Herrmann for the amazing technical support and for showing me a spin-coater for the first time. Herr. Dirk Richter for elaborating with me the electronics of my setup. Thomas Wagner for synthesizing high quality polymers, and for spending such a long time to produce the few existing grams in the world of the PMPS I have. Hans-Josef Beauvisage for spending some of his time discussing with me about mathematics.

During my stay at Max Planck Institute for Polymer Research, I had the great opportunity of leading and supervising some other students in small projects I created, what gave me the feeling of what is to be a group manager. The best part is that these students were really good in learning fast, what allowed me to develop full projects in a short time with them. As the projects had a clear full story, *i.e.*, a beginning, middle part and an end, the students could understand how important the projects were, what made them to wish hard to achieve their goals. I learned a lot from that, and they also did so. Specially Jishna Sai Pulluru, who impressed me several times with his early abilities, and Burcu Aciksöz, contributed a lot to those projects.

My friends play an important role in my day by day life. They are the family I chose, the people I share issues other than science (this topic is

never excluded though). For this, I would like to thank the members of AK-Butt, specially Tiago Dos Santos Rodrigues, Dr. Vitor Deichmann (AK-Landfester), Dr. Emmanouil G. Anyfantakis (Manolis, Manos, etc), Karmena Jaskiewicz (AK-Landfester), and some ex-members: Dr. Ed de Jong, Dr. Nikos Gomopoulos, Dr. Sascha Pihan, Dr. Lizandra Castro, Dr. Akihiro Sato and Dr. Tim Still. Out of MPI-P: Guilherme Bollini (father and son), Marinho, Rafael Barbosa Rodrigues, Felipe Scopel, Jordana Barros, Lucas Faccioni Chanchetti, Colm Power, Bernhard Flohr, Matthias Müller and Marion Müller, Schuller, Manfred, and all my bavarian friends, which taught me how to speak and understand the "real German" and are too many to fit in this book. All these people were definitely necessary for the existence of this work.

I want to thank Dr. Tim Still (Univ. Pennsylvania), Tiago Rodrigues dos Santos (MPI-P), Dr. Manos Anyfantakis (MPI-P), Dr. Sascha Pihan (Heraeus), Veronika Beer (MPI-P), and my supervisors for proof reading this thesis. I really appreciate it.

I am forever indebted to my family for supporting me in any aspect since the day of my birth. My grandma Nazareth Matteus Dias, for giving me all she had in order to keep me able to study and become an engineer. My mother, Leni Dias Vianna and my father, Hélio Borges Vianna for working hard every day and night to feed us. My sister, for truly sharing with me a real love. My father for teaching me since I was a baby, how to think in a creative way and learn from the wise mother nature.

Coming to the end of this ritual, I am forever indebted with Dr. Ed de Jong, Prof. Hatice Duran and Dr. Tim Still, for helping me in one of the hardest months I ever had in my life. I will never forget it.

Finally, I want to thank you Katrin for being the woman of my life and standing me and my "weird Brazilian manners" everyday in our cozy home. You bring joy to my existence and make me feel a human everyday, since that great 31.10.2007. I love you !

I love you all.
Muitíssimo obrigado !!!

List of Symbols & Abbreviations

T_g	Glass transition temperature
CRR	Cooperative Rearrangement Regions
DSC	Differential Scanning Calorimetry
SPR	Surface Plasmon Resonance Spectroscopy
DLS	Dynamic Light Scattering
PCS	Photon Correlation Spectroscopy
X-PCS	X-ray photon correlation spectroscopy
REDLS	Resonance Enhanced Dynamic Light Scattering
WEDLS	Waveguide Enhanced Dynamic Light Scattering
QELS	Quasi Elastic Light Scattering
TDLS	Time Domain Light Scattering
BDS	Broadband Dielectric Spectroscopy
DMTA	dynamical mechanical thermal analysis
PM	Photomultiplier
APD	Avalanche Photodiode
PS	polystyrene
a-PS	atactic polystyrene
s-PS	syndiotactic polystyrene
i-PS	isotactic polystyrene
PMMA	polymethyl methacrylate
PB	polybutadiene
PDMS	polydimethylsiloxane
$\mathbf{q}$	experimental wave vector or wave number $(\mathbf{k}_s - \mathbf{k}_i)$
$\mathbf{k}$	wave vector or wave number of a capillary wave
ω_p	propagation frequency of a capillary wave
$\lambda_{C.W.}$	wave length of a capillary wave
M_e	entangled molecular weight
V&D	free-volume theory of Vrentas and Duda
(PGSE) NMR	pulsed gradient spin echo nuclear magnetic resonance
NTE	negative thermal expansion

Appendix A

SPR

All resonance curves were simulated using the software WinSpall, cf. Chapter 2.1.2.1. For this, the dielectric properties of the layers as well as their thicknesses had to be determined. The thickness of polymer and metal films were primarily measured with a profilometer, cf. Chapter 2.1.1.5. These thickness values were used for the multi-layer system, while the refractive index, or dielectric constant were determined by fitting the SPR curves with WinSpall. The working principle of WinSpall is also explained in Chapter 2.1.2.1. The obtained values of refractive indexes are in full agreement with literature values.

Table A.1: Dielectric constant values used.

Material	ϵ'	ϵ''
LaSFN9 (glass)	3.276	0
NLAK8 (glass)	2.89	0
Cr	-4	18
Au	-12	1.33
Polystyrene	2.51 ± (0.01)	0
N_2	1	0

Appendix B

DLS

B.1 The heterodyne detection modus

Regarding optical mixing methods (where no filter is inserted between the scattering medium and detector), when a local oscillator, usually a small portion of the laser beam (unscattered), is directed into the detector and mixed with the scattered signal from the sample, this is called the **heterodyne** detection method. If only the scattered light from the sample reaches the detector, this is called **homodyne** (or self-beat) method [99].

REDLS is a "natural" heterodyne method, as the surface roughness and small defects in the gold layer, in the glass substrate, or even in the polymer film, lead light to scatter statically, and this is the local oscillator in REDLS (the same is valid for WEDLS). As the sample is a thin film in this work, both, the scattered light from the sample and the local oscillator are in phase. Therefore, the autocorrelation function obtained by REDLS is denominated as G_1, the heterodyne autocorrelation function (or field autocorrelation function [99]), while G_2 is the homodyne autocorrelation function (or intensity autocorrelation function [99]) and relates to G_1 through the Siegert relation, cf. equation 2.32.

An important feature of the heterodyne method is the signal enhancement, due to the constructive superposition of waves from the local oscillator and from the scattered signal originated at the sample. Thus, REDLS enables signals with very small contrast to be resolved [122–124]. Another advantage of the heterodyne method is that, when several modes are present, the contrast (a) of each mode is directly related to the portion of the total

scattered light, due to the specific mode [54]. For example if the average scattered intensity is $I_{average} = 100$ kHz (in quantum language, equivalent to 100 000 photons/s reaching the detector [99]), and two modes are present, then the amplitude, a, of each mode, times the average intensity, gives the contribution of each mode individually to the scattered light. Thus, it is possible to affirm that the portion of light scattered by the fast-mode (when it is present), is much smaller than that of the slow-mode, as the fast-mode shows very small contrast levels in comparison to the slow-mode, cf. Figure 3.22. When just one mode is present, and has a contrast, *e.g.*, $a = 0.01$, with the above mentioned $I_{average} = 100$ kHz, this would mean that 1 % of this intensity value is due to this specific mode, *i.e.*, 1 kHz. The other 99 % of the intensity is due to the local oscillator.

The meaning of contrast in G_1. The amplitude, a, of the exponential function G_1 is finally related to the contribution of a given mode to the portion of scattered light from the absolute value of scattered intensity.

The meaning of total intensity in G_1. The total intensity I_{total} in heterodyne detection is given by:

$$I_{total} = I_{average} \cdot a \tag{B.1}$$

where $I_{average}$ is the average value of the detected intensity with time, a is the contrast of the heterodyne autocorrelation function G_1. In the example given before in B.1, $I_{total} = 1$ kHz, $I_{average} = 100$ kHz, and $a = 0.01$. This concept of total intensity plays a fundamental role in this work, because if the laser power impinging on the sample is kept constant (supposing a fairly good alignment), the contribution of different modes to the scattering process can be compared.

B.2 The concept of dispersion relations

In physics, the concept of dispersion relations was introduced by the work of Kramers and Kronig [160]. In the literature it is also found under the name **q**-dependence, *i.e.*, the dependence of the relaxation rate Γ (or frequency) as a function of wavenumber q.

Such a plot (ω or Γ *vs.* q) brings relevant information about the physics of movement in real systems. For example, a derivative of this function at

a given q value delivers velocity. For Brownian motion, Γ is a square law of q, and therefore, the derivative $\partial\Gamma/\partial q^2$, gives the diffusion coefficient D (as will be further shown). By knowing exactly the physics of motion, *i.e.*, how a system behaves, it is possible to predict the function $\Gamma(q)$.

This concept is important for this work when it comes to the derivation of such dispersion relations for capillary waves, such as the theory derived by Jäckle [47]. But before, as an example, let us start with the simpler case of a colloidal particle undergoing Brownian motion. The precise derivation is given in ref. [99], but the here shown is simple and intuitive, leading to an equivalent final result.

When a particle diffuses undergoing this kind of movement, the mean-square displacement takes the form:

$$< x^2 > = \ 2D_x t; \ \ < y^2 > = \ 2D_y t; \ \ < z^2 > = \ 2D_z t \tag{B.2}$$

where $|D_x| = |D_y| = |D_z| = |D'|$ are the diffusion coefficients in the respective canonical directions. Finally the 3-dimensional case gives:

$$< R^2 >= 6D't \tag{B.3}$$

where $D = 6D'$ is the spatial diffusion coefficient and t is the time the particle takes to diffuse the length R. If $R = r$, the particle radius, t is the relaxation time τ. This equation can be rewritten in the form:

$$\frac{1}{\tau} \approx \frac{D}{< r^2 >} \tag{B.4}$$

and since the inverse space $q = |\mathbf{q}|$ can be related to $2\pi/R$, one can write:

$$\frac{1}{\tau} \approx D|\mathbf{q}|^2 \tag{B.5}$$

that is the well-known $\mathbf{q}$-dependence of the relaxation rate (or inverse relaxation time) for particles in Brownian motion [33].

This result means the following: if a particle undergoes Brownian diffusion, its **mean-square displacement,** $< R^2 >$, is related to the diffusion coefficient and to the time. If one observes by means of DLS this type movement, from a certain scattering angle θ_s, a $\mathbf{q}$ value can be calculated[1], and the dispersion-relation B.5 will be satisfied. A plot $\Gamma = 1/\tau$ *vs.* $|\mathbf{q}|^2$ yields a straight line passing through the origin with slope D. Thus, if one knows

[1] $|\mathbf{q}| = |\mathbf{k}_s - \mathbf{k}_i| = [4\pi n_i/\lambda]\sin(\theta_s/2)$, the experimental wavevector.

the dependence of D with the particle and medium physical properties, the Brownian motion can be fully predicted. The Brownian motion is described by a well-established law given by the combination of the Einstein relation and the Stokes-law (therefore Einstein-Stokes equation).

Einstein-relation:

$$D = \frac{k_B T}{\zeta} \tag{B.6}$$

where k_B is the Boltzmann constant, T is the temperature, and ζ is the friction coefficient between the particle and the medium in which the particle is diffusing.

Stokes-law:

$$\zeta = 6\pi\eta R \tag{B.7}$$

where η is the viscosity of the medium, and R is the particle radius. Combining both we find:

$$D \equiv \frac{k_B T}{6\pi\eta R_h} \tag{B.8}$$

where R_h is the particle hydrodynamic radius. The $\mathbf{q}$-dependence (or dispersion relation) for the Brownian motion takes the form:

$$\frac{1}{\tau} \equiv \left[\frac{k_B T}{6\pi\eta R_h}\right] |\mathbf{q}|^2 \tag{B.9}$$

Thus the Brownian motion can be fully described by knowing the particle hydrodynamic radius, the viscosity of the medium and of course the experimental conditions (as T, λ, and scattering angle θ_s).

B.3 The concept of Power spectrum

The "power spectrum" also called, "spectral density" or "dynamic structure factor", $S(\omega)$ (or sometimes $I_A(\omega)$ as in ref. [99]) of a time-autocorrelation function $< A(0)A(t) >$ is precisely defined as:

$$S(\omega) = \lim_{\epsilon \to +0} \frac{1}{2\pi} \int_{-\infty}^{+\infty} e^{-i\ \omega t} e^{-\epsilon|t|} < A(0)A(t) > \mathrm{d}t \tag{B.10}$$

The power spectrum $S(\omega)$ is therefore the time Fourier transform of the autocorrelation function, $< A(0)A(t) >$. Thus:

$$< A(0)A(t) > = \int_{-\infty}^{+\infty} e^{+i\ \omega t}\ S(\omega)\, \mathrm{d}\omega \tag{B.11}$$

The power spectrum is a very important quantity in light scattering, since what is sometimes measured in some experiments is the power spectrum of the electric field of the scattered light instead of the autocorrelation function [99].

Here, it is relevant because the development of the theory of thermally activated capillary waves given by Jäckle [47] is described in terms of a "dynamic susceptibility", χ_{zz}, which is related to the power spectrum through its imaginary component:

$$S(q, \omega) = \frac{2k_B T \chi''_{z\,z}(q, \omega)}{\omega} \tag{B.12}$$

Therefore, the theory from Jäckle is given in terms of the power spectrum instead of the autocorrelation function itself. The explicit form of the relaxation time, $\tau(q, h, T)$, derived by Jiang *et al.* [82] using Jäckle's theory, can describe the results obtained by REDLS, by substituting μ by $G'(\omega, T)$, cf. equation 1.44 and 1.48. Even though the dispersion relations of thermally activated capillary waves given by Jäckle [47] was derived following a different methodology of the theory delivered by Herminghaus [81], both results are equivalent, except due to the use of different moduli (μ and E, respectively), cf. Chapter 1.2.3.

Appendix C

Description of capillary waves from Jäckle

A general expression that predicts the dynamical behavior of surface waves in viscous liquids of arbitrary thickness was first derived by Jäckle [47]. This description includes the elastic high-frequency waves contribution[1] that was missing in the lubrication approximation derived by Levich [87], and is based on the linear response theory from Kadanoff [94], where the power spectrum, $S(\mathbf{q},\omega)$, of thermal height fluctuations, u_z, of a liquid free-surface is derived:

$$S(\mathbf{q},\omega) = \frac{2k_BT\chi''_{zz}(\mathbf{q},\omega)}{\omega} \tag{C.1}$$

where $\chi''_{zz}(\mathbf{q},\omega)$, is the imaginary part of the dynamic susceptibility:

$$\chi_{zz}(\mathbf{q},\omega) = \frac{u_z}{p} \tag{C.2}$$

the ratio between the surface displacement, u_z, due to an external force, per unit area, A, *i.e.*, an external pressure, p. Here the vertical displacement u_z of the free-surface, Figure 1.1, is of analogous importance for the derivation of the dispersion relations of capillary waves, as the displacement R of the particle in Brownian motion, as derived in appendix B.2.

The full calculation of $\chi''_{zz}(q,\omega)$ follows from the linearized Navier-Stokes equation ($v_z = \frac{du_z}{dt}$):

[1] the elastic contribution consists of resonance modes corresponding to elastic waves in a thin plate [47].

$$\frac{\partial v}{\partial t} = -\frac{1}{\rho}\nabla p + \nu\Delta v \tag{C.3}$$

where v is the velocity, $\Delta v = \partial^2 v/\partial^2 \mathrm{r}$, p is the pressure, and ν is the kinematic viscosity η/ρ, with the corresponding Ansatz for monochromatic plane waves and no-slip boundary conditions at $z = -h$. The z-axis (perpendicular to the liquid surface) and therefore the thickness h comes explicitly into play by solving the differential equation C.3:

$$w(z) = B\cosh(\kappa z) + C\sinh(\kappa z) \tag{C.4}$$

where:

$$w(z) = \frac{\partial v_x(z)}{\partial z} - ikv_z(z) \tag{C.5}$$

the arguments of these hyperbolic functions contain the term z, that is the thickness axis. If one considers $|\mathrm{z}_{max}| = \mathrm{h}$, the dependence of the relaxation times τ of the capillary waves with the film thickness h, is obtained. Since no-slip boundary condition, $v_{z=-h} = 0$, was used in the derivation, it results that thinner films will move slower due to the presence of the solid interface (this would not be the case for a free-standing film). These results are in correspondence to the derivation from Herminghaus, cf. section 1.2.3.

From this theory, the dispersion relations for thermally activated capillary waves takes the general form [82]:

$$\frac{1}{\tau(q_{\|})} \approx \frac{1}{\tau_0(q_{\|})} + \frac{\mu}{\eta} \tag{C.6}$$

where

$$\tau_0(q_{\|}) \approx \frac{2\eta[cosh^2(q_{\|}h) + q_{\|}^2h^2]}{\gamma q_{\|}[sinh(q_{\|}h)cosh(q_{\|}h) - q_{\|}h]} \tag{C.7}$$

meaning that the relaxation time, $\tau(q_{\|})$, is directly proportional to the material viscosity η, and therefore, the temperature dependence of the relaxation times of capillary waves will be Vogel-Fulcher-Tamman (VFT), and an approximate parallel shift from the bulk viscosity (or α-relaxation).

Actually, the term G', substituting μ, decreases with increasing temperature, explaining the deviation in high temperatures from the perfect parallel shift from the bulk VFT behavior of the viscosity. Also, $\tau_0(q_{\|}) \propto \eta/\gamma$ and since γ is temperature dependent (γ decays linearly with the temperature for PS 1821 g/mol [101]), $\tau_0(q_{\|})$ deviates a little from the VFT dependence of the bulk viscosity.

Appendix D

Polymer Physics

The bulk relaxation times of the α-relaxation (or segmental relaxation times), $\tau_\alpha(T)$, as well as the bulk viscosity $\eta(T)$ for all used materials were measured by rheology. The experimental setup was in plate-plate geometry, ARES-Rheometric Scientific. The plates were 6 mm in diameter and the space between plates was about 1 mm in all cases (*i.e.*, the film thickness). A conventional master curve is represented as shown in Figure D.1.

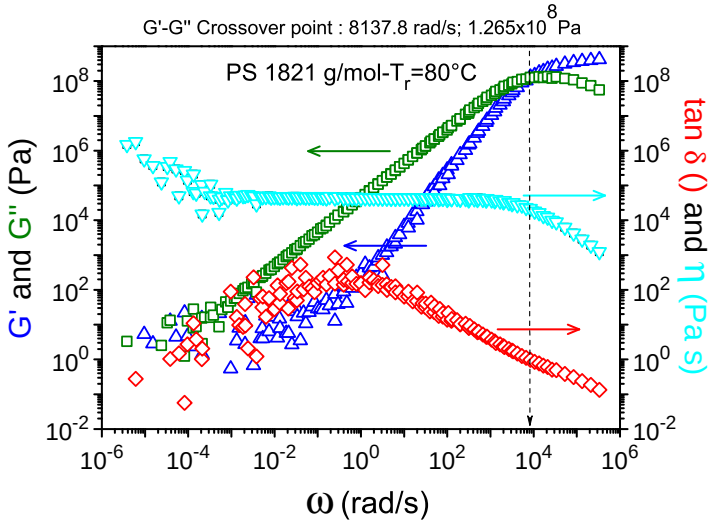

Figure D.1: Master Curve PS 1821 g/mol. The viscosity (η), storage shear modulus (G$'$), and loss modulus (G$''$) are represented at the reference temperature, T = 80 °C.

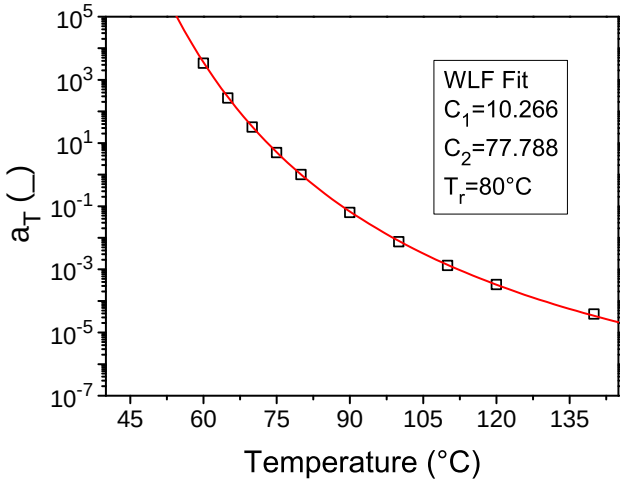

Figure D.2: Shift factors, PS 1821 g/mol. T_r = 80 °C. WLF parameters are shown in the inset.

The crossover point between the storage shear modulus, G', and the loss shear modulus, G'', happens in general at $\approx 10^8$ Pa for PS. The master curve's abscissa gives the frequency $\omega = 2\pi f$ rad/s, which has to be converted into the frequency f in Hz, in order to obtain the relaxation time, $\tau_\alpha(T_r)$, at this specific reference temperature, T_r (in Figure D.1, T_r = 80 °C). After determining the relaxation time of the α-relaxation at the reference temperature, one can find the α-relaxation time, τ_α(T), for all temperatures by multiplying $\tau_\alpha(T_r)$ by the shift factor $a_T(T_i)$ (Figure D.2), at the desired temperature, T_i. Multiplying the whole points of the curve in Figure D.2 by $\tau_\alpha(T_r)$ delivers the full values necessary to calculate the activation plot for the α-relaxation times at any temperature.

The same procedure can be done with the viscosity, so that for each temperature, a corresponding viscosity is found. For this purpose, not the crossover point is taken at the reference temperature, but the viscosity value at the zero shear frequency or the static viscosity. The viscosity is approximately constant in the here studied range of frequency, for a low molecular weight polymer as PS 1821 g/mol, Figure D.1. This zero frequency shear viscosity value has to be multiplied by the shift factors delivering the full temperature range curve. For high molecular weight polymers, the frequency dependence of the viscosity has to be taken into account, *i.e.*, instead of taking the zero frequency shear viscosity, $\eta(\omega, T)$ has to be considered.

The shape of the curve D.2 can be fit by the Williams-Landel-Ferry (WLF) equation [161], (cf. section 1.1.1.2):

$$log(a_T) = \frac{-C_1 \cdot (T - T_r)}{C_2 + (T - T_r)}$$

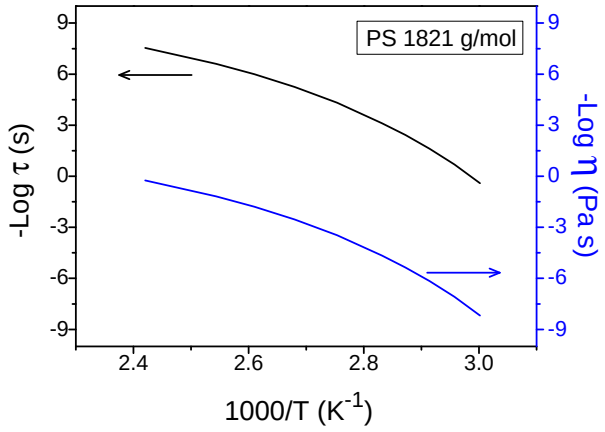

Figure D.3: Zero frequency shear viscosity and α-relaxation times as a function of temperature in an activation plot, PS 1821 g/mol.

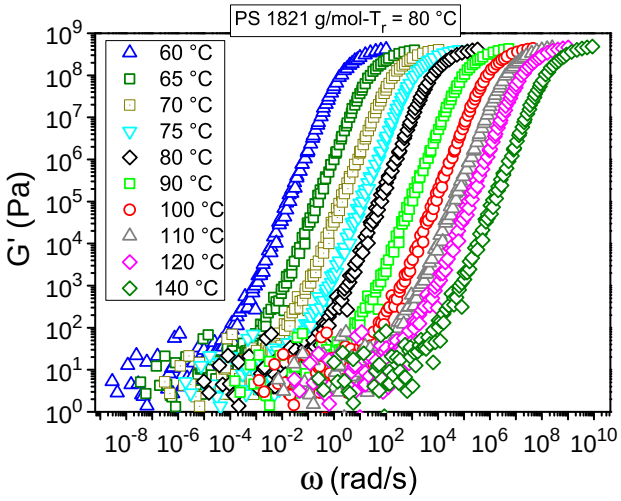

Figure D.4: Shear modulus as a function of temperature, PS 1821 g/mol. The curves are shifted using the corresponding shift factors, $a_T(T)$.

D.1 Rheology for PS of other molecular weights

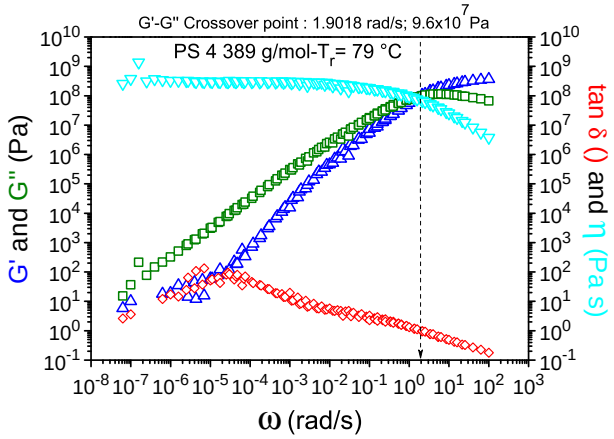

Figure D.5: Master Curve PS 4 389 g/mol. The viscosity (η), storage shear modulus (G'), and loss modulus (G'') and tanδ are represented at the reference temperature, T_r = 79 °C.

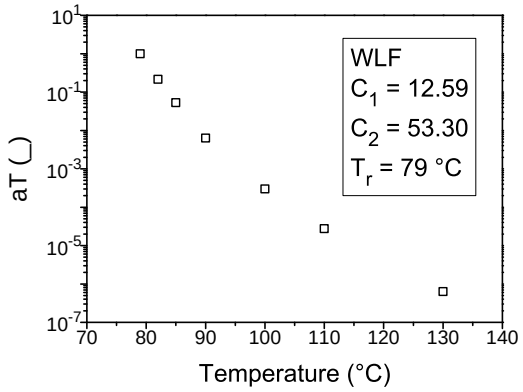

Figure D.6: Shift factors, PS 4 389 g/mol. T_r = 79 °C. WLF parameters are shown in the inset.

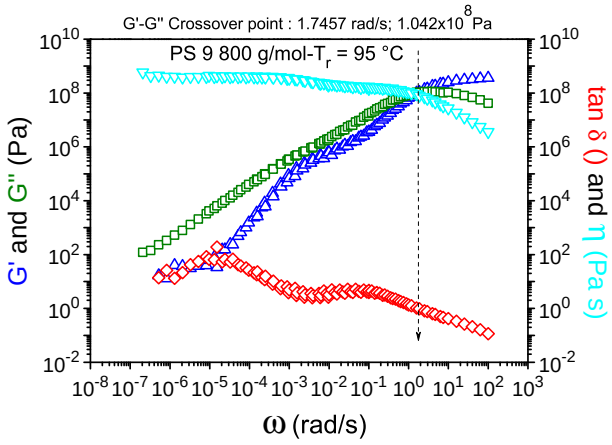

Figure D.7: Master Curve PS 9 800 g/mol. The viscosity (η), storage shear modulus (G'), and loss modulus (G'') and tanδ are represented at the reference temperature, $T_r = 95$ °C.

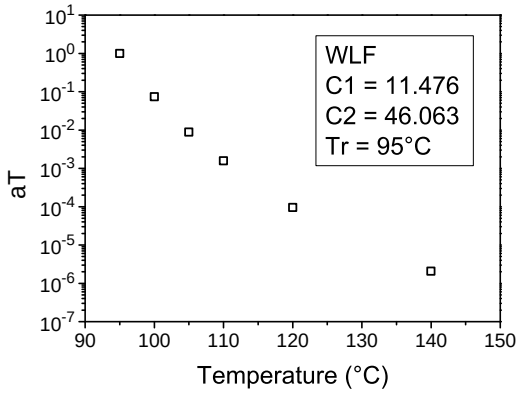

Figure D.8: Shift factors, PS 9 800 g/mol. $T_r = 95$ °C. WLF parameters are shown in the inset.

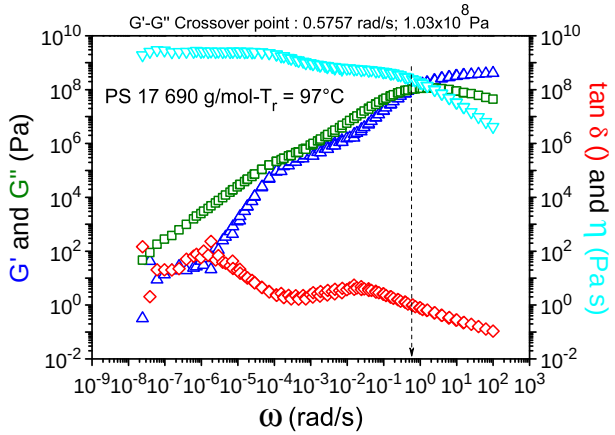

Figure D.9: Master Curve PS 17 690 g/mol. The viscosity (η), storage shear modulus (G′), and loss modulus (G″) and tanδ are represented at the reference temperature, T_r = 97 °C.

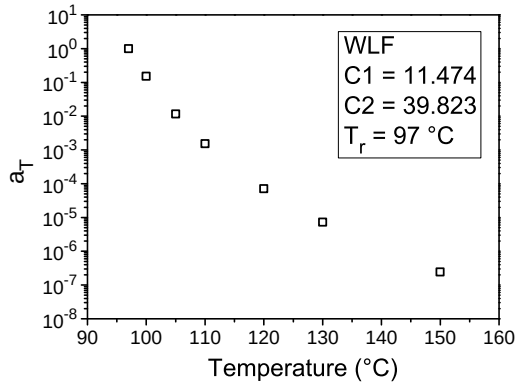

Figure D.10: Shift factors, PS 17 690 g/mol. T_r = 97 °C. WLF parameters are shown in the inset.

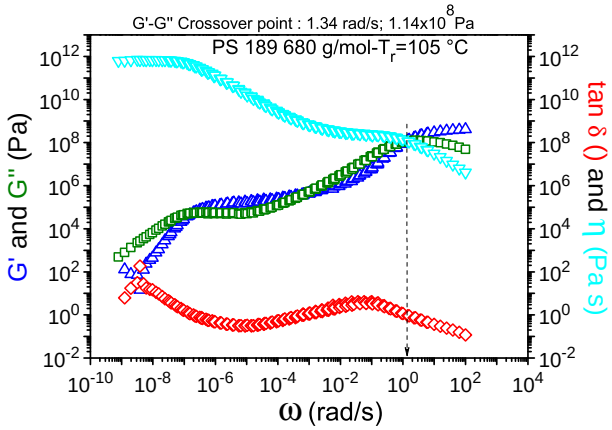

Figure D.11: Master Curve PS 189 680 g/mol. The viscosity (η), storage shear modulus (G$'$), and loss modulus (G$''$) and tanδ are represented at the reference temperature, T$_r$ = 105 °C.

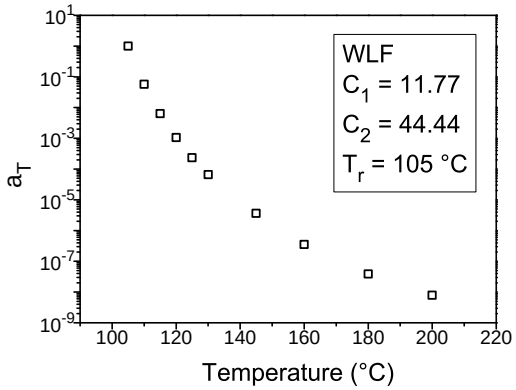

Figure D.12: Shift factors, PS 189 680 g/mol. T$_r$ = 105 °C. WLF parameters are shown in the inset.

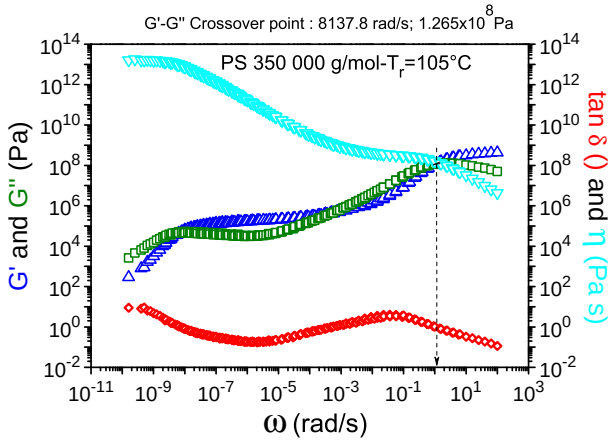

Figure D.13: Master Curve PS 350 000 g/mol. The viscosity (η), storage shear modulus (G'), and loss modulus (G'') and tanδ are represented at the reference temperature, T_r = 105 °C.

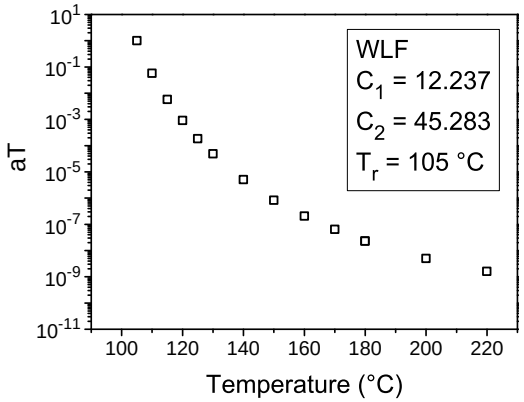

Figure D.14: Shift factors, PS 350 000 g/mol. T_r = 105 °C. WLF parameters are shown in the inset.

D.2 Calculation of Activation energy of the fast-mode

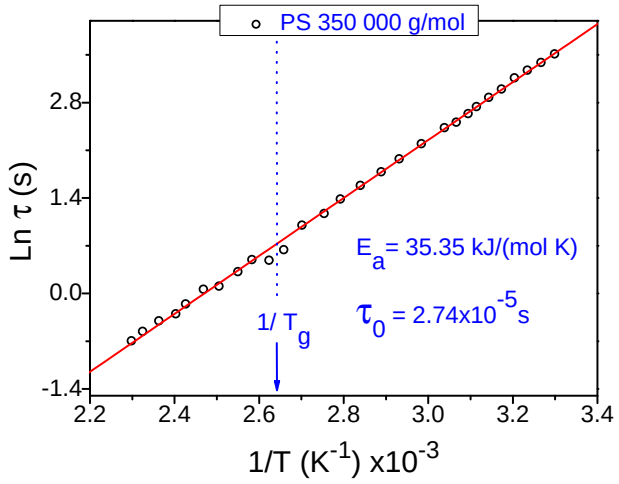

Figure D.15: The calculated activation energy of the fast-mode in PS 350 000 g/mol is about 35 kJ/(mol K), which is around half of the energy found for the β-relaxation by many authors. At T_g a deviation from the linear behavior is found. This might be the manifestation of the α-relaxation at this point, leading to a sort of "coupling" of the fast-mode with the α-relaxation, and to an apparent faster mobility at this point.

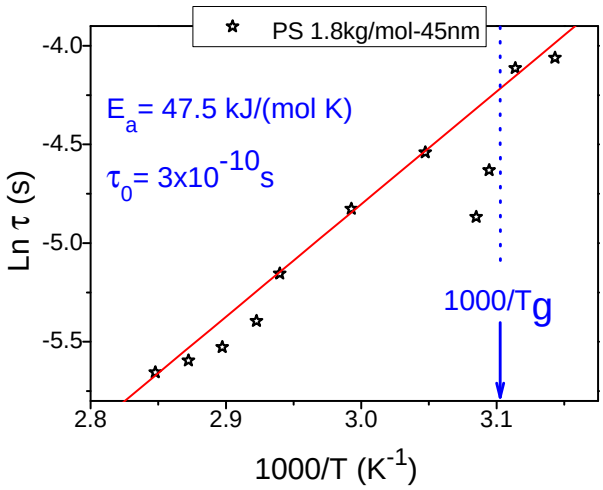

Figure D.16: The activation energy of the fast-mode in PS 1821 g/mol is about 47.5 kJ/(mol K). It seems to be a little higher than the E_a in the entangled PS 350 kg/mol in which the value of 35.5 kJ/(mol K) was found.

Bibliography

[1] S. Granick, S. Kumar, E. Amis, M. Antonietti, A. Balazs, A. Chakraborty, G. Grest, C. Hawker, P. Janmey, and E. Kramer, "Macromolecules at surfaces: Research challenges and opportunities from tribology to biology," *Journal of Polymer Science Part B: Polymer Physics*, vol. 41, no. 22, pp. 2755–2793, 2003.

[2] S. Bae and S. Granick, "Molecular motion at soft and hard interfaces: from phospholipid bilayers to polymers and lubricants," *Annu. Rev. Phys. Chem.*, vol. 58, pp. 353–374, 2007.

[3] C. Jackson and G. McKenna, "The glass transition of organic liquids confined to small pores," *Journal of Non-Crystalline Solids*, vol. 131, pp. 221–224, 1991.

[4] J. Keddie, R. Jones, and R. Cory, "Size-dependent depression of the glass transition temperature in polymer films," *EPL (Europhysics Letters)*, vol. 27, p. 59, 1994.

[5] A. Serghei, M. Tress, and F. Kremer, "Confinement effects on the relaxation time distribution of the dynamic glass transition in ultrathin polymer films," *Macromolecules*, vol. 39, no. 26, pp. 9385–9387, 2006.

[6] J. Forrest, K. Dalnoki-Veress, J. Stevens, and J. Dutcher, "Effect of free surfaces on the glass transition temperature of thin polymer films," *Physical Review Letters*, vol. 77, no. 10, pp. 2002–2005, 1996.

[7] J. Forrest, K. Dalnoki-Veress, and J. Dutcher, "Interface and chain confinement effects on the glass transition temperature of thin polymer films," *Physical Review E*, vol. 56, no. 5, pp. 5705–5716, 1997.

[8] C. Ellison and J. Torkelson, "The distribution of glass-transition temperatures in nanoscopically confined glass formers," *Nature Materials*, vol. 2, no. 10, pp. 695–700, 2003.

[9] Z. Fakhraai, J. Sharp, and J. Forrest, "Effect of sample preparation on the glass transition of thin polystyrene films," *Journal of Polymer Science Part B: Polymer Physics*, vol. 42, no. 24, pp. 4503–4507, 2004.

[10] J. Sharp, J. Teichroeb, and J. Forrest, "The properties of free polymer surfaces and their influence on the glass transition temperature of thin polystyrene films," *The European Physical Journal E*, vol. 15, no. 4, pp. 473–487, 2004.

[11] Z. Fakhraai and J. Forrest, "Probing slow dynamics in supported thin polymer films," *Physical Review Letters*, vol. 95, no. 2, p. 25701, 2005.

[12] Z. Fakhraai, S. Valadkhan, and J. Forrest, "Qualitative discrepancy between different measures of dynamics in thin polymer films," *The European Physical Journal E*, vol. 18, no. 2, pp. 143–148, 2005.

[13] D. Qi, Z. Fakhraai, and J. Forrest, "Substrate and chain size dependence of near surface dynamics of glassy polymers," *Physical Review Letters*, vol. 101, no. 9, p. 96101, 2008.

[14] A. Raegen, M. Massa, J. Forrest, and K. Dalnoki-Veress, "Effect of atmosphere on reductions in the glass transition of thin polystyrene films," *The European Physical Journal E: Soft Matter and Biological Physics*, vol. 27, no. 4, pp. 375–377, 2008.

[15] D. A. Savin, G. D. Patterson, and J. R. Stevens, "Evidence for the gamma-relaxation in the light scattering spectra of poly (n-hexyl methacrylate) near the glass transition," *Journal of Polymer Science Part B-Polymer Physics*, vol. 43, no. 12, pp. 1504–1519, 2005.

[16] Z. Fakhraai and J. Forrest, "Measuring the surface dynamics of glassy polymers," *Science*, vol. 319, no. 5863, p. 600, 2008.

[17] Z. Yang, Y. Fujii, F. Lee, C. Lam, and O. Tsui, "Glass transition dynamics and surface layer mobility in unentangled polystyrene films," *Science*, vol. 328, no. 5986, p. 1676, 2010.

[18] A. Serghei, H. Huth, M. Schellenberger, C. Schick, and F. Kremer, "Pattern formation in thin polystyrene films induced by an enhanced mobility in ambient air," *Physical Review E*, vol. 71, no. 6, p. 61801, 2005.

[19] M. Tress, M. Erber, E. Mapesa, H. Huth, J. Mu ller, A. Serghei, C. Schick, K. Eichhorn, B. Voit, and F. Kremer, "Glassy dynamics

and glass transition in nanometric thin layers of polystyrene," *Macromolecules*, pp. 139–473, 2010.

[20] E. Mapesa, M. Erber, M. Tress, K. Eichhorn, A. Serghei, B. Voit, and F. Kremer, "Glassy dynamics in nanometer thin layers of polystyrene," *The European Physical Journal-Special Topics*, vol. 189, no. 1, pp. 173–180, 2010.

[21] A. Serghei, H. Huth, C. Schick, and F. Kremer, "Glassy dynamics in thin polymer layers having a free upper interface," *Macromolecules*, vol. 41, no. 10, pp. 3636–3639, 2008.

[22] M. Erber, M. Tress, E. Mapesa, A. Serghei, K. Eichhorn, B. Voit, and F. Kremer, "Glassy dynamics and glass transition in thin polymer layers of pmma deposited on different substrates," *Macromolecules*, 2010.

[23] M. Efremov, E. Olson, M. Zhang, Z. Zhang, and L. Allen, "Glass transition in ultrathin polymer films: Calorimetric study," *Physical Review Letters*, vol. 91, no. 8, p. 85703, 2003.

[24] K. Deutsch, E. Hoff, and W. Reddish, "Relation between the structure of polymers and their dynamic mechanical and electrical properties. part i. some alpha substituted acrylic ester polymers," *Journal of Polymer Science*, vol. 13, no. 72, pp. 565–582, 1954.

[25] N. McCrum, "Be read, and g. williams," *Anelastic and Dielectric Effects in Polymeric Solids*, p. 355.

[26] M. Cicerone, F. Blackburn, and M. Ediger, "Anomalous diffusion of probe molecules in polystyrene: evidence for spatially heterogeneous segmental dynamics," *Macromolecules*, vol. 28, no. 24, pp. 8224–8232, 1995.

[27] U. Tracht, M. Wilhelm, A. Heuer, H. Feng, K. Schmidt-Rohr, and H. Spiess, "Length scale of dynamic heterogeneities at the glass transition determined by multidimensional nuclear magnetic resonance," *Physical Review Letters*, vol. 81, no. 13, pp. 2727–2730, 1998.

[28] I. Bahar, B. Erman, F. Kremer, and E. Fischer, "Segmental motions of cis-polyisoprene in the bulk state: interpretation of dielectric relaxation data," *Macromolecules*, vol. 25, no. 2, pp. 816–825, 1992.

[29] C. Angell, "Glass-formers and viscous liquid slowdown since david tumbull: Enduring puzzles and new twists," *MRS bulletin*, vol. 33, no. 5, pp. 544–555, 2008.

[30] M. Fuchs, W. Götze, S. Hildebrand, and A. Latz, "A theory for the beta-relaxation process near the liquid-to-glass crossover," *Journal of Physics: Condensed Matter*, vol. 4, p. 7709, 1992.

[31] E. W. Fischer, "Light-scattering and dielectric studies on glass-forming liquids," *Physica A*, vol. 201, no. 1-3, pp. 183–206, 1993.

[32] P. Rouse Jr, "A theory of the linear viscoelastic properties of dilute solutions of coiling polymers," *The Journal of Chemical Physics*, vol. 21, p. 1272, 1953.

[33] M. Rubenstein and R. Colby, "Polymer physics," 2003.

[34] E. Riande, *Polymer viscoelasticity: stress and strain in practice*, vol. 55. CRC, 2000.

[35] M. Doi and S. Edwards, *The theory of polymer dynamics*, vol. 73. Oxford University Press, USA, 1988.

[36] D. Boese and F. Kremer, "Molecular dynamics in bulk cis-polyisoprene as studied by dielectric spectroscopy," *Macromolecules*, vol. 23, no. 3, pp. 829–835, 1990.

[37] P. de Gennes, "Reptation of a polymer chain in the presence of fixed obstacles," *The Journal of Chemical Physics*, vol. 55, p. 572, 1971.

[38] M. Doi, "Explanation for the 3. 4-power law for viscosity of polymeric liquids on the basis of the tube model," *Journal of Polymer Science Polymer Physics Edition*, vol. 21, no. 5, pp. 667–684, 1983.

[39] S. Milner and T. McLeish, "Reptation and contour-length fluctuations in melts of linear polymers," *Physical Review Letters*, vol. 81, no. 3, pp. 725–728, 1998.

[40] J. Cloizeaux, "Double reptation vs. simple reptation in polymer melts," *EPL (Europhysics Letters)*, vol. 5, p. 437, 1988.

[41] J. Des Cloizeaux, "Relaxation of entangled polymers in melts," *Macromolecules*, vol. 23, no. 17, pp. 3992–4006, 1990.

[42] J. Des Cloizeaux, "Relaxation and viscosity anomaly of melts made of long entangled polymers: time-dependent reptation," *Macromolecules*, vol. 23, no. 21, pp. 4678–4687, 1990.

[43] J. Des Cloizeaux, "Relaxation of entangled and partially entangled polymers in melts: time-dependent reptation," *Macromolecules*, vol. 25, no. 2, pp. 835–841, 1992.

[44] H. Chen, E. Stepanov, S. Chum, A. Hiltner, and E. Baer, "Linear stress relaxation behavior of amorphous ethylene-styrene interpolymers," *Macromolecules*, vol. 33, no. 23, pp. 8870–8877, 2000.

[45] A. Bakai and E. Fischer, "Nature of long-range correlations of density fluctuations in glass-forming liquids," *The Journal of Chemical Physics*, vol. 120, p. 5235, 2004.

[46] M. Vasin and V. Lad'yanov, "A description of fischer cluster formation in supercooled liquids within the framework of the continuous theory of defects," *Journal of Physics: Condensed Matter*, vol. 17, p. S1287, 2005.

[47] J. Jäckle, "The spectrum of surface waves on viscoelastic liquids of arbitrary depth," *Journal of Physics: Condensed Matter*, vol. 10, p. 7121, 1998.

[48] H. Nakanishi and S. Kubota, "Absence of surface mode in a viscoelastic material with surface tension," *Physical Review E*, vol. 58, no. 6, p. 7678, 1998.

[49] H. Lee, A. Jamieson, and R. Simha, "Photon correlation spectroscopy of polystyrene in the glass transition region," *Macromolecules*, vol. 12, no. 2, pp. 329–332, 1979.

[50] R. Coakley, R. Mitchell, J. Stevens, and J. Hunt, "Rayleigh-brillouin light scattering studies on atactic polystrene," *Journal of Applied Physics*, vol. 47, no. 10, pp. 4271–4277, 1976.

[51] C. Demoulin, C. Montrose, and N. Ostrowsky, "Structural relaxation by digital-correlation spectroscopy," *Physical Review A*, vol. 9, pp. 1740–1742, 1974.

[52] C. LAI, P. Macedo, and C. Montrose, "Light scattering measurements of structural relaxation in glass by digital correlation spectroscopy," *Journal of the American Ceramic Society*, vol. 58, no. 3-4, pp. 120–123, 1975.

[53] J. Bucaro, H. Dardy, and R. Corsaro, "Strain relaxation in glass by optical correlation and pressure jump relaxation," *Journal of Applied Physics*, vol. 46, no. 2, pp. 741–746, 1975.

[54] G. Patterson, C. Lindsey, and J. Stevens, "Depolarized rayleigh spectroscopy of polystyrene near the glass-rubber relaxation," *The Journal of Chemical Physics*, vol. 70, p. 643, 1979.

[55] G. Adam, "On molecular kinetic theory of cooperative relaxation processes in dipolar liquid and crystalline phases," *Journal of Chemical Physics*, vol. 43, no. 2, p. 662, 1965.

[56] C. Angell, K. Ngai, G. McKenna, P. McMillan, and S. Martin, "Relaxation in glassforming liquids and amorphous solids," *Journal of Applied Physics*, vol. 88, p. 3113, 2000.

[57] C. Angell, "Relaxation in liquids, polymers and plastic crystals–strong/fragile patterns and problems," *Journal of Non-Crystalline Solids*, vol. 131, pp. 13–31, 1991.

[58] M. Cohen and D. Turnbull, "Molecular transport in liquids and glasses," *The Journal of Chemical Physics*, vol. 31, p. 1164, 1959.

[59] A. Doolittle, "Studies in newtonian flow. ii. the dependence of the viscosity of liquids on free space," *Journal of Applied Physics*, vol. 22, no. 12, pp. 1471–1475, 1951.

[60] G. McKenna, "Glass dynamics: Diverging views on glass transition," *Nature Physics*, vol. 4, no. 9, pp. 673–673, 2008.

[61] J. Phillips, "Microscopic theory of the kohlrausch relaxation constant [beta] k," *Journal of Non-Crystalline Solids*, vol. 172, pp. 98–103, 1994.

[62] J. Phillips, "Stretched exponential relaxation in molecular and electronic glasses," *Reports on Progress in Physics*, vol. 59, p. 1133, 1996.

[63] S. Lovejoy, "Area-perimeter relation for rain and cloud areas," *Science*, vol. 216, no. 4542, p. 185, 1982.

[64] B. Spehar, C. Clifford, B. Newell, and R. Taylor, "Universal aesthetic of fractals," *Computers Graphics*, vol. 27, no. 5, pp. 813–820, 2003.

[65] A. Serghei and F. Kremer, "Metastable states of glassy dynamics, possibly mimicking confinement-effects in thin polymer films," *Macromolecular Chemistry and Physics*, vol. 209, no. 8, pp. 810–817, 2008.

[66] G. Reiter, M. Hamieh, P. Damman, S. Sclavons, S. Gabriele, T. Vilmin, and E. Raphaël, "Residual stresses in thin polymer films cause rupture and dominate early stages of dewetting," *Nature Materials*, vol. 4, no. 10, pp. 754–758, 2005.

[67] J. Keddie, R. Jones, and R. Cory, "Interface and surface effects on the glass-transition temperature in thin polymer films," *Faraday Discuss.*, vol. 98, pp. 219–230, 1994.

[68] S. Ge, Y. Pu, W. Zhang, M. Rafailovich, J. Sokolov, C. Buenviaje, R. Buckmaster, and R. Overney, "Shear modulation force microscopy study of near surface glass transition temperatures," *Physical Review Letters*, vol. 85, no. 11, pp. 2340–2343, 2000.

[69] V. Lupascu, H. Huth, C. Schick, and M. Wubbenhorst, "Specific heat and dielectric relaxations in ultra-thin polystyrene layers," *Thermochimica acta*, vol. 432, no. 2, pp. 222–228, 2005.

[70] M. Efremov, E. Olson, M. Zhang, Z. Zhang, and L. Allen, "Probing glass transition of ultrathin polymer films at a time scale of seconds using fast differential scanning calorimetry," *Macromolecules*, vol. 37, no. 12, pp. 4607–4616, 2004.

[71] H. Huth, A. Minakov, and C. Schick, "Differential ac chip calorimeter for glass transition measurements in ultrathin films," *Journal of Polymer Science Part B: Polymer Physics*, vol. 44, no. 20, pp. 2996–3005, 2006.

[72] Z. Yang, D. Peng, A. Clough, C. Lam, and O. Tsui, "Is the dynamics of polystyrene films consistent with their glass transition temperature?," *The European Physical Journal-Special Topics*, vol. 189, no. 1, pp. 155–164, 2010.

[73] O. Tsui and H. Zhang, "Effects of chain ends and chain entanglement on the glass transition temperature of polymer thin films," *Macromolecules*, vol. 34, no. 26, pp. 9139–9142, 2001.

[74] O. Tsui, T. Russell, and C. Hawker, "Effect of interfacial interactions on the glass transition of polymer thin films," *Macromolecules*, vol. 34, no. 16, pp. 5535–5539, 2001.

[75] K. Fukao and Y. Miyamoto, "Slow dynamics near glass transitions in thin polymer films," *Physical Review E*, vol. 64, no. 1, p. 011803, 2001.

[76] C. Ellison, M. Mundra, and J. Torkelson, "Impacts of polystyrene molecular weight and modification to the repeat unit structure on the glass transition-nanoconfinement effect and the cooperativity length scale," *Macromolecules*, vol. 38, no. 5, pp. 1767–1778, 2005.

[77] O. Tsui and T. P. Russell, "Anomalous dynamics of polymer films," *Polymer Thin Films*, p. 267, 2008.

[78] A. Mayes, "Glass transition of amorphous polymer surfaces," *Macromolecules*, vol. 27, no. 11, pp. 3114–3115, 1994.

[79] P. De Gennes, "Glass transitions in thin polymer films," *The European Physical Journal E: Soft Matter and Biological Physics*, vol. 2, no. 3, pp. 201–205, 2000.

[80] S. Herminghaus, K. Jacobs, and R. Seemann, "The glass transition of thin polymer films: some questions, and a possible answer," *The European Physical Journal E: Soft Matter and Biological Physics*, vol. 5, no. 5, pp. 531–538, 2001.

[81] S. Herminghaus, "Polymer thin films and surfaces: Possible effects of capillary waves," *The European Physical Journal E: Soft Matter and Biological Physics*, vol. 8, no. 2, pp. 237–243, 2002.

[82] Z. Jiang, H. Kim, X. Jiao, H. Lee, Y. Lee, Y. Byun, S. Song, D. Eom, C. Li, and M. Rafailovich, "Evidence for viscoelastic effects in surface capillary waves of molten polymer films," *Physical Review Letters*, vol. 98, no. 22, p. 227801, 2007.

[83] D. Long and F. Lequeux, "Heterogeneous dynamics at the glass transition in van der waals liquids, in the bulk and in thin films," *The European Physical Journal E: Soft Matter and Biological Physics*, vol. 4, no. 3, pp. 371–387, 2001.

[84] A. Love, "Some problems of geodynamics" chap," 1911.

[85] A. Love, *Some Problems of Geodynamics: Being an Essay to which the Adams Prize in the University of Cambridge was Adjudged in 1911.* CUP Archive, 1967.

[86] I. Viktorov, "Rayleigh and lamb waves: Physical theory and applications," 1967.

[87] V. Levich, "Physicochemical hydro dynamics, pp, 472-531," 1962.

[88] V. Levich and V. Krylov, "Surface-tension-driven phenomena," *Annual Review of Fluid Mechanics*, vol. 1, no. 1, pp. 293–316, 1969.

[89] D. Buzza, "General theory for capillary waves and surface light scattering," *Langmuir*, vol. 18, no. 22, pp. 8418–8435, 2002.

[90] D. Aarts, M. Schmidt, and H. Lekkerkerker, "Direct visual observation of thermal capillary waves," *Science*, vol. 304, no. 5672, p. 847, 2004.

[91] M. von Smoluchowski, "Molecular-kinetic theory of the opalescence of gases in a critical state, as well as several related occurrences," *Annalen Der Physik*, vol. 25, no. 2, pp. 205–226, 1908.

[92] A. Madsen, T. Seydel, M. Sprung, C. Gutt, M. Tolan, and G. Grübel, "Capillary waves at the transition from propagating to overdamped behavior," *Physical Review Letters*, vol. 92, no. 9, p. 96104, 2004.

[93] J. Jäckle and K. Kawasaki, "Intrinsic roughness of glass surfaces," *Journal of Physics: Condensed Matter*, vol. 7, p. 4351, 1995.

[94] L. Kadanoff and P. Martin, "Hydrodynamic equations and correlation functions," *Annals of Physics*, vol. 24, pp. 419–469, 1963.

[95] L. Landau and E. Lifshitz, "Theory of elasticity, vol. vii," 1995.

[96] L. Landau and E. Lifshitz, *Course of Theoretical Physics: Vol.: 6 : Fluid Mechanics*. Pergamon Press, 1963.

[97] F. Brochard-Wyart, P. De Gennes, H. Hervert, and C. Redon, "Wetting and slippage of polymer melts on semi-ideal surfaces," *Langmuir*, vol. 10, no. 5, pp. 1566–1572, 1994.

[98] H. Kim, A. Rühm, L. Lurio, J. Basu, J. Lal, D. Lumma, S. Mochrie, and S. Sinha, "Surface dynamics of polymer films," *Physical Review Letters*, vol. 90, no. 6, p. 68302, 2003.

[99] B. Berne and R. Pecora, *Dynamic light scattering: with applications to chemistry, biology, and physics*. Dover Pubns, 2000.

[100] D. Champeney, "Fourier transforms and their physical applications," *Techniques of Physics, London: Academic Press, 1973*, vol. 1, 1973.

[101] G. Dee and B. Sauer, "The molecular weight and temperature dependence of polymer surface tension: Comparison of experiment with interface gradient theory," *Journal of colloid and interface science*, vol. 152, no. 1, pp. 85–103, 1992.

[102] H. Butt, K. Graf, M. Kappl, and J. Wiley, *Physics and chemistry of interfaces*, vol. 1. Wiley Online Library, 2003.

[103] D. Schubert and T. Dunkel, "Spin coating from a molecular point of view: its concentration regimes, influence of molar mass and distribution," *Materials Research Innovations*, vol. 7, no. 5, pp. 314–321, 2003.

[104] T. Faravelli, M. Pinciroli, F. Pisano, G. Bozzano, M. Dente, and E. Ranzi, "Thermal degradation of polystyrene," *Journal of analytical and applied pyrolysis*, vol. 60, no. 1, pp. 103–121, 2001.

[105] M. Guaita, "Thermal degradation of polystyrene," *British Polymer Journal*, vol. 18, no. 4, pp. 226–230, 1986.

[106] K. Kishore, V. Verneker, and M. Nair, "Thermal degradation of polystyrene," *Journal of Applied Polymer Science*, vol. 20, no. 9, pp. 2355–2365, 1976.

[107] G. Knight, "Thermal degradation of polystyrene," *Journal of Polymer Science Part B: Polymer Letters*, vol. 5, no. 9, pp. 855–857, 1967.

[108] J. Wegner and F. Patat, "Thermal degradation of polystyrene," vol. 31, pp. 121–135, Wiley Online Library.

[109] M. A. Plum, S. Dias Borges Vianna, A. Unger, R. F. Roskamp, H.-J. Butt, B. Menges, and W. Steffen, "Probing dynamics near surfaces: waveguide enhanced dynamic light scattering," *Soft Matter*, 2010.

[110] I. Anac, A. Aulasevich, M. J. N. Junk, P. Jakubowicz, R. F. Roskamp, B. Menges, U. Jonas, and W. Knoll, "Optical characterization of cononsolvency effects in thin responsive pnipaam-based gel layers exposed to ethanol/water mixtures," *Macromolecular Chemistry and Physics*, vol. 211, no. 9, pp. 1018–1025, 2010.

[111] F. de Fornel, *Evanescent waves: from Newtonian optics to atomic optics*, vol. 73. Springer Verlag, 2001.

[112] T. Fliessbach, *Elektrodynamik: Lehrbuch zur Theoretischen Physik II*. Spektrum Akademischer Verlag, 2004.

[113] W. Nolting, *Grundkurs Theoretische Physik 3: Elektrodynamik*. Springer, 2007.

[114] J. Chilwell and I. Hodgkinson, "Thin-films field-transfer matrix theory of planar multilayer waveguides and reflection from prism-loaded waveguides," *JOSA A*, vol. 1, no. 7, pp. 742–753, 1984.

[115] P. Yeh, *Optical waves in layered media*, vol. 95. Wiley Online Library, 1988.

[116] E. Kretschmann and H. Raether, "Radiative decay of non radiative surface plasmons excited by light(surface plasma waves excitation by light and decay into photons applied to nonradiative modes)," *Zeitschrift Fuer Naturforschung, Teil A*, vol. 23, p. 2135, 1968.

[117] O. Prucker, S. Christian, H. Bock, J. Rühe, C. Frank, and W. Knoll, "On the glass transition in ultrathin polymer films of different molecular architecture," *Macromolecular Chemistry and Physics*, vol. 199, no. 7, pp. 1435–1444, 1998.

[118] S. Rostami and D. Walsh, "Simulation of upper and lower critical phase diagrams for polymer mixtures at various pressures," *Macromolecules*, vol. 18, no. 6, pp. 1228–1235, 1985.

[119] S. Krause and Z. Lu, "Refractive index temperature measurements on anionically polymerized polystyrene," *Journal of Polymer Science: Polymer Physics Edition*, vol. 19, no. 12, pp. 1925–1928, 1981.

[120] K. Schmitz, "An introduction to dynamic light scattering of macromolecules," 1990.

[121] W. Schärtl, *Light scattering from polymer solutions and nanoparticle dispersions*. Springer Verlag, 2007.

[122] M. Plum, W. Steffen, G. Fytas, W. Knoll, and B. Menges, "Probing dynamics at interfaces: resonance enhanced dynamic light scattering," *Optics express*, vol. 17, no. 12, pp. 10364–10371, 2009.

[123] M. Plum, B. Menges, G. Fytas, H. Butt, and W. Steffen, "Resonance enhanced dynamic light scattering," *Review of Scientific Instruments*, vol. 82, no. 1, p. 5102, 2011.

[124] M. Plum, J. Ricka, H. Butt, and W. Steffen, "Anisotropic hindered motion close to an interface studied by resonance-enhanced dynamic light scattering," *New Journal of Physics*, vol. 12, p. 103022, 2010.

[125] M. Sanyal, S. Sinha, K. Huang, and B. Ocko, "X-ray-scattering study of capillary-wave fluctuations at a liquid surface," *Physical Review Letters*, vol. 66, no. 5, pp. 628–631, 1991.

[126] B. Ocko, X. Wu, E. Sirota, S. Sinha, and M. Deutsch, "X-ray reflectivity study of thermal capillary waves on liquid surfaces," *Physical Review Letters*, vol. 72, no. 2, pp. 242–245, 1994.

[127] M. Tolan, O. Seeck, J. Schlomka, W. Press, J. Wang, S. Sinha, Z. Li, M. Rafailovich, and J. Sokolov, "Evidence for capillary waves on dewetted polymer film surfaces: A combined x-ray and atomic force microscopy study," *Physical Review Letters*, vol. 81, no. 13, pp. 2731–2734, 1998.

[128] J. Wang, M. Tolan, O. H. Seeck, S. K. Sinha, O. Bahr, M. H. Rafailovich, and J. Sokolov, "Surfaces of strongly confined polymer thin films studied by x-ray scattering," *Physical Review Letters*, vol. 83, no. 3, p. 564, 1999.

[129] C. Gutt, T. Ghaderi, V. Chamard, A. Madsen, T. Seydel, M. Tolan, M. Sprung, G. Grübel, and S. Sinha, "Observation of heterodyne mixing in surface x-ray photon correlation spectroscopy experiments," *Physical Review Letters*, vol. 91, no. 7, p. 76104, 2003.

[130] L. Lurio, H. Kim, A. Rühm, J. Basu, J. Lal, S. Sinha, and S. Mochrie, "Surface tension and surface roughness of supported polystyrene films," *Macromolecules*, vol. 36, no. 15, pp. 5704–5709, 2003.

[131] C. Li, T. Koga, J. Jiang, S. Sharma, S. Narayanan, L. Lurio, X. Hu, X. Jiao, and S. Sinha, "Viscosity measurements of very thin polymer films," *Macromolecules*, vol. 38, no. 12, pp. 5144–5151, 2005.

[132] K. Shin, Y. Pu, M. Rafailovich, J. Sokolov, O. Seeck, S. Sinha, M. Tolan, and R. Kolb, "Correlated surfaces of free-standing polystyrene thin films," *Macromolecules*, vol. 34, no. 16, pp. 5620–5626, 2001.

[133] H. Raether, "Surface plasmons on smooth and rough surfaces and on gratings," *Springer Tracts in Modern Physics (Springer, Berlin, 1988)*, 1997.

[134] J. Pitarke, V. Silkin, E. Chulkov, and P. Echenique, "Theory of surface plasmons and surface-plasmon polaritons," *Reports on Progress in Physics*, vol. 70, p. 1, 2007.

[135] A. Tudos and R. Schasfoort, "Introduction to surface plasmon resonance," *Handbook of surface Plasmon resonance*, pp. 1–14, 2008.

[136] J. Evans, "Negative thermal expansion materials," *J. Chem. Soc., Dalton Trans.*, no. 19, pp. 3317–3326, 1999.

[137] P. Tipler and G. Mosca, *Physics for scientists and engineers*, vol. 1. Macmillan, 2008.

[138] P. W. Atkins, *Physical chemistry*. New York: Freeman, 6th ed., 1998.

[139] M. Mukherjee, M. Bhattacharya, M. Sanyal, T. Geue, J. Grenzer, and U. Pietsch, "Reversible negative thermal expansion of polymer films," *Physical Review E*, vol. 66, no. 6, p. 061801, 2002.

[140] R. Boyer and R. Spencer, "Thermal expansion and second order transition effects in high polymers: Part ii. theory," *Journal of Applied Physics*, vol. 16, no. 10, pp. 594–607, 1945.

[141] K. Illers and E. Jenckel, "Dynamic mechanical behavior of polystyrene, poly-p-chlorostyrene, and poly-p-bromostyrene at low temperatures," *Journal of Polymer Science*, vol. 41, no. 138, pp. 528–531, 1959.

[142] K. Illers, "Untersuchung der molekülbewegungen in polystyrol und poly-p-halogenstyrolen," *Zeitschrift für Elektrochemie, Berichte der Bunsengesellschaft für physikalische Chemie*, vol. 65, no. 7-8, pp. 679–686, 1961.

[143] R. Buchdahl and L. Nielsen, "Multiple dispersion regions in rigid polymeric systems," *Journal of Polymer Science*, vol. 15, no. 79, pp. 1–8, 1955.

[144] M. Takayanagi, H. Harima, and Y. Iwata, "Viscoelastic behaviour of polymer blends and its comparison with model experiments," *Mem. Fac. Eng. Kyusha Univ*, vol. 23, pp. 1–13, 1963.

[145] R. Boyer, "Dependence of mechanical properties on molecular motion in polymers," *Polymer Engineering Science*, vol. 8, no. 3, pp. 161–185, 1968.

[146] J. Cavaille, C. Jourdan, J. Perez, L. Monnerie, and G. Johari, "Time temperature superposition and dynamic mechanical behavior of atactic polystyrene," *Journal of Polymer Science Part B: Polymer Physics*, vol. 25, no. 6, pp. 1235–1251, 1987.

[147] R. Mininni, R. Moore, J. Flick, and S. Petrie, "The effect of excess volume on molecular mobility and on the mode of failure of glassy poly (ethylene terephthalate)," *Journal of Macromolecular Science, Part B: Physics*, vol. 8, no. 1-2, pp. 343–359, 1973.

[148] V. Lupascu, S. Picken, and M. Wübbenhorst, "Dynamics of t2g2 helices in atactic and syndiotactic polystyrene: new evidence from dielectric spectroscopy and ftir," *Macromolecules*, vol. 39, no. 15, pp. 5152–5158, 2006.

[149] F. Bovey and F. Hood *J. Chem. Phys*, vol. 42, p. 3900, 1965.

[150] B. Jasse, "Influence of conformational structure on the vibrational spectra of the different isomers of 2, 4, 6, 8-tetraphenylnonane, a polystyrene model molecule," *Journal of Molecular Structure*, vol. 39, no. 2, pp. 165–173, 1977.

[151] Y. Li and G. Xue, "Molecular conformation of syndiotactic polystyrene gel from octadecyl benzoate solution," *Macromolecular rapid communications*, vol. 19, no. 11, pp. 549–552, 1998.

[152] S. Cimmino, E. Pace, E. Martuscelli, and C. Silvestre, "Syndiotactic polystyrene: crystallization and melting behaviour," *Polymer*, vol. 32, no. 6, pp. 1080–1083, 1991.

[153] N. Ishihara, T. Seimiya, M. Kuramoto, and M. Uoi, "Crystalline syndiotactic polystyrene," *Macromolecules*, vol. 19, no. 9, pp. 2464–2465, 1986.

[154] J. Vrentas and J. Duda, "Diffusion in polymer-solvent systems. i. reexamination of the free-volume theory," *Journal of Polymer Science: Polymer Physics Edition*, vol. 15, no. 3, pp. 403–416, 1977.

[155] J. Duda, Y. Ni, and J. Vrentas, "An equation relating self-diffusion and mutual diffusion coefficients in polymer-solvent systems," *Macromolecules*, vol. 12, no. 3, pp. 459–462, 1979.

[156] S. Pickup and F. Blum, "Self-diffusion of toluene in polystyrene solutions," *Macromolecules*, vol. 22, no. 10, pp. 3961–3968, 1989.

[157] F. Blum, "Self diffusion of toluene in polystyrene solutions," tech. rep., DTIC Document, 1989.

[158] C. Kittel and P. McEuen, *Introduction to solid state physics*, vol. 7. Wiley New York, 1976.

[159] T. Still, W. Cheng, M. Retsch, R. Sainidou, J. Wang, U. Jonas, N. Stefanou, and G. Fytas, "Simultaneous occurrence of structure-directed and particle-resonance-induced phononic gaps in colloidal films," *Physical Review Letters*, vol. 100, no. 19, p. 194301, 2008.

[160] G. Arfken, H. Weber, and H. Weber, *Mathematical methods for physicists*, vol. 3. Academic press New York, 2005.

[161] M. Williams, R. Landel, and J. Ferry, "The temperature dependence of relaxation mechanisms in amorphous polymers and other glass-forming liquids," *Journal of the American Chemical Society*, vol. 77, no. 14, pp. 3701–3707, 1955.

Curriculum Vitæ

Sulivan Dias Borges Vianna

Date of Birth: June 25, 1985
Place of Birth: São Paulo, Brazil
Nationality: Brazilian
e-mail:sulivan.vianna@gmail.com
ResearcherID: B-4966-2011

February 2009 – January 2012
Max Planck Institute for Polymer Research, Mainz, Germany
Promotion by TU Darmstadt
Degree obtained: Doctor in natural science (Dr. rer. nat.)

February 2004 – December 2008
Department of Materials Engineering (DEMA), Federal University of São Carlos (UFSCar), Brazil
Degree obtained: Materials Engineer (Dipl.-Ing Materialwissenschaft)
Emphasis: polymeric materials
Thesis: Characterization of getter materials for the solar power collection technology

February 2003 – December 2003
Department of Materials Engineering, São Paulo State University (UNESP-Guaratingutá), Brazil

February 2000 – December 2002
Federal Center of Technological Education (CEFET-Uned-Cubatão) , Cubatão, Brazil

Publications

(1) S.D.B. Vianna, M.A. Plum, H.-J. Butt, H. Duran and W. Steffen *Dynamics in Ultrathin Films of Entangled and Non-Entangled Polymers.* **to be submitted**.

(2) M.A. Plum, **S.D.B. Vianna**, A.Unger, R.F. Roskamp, H.-J. Butt, B. Menges and W. Steffen *Probing dynamics near surfaces: waveguide enhanced dynamic light scattering.* Soft Matter 2011, 7, 1501-1505. DOI: 10.1039/C0SM00871K.

(3) H. Duran, K. Ogura, K. Nakao, **S.D.B. Vianna** *et al. High-Vacuum Vapor Deposition and in Situ Monitoring of N-Carboxy Anhydride Benzyl Glutamate Polymerization.* Langmuir 2009, **25**, 18. DOI: 10.1021/la9012125